이학박사 학위논문

Study on Rectifying Molecular Electronic Junctions in High-Yield Structure

고수율 구조에서의 정류 특성을 갖는 분자 전자 접합에 관한 연구

2018 년 2 월

서울대학교 대학원

물리·천문학부

정 현 학

Study on Rectifying Molecular Electronic Junctions in High-Yield Structure

고수율 구조에서의 정류 특성을 갖는 분자 전자 접합에 관한 연구

지도 교수 이 탁 희

이 논문을 이학박사 학위논문으로 제출함

2018년 1월

서울대학교 대학원

물리·천문학부 물리학전공

정 현 학

정현학의 이학박사 학위논문을 인준함

2018년 1월

위 원 장	홍 성 철	(인)
부위원장	이 탁 희	(인)
위 원	홍 승 훈	(인)
위 원	이 진 호	(인)
위 원	윤 효 재	(인)

Abstract

Study on Rectifying Molecular Electronic Junctions in High-Yield Structure

Hyunhak Jeong
Department of Physics and Astronomy
Seoul National University

The history of molecular electronics is generally considered to have begun with Aviram and Ratner with their early theoretical proposal entitled "Molecular Rectifiers" in 1974. The thrilling aspect of this research was that even a single molecule component that is contacted between electrodes, when it is rationally designed to exhibit functionality resembling its silicon-based device counterpart, can exhibit preferential electronic function in its ultimate downscale regime. Since then, the vast efforts for development of single molecule or self-assembled monolayers (SAMs) based electronic junctions with various experimental tools for investigating charge transport characteristics through molecules have been pursued. However at the same time, several major issues regarding ultimately downscaled molecular junctions were observed, especially in terms of junction reliability and device yield. This is mainly because of the absence of reliable, high-yield device platforms for testing molecular junctions that exhibit the distinctive and intrinsic functional properties of their component molecules. Recently, various types of these intrinsic molecular properties such as the change of chemical bonding, the redox process, photo- or charge-induced conformational change, and phase transition in molecular electronic devices have been widely investigated to understand the charge transport characteristics across molecules by resolving the issues. However, these intrinsic molecular properties in

molecular junctions are still under debate due to the difficulty in precise characterization. The issue represents a long-standing challenge for the advancement of molecular electronics as a viable technology for practical applications.

In this thesis, first I investigated the electrical properties of ferrocene-alkanethiolate SAMs on a high-yield, solid-state device structure. The devices were fabricated using a conductive polymer interlayer between the top electrode and the SAMs on both silicon-based rigid substrates and plastic-based flexible substrates. I observed asymmetric electrical transport characteristics that originated from the ferrocene moieties. In particular, I found an abnormal temperature dependence of the current-voltage characteristics at a large reverse bias (i.e., a decrease in current density as temperature increases), which is associated with the redox-induced conformational change of the molecules in the molecular junctions. Also, I applied temperature dependent transition voltage spectroscopy analysis to verify the validity of this claim. I further demonstrated that the molecular devices could function on flexible substrates under various mechanical stress configurations with consistent electrical characteristics.

Secondly, I proposed a new approach for creating high-yield molecular devices as a vertically structured metal-molecule-metal junction. I fabricated the top metal electrodes using a direct metal transfer method in which the top electrodes are formed on a different substrate and then transferred to the molecular layers, similar to the well-known graphene transfer method. Using this method, I was able to fabricate highly stable and reliable metal-molecule-metal junctions without the use of any additional interlayers, and the resulting junctions exhibited considerably improved device yields (~70 %) compared to those (typically less than a few %) of the molecular junctions in which the top electrodes are formed using the conventional metal-evaporation method. I compared this method with

other molecular device fabrication methods in terms of characteristic charge transport parameters, especially the electronic coupling interaction between the molecular layer and electrodes. Also, inelastic electron tunneling spectroscopy analysis were applied to examine molecular vibrational properties of the molecular junctions. Finally, I investigated the statistical variations in the length-dependent electrical characteristics from the molecular junctions, especially the Gaussian standard deviation σ of the current density histogram.

Keywords: Molecular electronics, Molecular junctions, Self-assembled monolayers, Electrical characteristics, Molecular diodes, Ferrocene-alkanethiolate, High device yield, Direct metal transfer, Inelastic electron tunneling spectroscopy, Transition voltage spectroscopy

Student Number: 2011-20423

List of Contents

List of Figures

Chapter 1.

Chapter 2.

Chapter 3.

List of Tables

Abbreviations

PEDOT:PSS	poly(3,4-ethylenedioxythiophene) stabilized with ploy(4-styrenesulfonic acid)
SAMs	self-assembled monolayers
PI	polyimide
PET	polyethylene terephthalate
PEN	polyethylene naphthalate
DMSO	dimethyl sulfoxide
RIE	reactive ion etching
RMS	root mean square
AFM	atomic force microscopy
FcC6	6-(ferrocenyl)hexanethiol
FcC8	8-(ferrocenyl)octanethiol
FcC11	11-(ferrocenyl)undecanethiol
J-V	current density-voltage
HOMO	highest occupied molecular orbital
LUMO	lowest unoccupied
TVS	transition voltage spectroscopy
IETS	inelastic electron tunneling spectroscopy
MBT	multibarrier tunneling
PR	photoresist
EGaIn	eutectic gallium-indium
rGO	reduced graphene oxide
GO	graphene oxide

IPA	isopropyl alcohol
SEM	scanning electron microscopy
PALO	polymer-assisted lift-off
DAC	digital-to-analog converter
NDR	negative differential resistance
RTD	resonant tunneling diode
M-M-M	metal-molecule-metal
XRD	X-ray diffraction
SPPs	surface plasmon polaritons
PPF	pyrolyzed photoresist films
eC	electron-beam deposited carbon films
PDMS	poly(dimethylsiloxane)
SDMD	surface diffusion mediated deposition

This work is dedicated to my loving wife Hyerin and our families.

Chapter 1. Introduction

1.1. General Concept of Molecular Electronics

Usually molecular electronics is regarded as a subfield of study of organic electronics.[1] Various organic compounds such as polymers have been studied for various applications in organic electronics such as a transistor, light-emitting diode, photovoltaic cell, non-volatile memory, etc.[2] In these applications, the thickness of the active electronic components is many times of the molecular diameter, so that only a small portion of molecules is in contact with metal electrodes. But if the molecular species are in contact with the metal electrodes in the form of a single molecule, or self-assembled monolayers (SAMs), there can be a prospect for more advanced physical phenomena of the charge transport characteristics of molecular species. Based on this view, molecular electronics is a subfield of organic electronics that specifically examines charge transport phenomena that is affected by physical/chemical properties of molecules which are directly connected to the electrodes. The molecular species can be either in a single molecule form or ensemble of molecules, i.e., SAMs. Contrary to the advances in organic electronics in which many practical applications are already found, however, this subfield is still in necessity of a lot of research which reflects its earlier, exploratory phase ever since the first theoretical proposal of a molecular electronic device in 1974.[3]

The genesis of molecular electronics is generally considered to have started with Aviram and Ratner with their early theoretical research entitled “Molecular Rectifiers” in 1974. The thrilling aspect of this study was that even a single molecule that is contacted

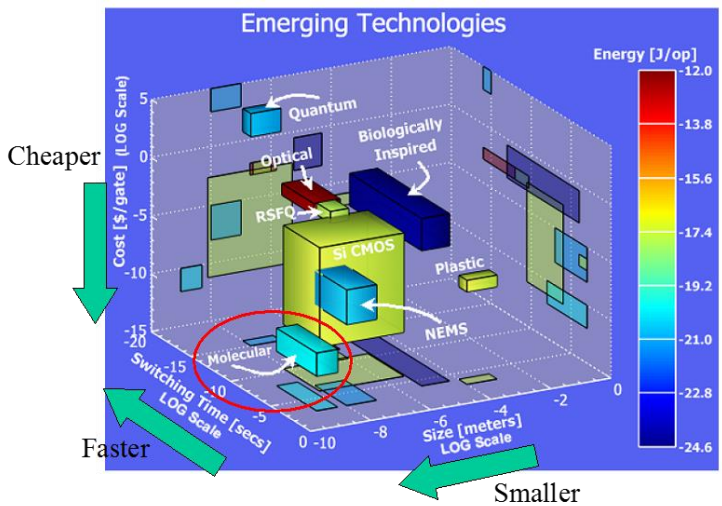

Figure 1.1.1. Schematic illustration of emerging technologies from International Technology Roadmap for Semiconductors (2005, 2007).

with electrodes, when rationally designed to resemble its silicon-based device counterpart, can exhibit preferential electronic function in the form of a 2-terminal wire junction in its ultimate downscale regime. Since then, the vast efforts for development of single molecule or SAMs based electronic junctions with various experimental tools for investigating charge transport characteristics through molecules have been pursued.[4-8] In this regard, molecular electronics is an active research field because it not only provides an ideal window for exploring the intrinsic properties of materials at the molecular level but may also be a promising complimentary electronics for the increasing technical demands of the miniaturization of traditional silicon-based electronics.[9]

In the view of practical applications, the concept of making an ultimately downscaled single molecule device, based on numerous degrees of freedom inherent in molecular structure, has potential for the future of next-generation electrical circuit units. Instead of utilizing the single molecules for an active device component, SAMs can be incorporated into the molecular junction while the functionalities are still exhibited in the molecular

structure, using an autonomous self-assembly of molecules. The SAMs are deposited by molecules in solution, which attach themselves to a specific substrate with an anchoring group, generating a densely packed molecular monolayer.[7] The unique nature of material self-assembly at the molecular level offers, in principle, numerous potential advantages. First, ultimately downscaling molecule size to the atomic scale may enable faster performance and high integration density with fewer heat issues. Second, the molecules' autonomous self-assembly process may reduce manufacturing production costs. Third, the great diversity of molecular structures may lead to the emergence of distinctive functionalities typically not accessible in traditional materials or approaches. These merits form a fundamental basis for attracting interdisciplinary interests to the field of molecular electronics as a promising candidate for alternative electronics, extending Moore's law beyond the foreseen limits. The advantage of molecular electronics with respect to other fields of electronics is schematically illustrated in Figure 1.1.1.

In this thesis, I will discuss my research work particularly focusing on the ensemble molecular junctions, which the molecular layer is organized by self-assembly process of molecules, i.e., the SAMs instead of the single molecule junction.

1.2. Experimental Testbeds for Ensemble Molecular Electronic Junctions

In the field of molecular electronics, extensive research has been performed to achieve reliable molecular junctions due to the fundamental difficulty of fabrication resulting from the ultimate scale of a molecule. Each approach to the realization of a

reliable molecular junction can be distinguished primarily depending on how many molecules can be characterized in the junction, and these approaches have their own advantages as well as disadvantages. For instance, although a few molecular junction techniques, including a that for the fabrication of a single molecule junction, can provide a platform for characterizing electronic properties of an individual molecule, it is a laborious task to utilize those techniques for practical application because these junctions are usually very delicate and show a low device yield. However, ensemble molecular junctions (the contacted molecules are more than ~1000) based on SAMs show relatively better device yield and can be used for practical applications based on a solid-state device platform. In this context, first we will discuss the development of various techniques for achieving ensemble molecular junctions in terms of the possibility of practical applications, for example, the device yield and manufacturability of a massive production based on a solid-state device platform.

1.2.1. General Experimental Testbeds for Ensemble Molecular Junctions

To manifest the electronic transport characteristics of ensemble molecular junctions, 2-terminal junction structures based on a metal-molecule-metal architecture have been widely adapted.[4-8] Especially in early days, many research groups have focused on a fundamental understanding of the electronic properties of molecules based on architecture rather than practical device application as a field of alternative electronics. Therefore, various techniques for fabricating ensemble molecular junctions have been proposed in many studies, but they were not suitable for practical applications due to extrinsic obstacles such as (i) low device yield, (ii) difficulty related to the fabrication of junctions (mostly

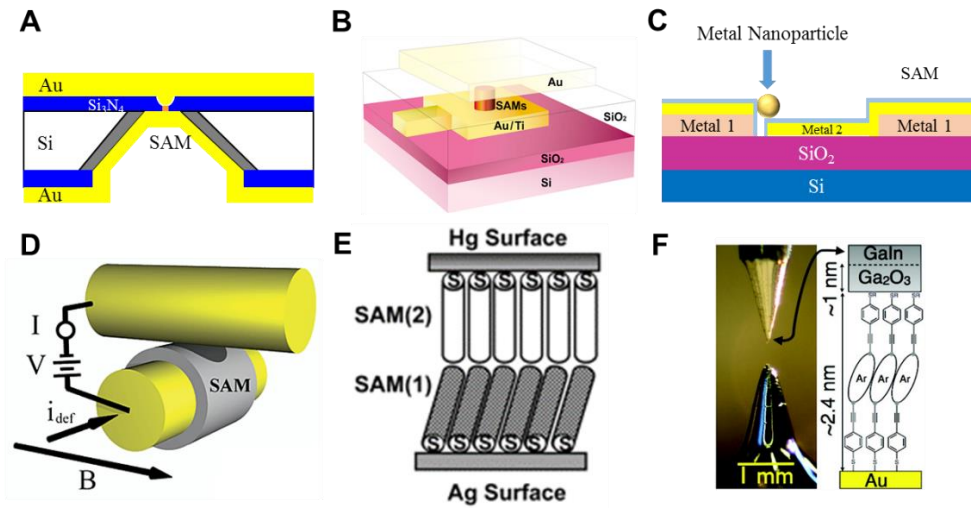

Figure 1.2.1. Examples of ensemble molecular junction platforms. (a) Nanopore. Reproduced from Ref. [10]. (b) Micro-scale via-hole. Reproduced from Ref. [11]. (c) Nanoparticles bridged. (d) Crosswire. Reproduced from Ref. [12]. (e) Hg liquid metal. Reproduced from Ref. [13]. (f) Eutectic gallium-indium based. Reproduced from Ref. [14].

due to poor addressability of molecules into gap electrodes), and (iii) low applicability for a massively parallel production of devices based on conventional lithography techniques such as the solid-state device platform. The schematics of these kinds of junctions are shown in Figure 1.2.1. Here, we will discuss these techniques from the perspective of potential device application.

Introducing an atomically thin molecular layer, which exhibits the transport characteristics of an active device component, into gap electrodes is a very challenging task due to the ultimate scale of the molecules. When SAMs of interest are deposited on metal-bottom electrodes, a prime way to sandwich the SAMs between two metallic contacts is the direct evaporation of metal electrodes. Nanopore and microscale via-hole techniques adopt this simple principle incorporated with a solid-state device platform based on conventional lithography as shown in Figure 1.2.1(a) and 1.2.1(b), respectively. The

creation of a nanopore junction is performed in an insulating material like SiO_2 or Si_3N_4.[15-20] After deposition of the vertically structured insulation layer, the nanopore, in which the SAMs will be deposited, is created by local etching using electron beam lithography and plasma etching or a focused ion beam. The remaining insulating membrane suspended over the substrate then acts as a window. By evaporating metal electrodes on both sides and depositing the SAMs on them, nanopore molecular junctions are obtained. All of the above steps can be performed using a conventional lithography-based solid-state device fabrication process. Therefore, this technique is a useful platform for massive production of the junctions and statistical determination of the intrinsic electronic transport characteristics.[15,16,21,22] This reproducibility is one of the most important aspects for massive production of a device with uniform device performance. Similar to the nanopore strategy, the microscale via-hole technique utilizes a direct metal evaporation method on bottom electrodes modified with SAMs.[23-25] Because of direct bombardment of the evaporated metal atoms with high kinetic energy on the SAMs; however, both techniques can induce mechanical damage, defects or even filamentary paths in the SAMs, resulting in poor device yield (~2 %).[23,26-32] To resolve this critical problem for practical applications of the molecular junctions, various countermeasures have been proposed. For example, (i) cooling of the evaporator stage during which the substrate is mounted, (ii) release of most of the kinetic energy of the metal atoms in collisions with inert gas atoms while the substrate is facing away from the boat, and (iii) maintenance of a very low evaporation rate.[15,16,21,33,34] Despite these measures, improvement of the device yield has remained doubtful.

Instead of direct evaporation of the metal atoms on the molecular layer resulting in poor device yield, one can deposit the electrodes by generating soft contacts on the SAMs.

Conceptually, this strategy involves a mechanical placement of pre-confined electrodes on the molecular layer, which is free from atomic defects caused by the metal evaporation. One example of this strategy is the fabrication of nanoparticle-bridged molecular junctions. The conceptual schematic of this junction is depicted in Figure 1.2.1(c). In this technique, a small gap between two metal electrodes is first fabricated using electromigration,[35] electron-beam lithography,[36] or the angled metal evaporation method.[37] Self-assembly of the molecular layer is then performed on the electrodes. Additionally, by trapping the nanoparticles in the gap, an electrical pathway consisting of metal-SAMs-nanoparticles-SAMs-metal is generated. Here, several methods can be applied to trap the metal nanoparticles in the gap. For example, (i) the application of an AC electric field between the electrodes to pull in the nanoparticles,[36] (ii) the application of a local magnetic field to ferromagnetic nanobeads coated with metal,[38,39] or simply (iii) the dispersal of the nanoparticles from solution.[37] Because this technique excludes the direct metal evaporation process, the device yield can be improved compared with the techniques mentioned in the previous paragraph. However, this technique may have several disadvantages in other aspects of device applications. First, precise control of the nanoparticles with a specific size and number at a well-defined location is quite challenging (i.e., the number of molecules connected by the nanoparticles at each electrode is variable), such that the charge transport characteristics of each molecular junction fabricated in a batch may seriously differ. Second, because this technique involves the nanoparticles between each molecular layer on both electrodes, the junctions are actually a double junction, wherein the charge transport characteristics may greatly be affected by the physical properties of the nanoparticles.[35] These issues may hinder the molecular junction manufactured by the nanoparticle-bridged technique to create a viable platform

for the practical application of molecular devices.

Another kind of soft contact method, evaporation-free on SAMs, is a crosswire technique. A schematic of the crosswire molecular junction is shown in Figure 1.2.1(d). Because the fabrication technique utilizes externally prepared long metal wires as the electrodes and makes a soft contact on SAMs similar to the nanoparticle-bridged junctions, it can prevent the unfavorable potential of metal atom penetration or defects associated with the monolayer during the device fabrication process, which result in an improved device yield compared with metal-evaporated molecular junctions.[40] In detail, this technique consists of two metal wires, one modified with SAMs of interest, mounted onto a stage with the wires are in a crossed geometry and with one wire perpendicular to the applied magnetic field.[12,41-44] To control the junction separation, a small DC current (< 5 mA) flows through the wire generating the Lorentz force in the magnetic field. The deflection current is then slowly increased to bring the wires together, forming a junction at the point contact. In spite of the device yield improvement, however, exact control of the number of contacted molecules is hard to achieve, and the orientation of the SAMs on the wire is not well defined because of the round curvature of the metal wire. This poor addressability of molecules may hinder a reliable and stable attainment of charge transport characteristics of the molecular junction ensemble when this technique is applied for molecular device fabrication. In addition, this technique is inadequate for massive production of the devices based on the solid-state device platform because of the requirement of the external magnetic field for the formation of the junctions.

Similar to the crosswire technique, the prevention of metal atom penetration or related defects in SAMs, which will improve the device yield, can be accomplished by the liquid metal contact. This technique takes advantage of the metal or alloy having a low

melting point that enables mechanical manipulation of the top electrode via a soft contact on the bottom electrode modified with the SAMs. Among the candidate materials, Race et al. first introduced a clean mercury (Hg) drop modified with SAMs as the top and bottom electrodes.[45] Figure 1.2.1(e) depicts a schematic of the Hg-SAMs-SAMs-metal junctions. In their experiment, the Hg drop as a top electrode is suspended from an amalgamated copper rod that can be lowered by a micrometer screw to make contact with the substrates containing barium, cadmium, calcium, copper and lead, on which the SAMs are formed on a microscope stage. There are several advantages of using the Hg drop as the electrodes.[46] First, because the liquid Hg drop has no structural features, such as edges, terraces, and pits, it is less likely to result in defects in the absorbed SAMs which forms a conformal contact. Second, this technique allows the exploration of the electrical properties of a wide range of organic/organometallic functionalities by diversifying the junction compounds. Finally, it is easy to assemble the junction over a large number of sites, which can generate several replicate experiments to collect a statistically large dataset number. However, this technique also has some drawbacks.[46-48] First, Hg is toxic, having harmful effects on the health of the user. Second, the junction stability is unsatisfactory, especially under the applied bias required for the electrical measurements originating from the intrinsic properties of Hg itself: high vapor pressure, easy to electromigrate, changes in shape under the applied potential, amalgamate with the bottom electrodes.[49-52] Thus, the junction yield is not dramatically improved compared with metal-evaporated junctions (less than 25%). Third, this technique requires external equipment such as a microscope, syringe, and micromanipulator for formation of the molecular junctions, and the measurements must be performed under a solvent bath, which is undesirable for functional molecular device applications.

Instead of Hg, stable and non-harmful liquid alloy electrodes may be beneficial to overcome the issues related to the abovementioned Hg electrodes. Whitesides group initially introduced an idea consisting of conformal electrodes from non-Newtonian fluid metal,[53] eutectic gallium-indium (EGaIn), and their use for studying charge transport characteristics across ensemble molecular junctions.[48,54-56] Figure 1.2.1(f) shows a microscopic and schematic image of the EGaIn-based molecular junction. In this technique, an EGaIn drop suspended from the needle of a syringe was brought into contact with the bare Ag surface, and the syringe was then retracted slowly until the EGaIn bifurcated on each side into conical tips. Because the conical tip protruding from the needle did not retract into a semispherical droplet (as would Hg), the contact area can be considerably reduced. Finally, using the micromanipulator, the EGaIn tip is brought into contact with the SAMs. The Ga_2O_3 interlayer (1~2 nm), which is formed by oxidation of EGaIn on the surface, is beneficial for the stability of the molecular junction as a protective layer leading to a high device yield (< 90 %). Nevertheless, the resistance of the interlayer is estimated to be low that is enough to characterize the electrical characteristics of the molecular junctions. There are several advantages when EGaIn electrodes are used for the molecular junctions instead of Hg electrodes: (i) unlike Hg, EGaIn does not flow until it experiences a critical surface stress, (ii) makes conformal, nondamaging contacts at room temperature, (iii) can be molded into nonspherical shapes with micrometer-scale (or larger) dimensions, (iv) has a low vapor pressure, and (v) is nontoxic. In addition, the work function of EGaIn (4.1-4.2 eV) is close to that of Hg (4.5 eV), but EGaIn does not form an alloy with many metals.[57,58] Thus, EGaIn could be an ideal replacement for Hg. However, there are some disadvantages related to the technique, impeding its suitability as a junction platform for practical device applications. For example, (i) although EGaIn exhibits better material

properties than Hg as an electrode, the fabrication method for the molecular junctions still requires external equipment like the Hg electrode-based technique, (ii) defining a reproducible junction size that determines the electrical characteristics of the junction remains uncertain, and (iii) the interfacial properties between the Ga_2O_3 layer and SAMs are ill-defined with respect to morphology and resistivity.[15,16,33] These disadvantages may hamper the viability of the liquid metal/alloy electrode technique for the practical application of molecule devices.

As one of the promising future candidates of alternative electronics against conventional Si-based electronics, which approaches its scalable limit, the realization of high-yield and stable molecular junctions has been a long-standing challenge in the field of molecular electronics, and it is an essential prerequisite for practical device applications. Although enormous efforts have been made by many research groups to develop reliable testbeds for the investigation of the fundamental transport characteristics, mentioned above, some critical disadvantages of the techniques still hinder their utilization for practical device platforms. Therefore, in the following chapter, we will discuss high-yield ensemble molecular junction fabrication techniques, which may overcome these obstacles and be applicable not only for examining the fundamental charge transport characteristics of molecular junctions but also potential device applications.

1.2.2. Realization of High-Yield Ensemble Molecular Junctions

As mentioned in the previous chapter, some of ensemble molecular junction fabrication techniques may be useful for investigating the electrical characteristics of the molecular layer, but they have the following limitations in terms of future device

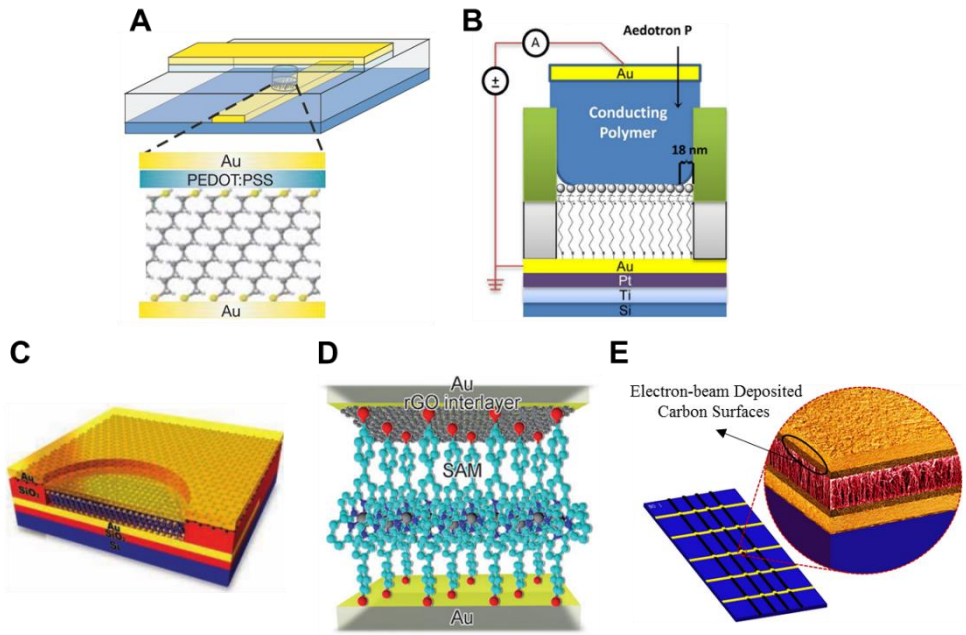

Figure 1.2.2. Approaches for high-yield solid-state based ensemble molecular junctions; Conducting interlayer based junctions. (a) Conducting polymer PEDOT:PSS. Reproduced from Ref. [60]. (B) Conducting polymer Aedotron P. Reproduced from Ref. [61]. (C) Graphene. Reproduced from Ref. [62]. (D) Reduced graphene oxide. Reproduced from Ref. [63]. (E) Electron-beam deposited carbon. Reproduced from Ref. [64].

applications: (i) low device yield, (ii) junction fabrication difficulties, and (iii) low applicability for massive device production based on conventional lithography techniques like the solid-state device platform. In the following, therefore, we will discuss two main approaches for fabricating the molecular junctions that have been presented by various research group to address these problems.

One of such approaches is interlayer technique. The low device yield problem of the metal-evaporated molecular junctions, which mostly resulted from metal atom penetration into the molecular layer, can be resolved by adhering to a simple idea: the introduction of a protective interlayer before evaporation of the top electrodes. Based on this strategy,

various materials have been proposed for the interlayer, such as thin oxide,[59] conducting polymer,[60,61] and carbon-based materials.[62,64] The schematics of the conducting polymer-based junction architectures are shown in Figure 1.2.2(a) and 1.2.2(b). To our knowledge, Boer group first introduced the conducting polymer interlayer technique to manufacture high-yield large area molecular junctions.[60,65-68] In this technique, they basically followed a similar fabrication process for the microscale via-hole technique except they incorporated a commercially available water-based suspension of PEDOT:PSS (poly(3,4-ethylenedioxythiophene) stabilized with ploy(4-styrenesulfonic acid)) as a top electrode on the SAMs and using a photoresist matrix as an insulating wall. While depositing the PEDOT:PSS interlayer, the SAMs can be protected from the formation of a filamentary path or contaminants under ambient conditions because the layer can be spin-coated on them. Moreover, each grain size of the macromolecules of the PEDOT:PSS is too large to penetrate the densely packed molecular layer, and the difference in water affinity between the PEDOT:PSS layer and the backbone of the SAMs makes them microscopically repulsive.[65] Based on this structural stability, large-area molecular junctions could be fabricated. Additionally, the aging effect on molecular junctions were confirmed to be minimal for at least several months in air, and there was no visible degradation upon sweeping. Most importantly, a large collection of molecular junctions can be easily manufactured with standard integrated device fabrication processes with a yield of working devices of ~100 %. As a similar strategy, Figure 1.2.2(b) shows a device schematic of an Aedotron P (1 % poly(3,4-ethylenedioxythiophene)-block-poly(ethylene glycol)) interlayer-based molecular junction.[61] Using this technique, they modified the fabrication process proposed by Boer group by replacing the photoresist insulating layer with an inorganic dielectric (alumina and silicon nitride), which was deposited using

conformal coating methods and the PEDOT:PSS interlayer with a commercially available Aedotron P dispersed in an organic solvent. Although the Aedotron P interlayer shows higher resistivity than PEDOT:PSS, submicrometer scaling of the molecular junctions was possible because of the better wetting properties and low viscosity of nitromethane on a conformal inorganic insulating wall. These properties allow the deposition of the interlayer into pores as small as 100 nm in diameter and 50 nm deep. This aggressive scaling of the junction fabrication technique to the limits of conventional lithographic methods may enable the realization of high-yield, low variation-integrated molecular junctions. Nevertheless, some issues regarding the use of the conducting polymer interlayer contact remain to be addressed. (i) The interface characteristics between the interlayer and SAMs are not fully understood. Moreover, the interlayer may dominate the charge transport characteristics in the junctions, especially when the resistivity of the interlayer is comparable with that of the molecular layer.[60,61,65,68,69] (ii) The intrinsic material properties of the conducting layer may limit the variety use of species of molecules due to their compatibility. Thus, there is still a plenty of room to improve the interlayer materials for the realization of robust ensemble molecular junctions.

Carbon-based materials ranging from activated carbons to carbon nanotubes and graphene have attracted a large amount of interest as the most promising electrodes because of their desirable physical and chemical properties. These properties include robust electronic transport characteristics, low cost, a variety of forms (powders, fibers, aerogels, composites, sheets, monoliths, and tubes, among others), ease of processability, a relatively inert electrochemistry, controllable porosity and electrocatalytic active sites for a variety of redox reactions.[70-72] In particular, there have recently been comprehensive investigations of graphene in various research fields.[73,74] Among these, graphene is a

two-dimensional array of carbon atoms arranged in a honeycomb lattice. Each carbon atom is sp^2-hybridized and is bound to its three neighbors.[73,74] Especially because its outstanding material properties such as high conductivity, transparency, chemical stability, and mechanical strength, graphene is considered a future candidate for optoelectronic device applications.[75,76] Regarding high-yield molecular junctions, Wang et al. first suggested the use of the multilayer graphene electrode for manufacturing high-yield ensemble molecular junctions. In their study, they transferred a multilayer graphene sheet synthesized by chemical vapor deposition on a Ni substrate, onto the SAMs as the buffer layer instead of spin coating the conducting polymer, as shown in Figure 1.2.2(c).[62] Using this graphene interlayer before the deposition of the top metal electrodes prevents the formation of filamentary paths that result in a low device yield. In this case, the device yield have been found to be > ~90 %, regardless of the properties of the isolating layer and contact groups (hydrophobic vs hydrophilic). Compared with earlier conducting polymer-based molecular devices, graphene interlayer-based devices may have potential advantages in terms of better charge transport characteristics due to a low contact resistance with a wide range of variable molecular lengths and different contacts.

One disadvantage of graphene interlayer-based molecular junctions is that the prepared graphene film should be transferred onto the SAMs using a mechanical method because graphene is atomically thin and chemically stable. To resolve this issue, the use as the top layer of reduced graphene oxide (rGO), which can be achieved from chemically exfoliated graphene oxide (GO), has been suggested.[63,77-79] GO consists of atomically thin flakes of oxidized graphite that is dispersible in various solutions and can produce dispersible rGO by chemical reduction.[80,81] The resistivity of the rGO is comparable to that of single-welled carbon nanotubes [82,83] and can be improved by thermal

treatment.[84,85] Because rGO is dispersible in organic solvents compared with graphene, one advantage of the use of rGO as electrodes is solution processability. For example, an rGO film electrode can be easily spin- and spray-coated directly onto a substrate, or generated by vapor reduction of spin-coated GO film.[86,87] Seo et al. first introduced the use of rGO as an interlayer electrode in molecular junctions, as shown in Figure 1.2.2(d).[63] In their study, they prepared the solvent-dispersed rGO sheets by reduction of GO sheets dispersed in water using a chemical reduction process. It has been demonstrated that there is no hysteresis or electrical short conduction in the current-voltage characteristics, indicating a high-device yield (> 99 %). Not only the high device yield but also the good stability and accessible processability of rGO interlayer-based molecular junctions enable this fabrication technique to be applicable for functional molecular electronic device applications. For example, there have been various rGO-based functional molecular device applications even on flexible substrates, such as a nonvolatile memory, photoswitching device.[77-79]

Other uses of sp^2-hybridized carbon material family members for molecular junctions, such as pyrolyzed photoresist films (PPF) and electron-beam deposited carbon films (eC), have been introduced by McCreery group.[64,88-93] PPF is disordered and partially graphitic carbon with a relatively low resistivity (~0.006 Ω cm) that is prepared by pyrolyzing patterned photoresistant stripes under a reducing atmosphere (5 % H_2 and 95 % N_2) at 1000 °C for 1 h.[88,94,95] This material is patternable by photolithography, which is thermally stable, and it is not subject to electromigration-like metals. And the surface of PPF is flat, with a root-mean-square (rms) roughness value similar to that of the substrate upon which it is formed. However, PPF has a relatively poor conductivity (~200 S/cm) compared with graphene or conducting polymers, and the requirement for slow

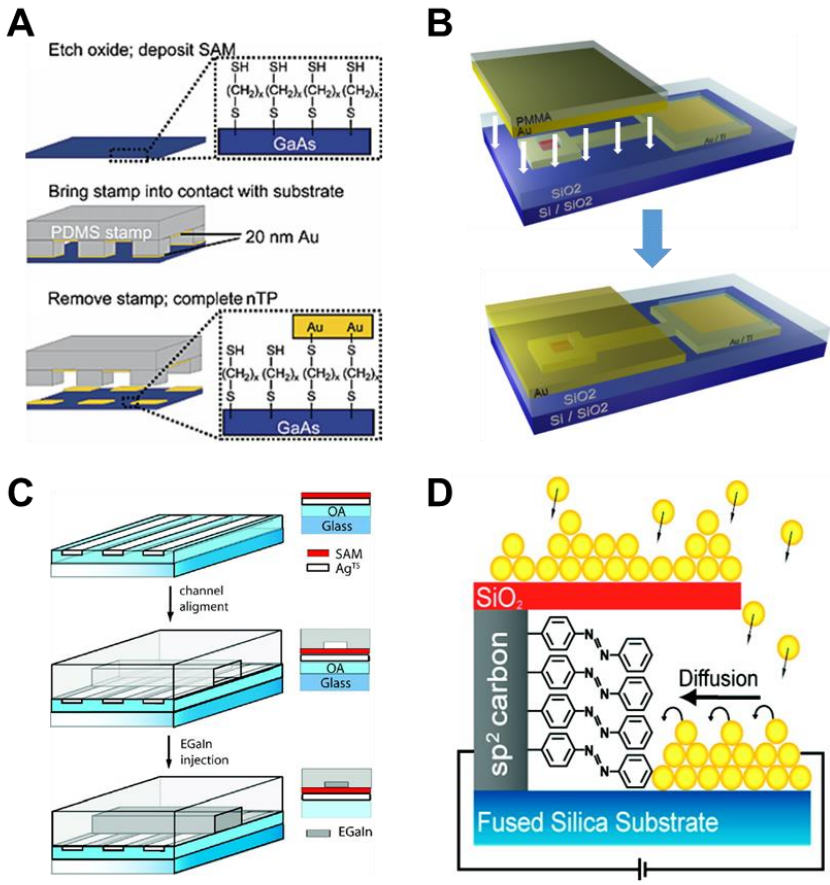

Figure 1.2.3. Approaches for high-yield solid-state based ensemble molecular junctions; Distinctive fabrication techniques. (a) Nanotransfer imprint. Reproduced from Ref. [96]. (b) Direct metal transfer. Reproduced from Ref. [97]. (c) PDMS based microfluidic channel. Reproduced from Ref. [98]. (d) Surface diffusion mediated deposition. Reproduced from Ref. [99].

pyrolysis at an extremely high temperature in forming gas is not readily amenable for use as the buffer interlayer for molecular junctions because the buffer layer is usually generated after the deposition of the molecular layer. Therefore, the high conductivity and partial transparency of thin metal films must be combined with the flatness and surface modification chemistry of PPF while also avoiding high temperature processing. Instead of PPF, eC has been described previously for conducting the carbon interlayer, resulting in a

partially transparent electrode. Figure 1.2.2(e) shows a schematic image of the molecular junctions using eC interlayer electrodes. To fabricate the molecular junctions, patterned bottom electrodes composed of Cr, Au, and eC are first vapor-deposited on the substrate using a shadow mask. The target source for the eC layer is high purity graphite, and the deposition rates are kept low, resulting in highly smooth surface morphology. Based on the electrical characterization of the fabricated Cr/Au/eC-SAMs//eC/Au junctions, a top contact of the eC interlayer yields molecular junctions with a high-yield (> 90 %), good reproducibility, a long cycle life (> 10^9 scans) and a wide temperature tolerance (6-600 K). Additionally, the resulting molecular junctions are compatible with conventional semiconductor device fabrication technology for massively parallel production with high device yield and excellent stability while avoiding the high temperatures and material transfer steps often required for graphene-based molecular junction designs.

Despite the improved device yield and several advantages of interlayer-incorporated molecular junctions using various distinctive materials as mentioned above, no possible variation of the top electrode materials may restrict the manifestation of diverse molecular functionalities due to the limited interactions between the molecular layer and top electrode. In addition, no in-depth investigations of the contact properties between the SAMs and interlayer have been conducted to provide an unambiguous understanding of the charge transport characteristics of the molecular junctions. In the following, we will briefly discuss other high-yield ensemble molecular junction fabrication techniques that can resolve the issues without the use of buffer interlayers.

Nanotransfer imprint technology where a thin metal layer is transferred from elastomeric stamps like poly(dimethylsiloxane) (PDMS) onto a designated surface [100] was first introduced by Loo et al. for fabricating large-area molecular junctions.[96] This

technique depends on the surface chemistry of the designated target surface, to which the thin metal layer on the stamp bonds chemically and releases it from the stamp.[101,102] Thus, it results in well-defined and highly reproducible nano-structures with various contact areas. As shown in Figure 1.2.3(a), the fabrication process is briefly described as follows: (i) SAMs are formed by vapor deposition on the GaAs surface, on which the native oxide layer is etched away using chemical etchants; (ii) a gold-coated elastomeric PDMS stamp with appropriate relief features is brought into contact with the substrate, and gold on the raised part of the PDMS stamp is bonded and transferred to the SAMs-coated GaAs; (iii) removal of the stamp from the substrate completes the printing process. Because the molecules chemically bind the gold patterns to the substrate, the patterns can be anchored permanently to the substrate. Since this technique involves the transfer of the thin metal electrode prepared in advance onto the designated SAMs, the resulting structures do not suffer from filamentary path formation, which results in a low device yield of the molecular junctions, as observed for the direct evaporation of metals on the SAMs.[103-106] In addition, due to chemical bonds between the transferred metal electrode and end group of the SAMs, the contact resistance usually exhibits lower values compared with the case of the physisorbed contact.[105,107,108]

Instead of using the molds, in which the removal of the stamps from the top electrode is affected by surface chemistry between the top electrode and SAMs, generation of the soft contact can be achieved without the molds but by using a sacrificial layer like a polymer, which can be washed away after junction formation as the support for the thin metal layer.[97,109,110] Thus, this technique, which is called direct metal transfer or the polymer-assisted lift-off (PALO) method, possesses several advantages of the nanotransfer imprint technique, namely, parallel device fabrication, nanoscale-to-centimeter device sizes,

high-quality metal films, and a non-damaging deposition. Figure 1.2.3(b) shows a schematic of the device fabrication procedure using this technique. The details of the method will be discussed in chapter 3 in detail.

Because the mold or sacrificial polymer layer on which the top electrode is deposited greatly influences the contact properties of the molecular junctions, establishing a reliable interface is a challenge that must be overcome to obtain reproducible molecular junctions fabricated using the above techniques. One possible solution for this issue would be the use of a liquid metal electrode, as we mentioned in chapter 1.2.1. This technique takes advantage of the metal or alloy having a low meting point that enables mechanical manipulation of the top electrode as a soft contact, so the electrode has no structural features such as edges, terraces, and pits, and it is less likely to result in defects in the absorbed SAMs. In addition, it conforms to the topography of the contacted surfaces, thus forming an intimate contact with SAMs on the surfaces. For example, the Ga_2O_3/EGaIn electrode is beneficial for the stability of the molecular junction leading to high device yield. Nevertheless, this technique requires external equipment such as a microscope, syringe, and micromanipulator for the formation of molecular junctions, which is not practical for parallel manufacturing of the functional molecular devices. Additionally, they lack the encapsulation and addressability needed to operate in a pressure- and temperature-controlled chamber.[98] To overcome this shortcoming, Nijhuis group proposed a method to create solid-state-based molecular junction arrays using the Ga_2O_3/EGaIn electrode stabilized in microfluidic channels made with an elastomeric polymer (e.g. PDMS).[58,98,111,112] A microfluidic channel is based on capillaries that typically have lateral dimensions of 10-1000 μm, and a simple two-dimensional channel systems can be used for many applications.[113] A schematic of the fabrication process for the microfluidic

channel-based molecular junction structure is shown in Figure 1.2.3(c). In this technique, a microfluidic channel in PDMS was aligned perpendicular to the Ag electrodes after the formation of the SAMs. Then, the fabrication was completed by filling the microfluidic channels with Ga_2O_3/EGaIn electrodes. The advantage of this technique is that encapsulation of the top electrodes in PDMS eliminates the instabilities associated with micromanipulators (device yield was 70-90 %) such as drift or vibrations and minimizes user-to-user variations in the details of the formation of the top electrode. Due to this stability, the obtained data shows high precision and replicability. These features enable the study of the electrical characteristics of the junctions over a long period of time and the various range of temperatures from 160-297 K. Additionally, the cone-shaped tips of EGaIn electrodes can only be prepared one at a time per setup, while the microfluidic channel technique can be performed in parallel to fabricate large numbers of junctions.[58]

Another distinctive fabrication method for a high-yield ensemble molecular junction would be the surface diffusion mediated deposition (SDMD) technique.[99,114] This technique involves remote diffusion-mediated deposition of the metal electrode onto the molecular layer, which leads to a horizontally aligned junction architecture. Due to the indirect deposition of one metal electrode, one can resolve the low device yield problem resulting from metal atom penetration or damage in the molecular layer when a metal electrode evaporation step is included in the fabrication process. The molecular junction structure based on the SDMD technique is illustrated schematically in Figure 1.2.3(d). In this technique, angled deposition of the metal electrode on the molecular layer was optimized to create a soft contact by a metal atom diffusion process. The remote diffusion of metal atoms instead of direct evaporation reduces the risk of penetration and damage in the molecular layer, which leads to excellent device yield (> 90 %) and reproducibility of

the molecular junctions. In addition, the conductance steps were readily observable because the electrical contact was controlled through surface diffusion of the metal atom on individual molecules one at a time, which allows characterization of a wide range of molecular junctions containing single/several molecules to bundle molecules. However, it is somewhat challenging to control the exact number of molecules in the junction because this technology depends on a remote diffusion process, the detailed physics of which are unknown. Additionally, possible choices of the molecule species may be limited because of the PPF bottom electrode surface. Nevertheless, the resulting molecular junctions are compatible with conventional semiconductor device fabrication technology for parallel production with high device yield and excellent reproducibility.

1.2.3. Statistical Analysis of High-Yield Molecular Junctions

Among various merits of fabricating high-yield molecular junctions using a solid-state device structure, one of the most remarkable advantages is the capability of mass production because the fabrication can be performed following conventional manufacturing processes. Mass production provides a statistically sufficient number of molecular devices for analysis, which enables us to distinguish the genuine transport characteristics of molecular junctions from uncertain electrical information.[11,23,58,62,111,115] Due to its ultimate scale of molecules, the electrical characteristics in molecular junctions should be rigorously identified not to involve any artificial defect in the data which is easy to be incorporated in the electrical characterization. Such a statistical investigation is especially beneficial to typical methods for electrical characterization of molecular electronic devices, for example, length/temperature variation, transition voltage spectroscopy (TVS), and inelastic electron tunneling spectroscopy

(IETS).[110,116]

1.3. Brief Introduction of Theoretical Background

1.3.1. Fundamental Charge Transport Mechanism in Ensemble Molecular Junctions

Conduction mechanism	Characteristic formula	Temperature dependence	Bias dependence	Length dependence
Direct tunneling	$J \approx \left(\frac{e^2 V\sqrt{2m^*\Phi_B}}{h^2 d}\right)\exp\left(-\frac{4\pi d\sqrt{2m^*\Phi_B}}{h}\right)$	None	J ~ V (low bias)	ln(J) ~ d
Fowler-Nordheim tunneling	$J \approx \left(\frac{2\pi e^3 V^2}{h d^2 \Phi_B}\right)\exp\left(-\frac{8\pi d\sqrt{2m^*}\Phi_B^{3/2}}{3heV}\right)$	None	$\ln(J/V^2) \sim 1/V$ (high bias)	ln(J) ~ d
Hopping conduction	$J \sim \frac{V}{d}\exp\left(-\frac{E_a}{k_B T}\right)$	ln(J) ~ 1/T	J ~ V	J ~ 1/d
Thermionic conduction	$J = AT^2\exp\left(-\frac{e\Phi_{TE} - e\sqrt{\frac{qV}{4\pi\varepsilon_0\varepsilon_r d}}}{kT}\right)$	$\ln(J/T^2) \sim 1/T$	ln(J) ~ √V	ln(J) ~ 1/√d

Table 1.3.1. A summary of conduction mechanisms in M-M-M junctions.

In SAMs based M-M-M junction system, intermolecular interactions such as van der Waals interaction between molecular backbone result in an induced molecular dipole or conformational changes which affect the conduction path through the molecular backbone. Therefore, this may complicate the investigation of charge transport mechanism from single molecule junction analysis.[117] It is usually adopted that the conduction mechanism can be categorized into two distinctive parts depending on whether there is thermal activation or not: (i) thermionic or hopping conduction which has temperature dependency in current-voltage characteristics and (ii) tunneling transport which does not have temperature dependency in current-voltage characteristics.[10,118]

When short molecules are in contact with electrodes having no molecular energy states in the bias window (low bias regime), this situation can be described as a simple

rectangular barrier system. This case, so called coherent tunneling (or direct tunneling), can be interpreted based on the probability to find an electron tunnel through the barrier with the barrier height (Φ_B) and width (d). A quantitative determination of the tunneling current density in this system is given by the Simmons model (see Table 1.3.1). On the other hands, in the high bias regime ($eV > \Phi_B$), i.e. molecular energy states are available in the accessible bias window, the barrier starts to be thinning into a triangular barrier which results in electric field-induced enhancement of tunneling rate of electron. This is so called Fowler-Nordheim tunneling that refers to an enhanced tunneling rate due to molecular orbital-mediated tunneling. Related to this behavior, one can estimate relative barrier height by investigating transition voltage of the tunneling transport from direct tunneling to Fowler-Nordheim tunneling that we will discuss in the following chapter. Both mechanisms show that the current density is exponentially dependent on the barrier width, while they are independent on temperature (see Table 1.3.1).

In contrast to temperature independent tunneling mechanisms, hopping conduction and thermionic conduction involves temperature dependent behaviors in charge transport characteristics. The hopping mechanism is usually defect- or trap-mediated, and thermally activated electrons hop from individual isolated state to another following a classical Arrhenius relation. Therefore, hopping mechanism involves sequential transfers of electrons between different sites, and shows a distance dependence of ~ 1/d. But in case of hopping conduction, there is no barrier-lowering effect as in thermionic emission. Another transport mechanism that is temperature dependent is thermionic emission. Thermionic emission is a process in which carriers overcome the metal-molecule barrier by thermal agitation, and therefore, the current has a strong dependence on temperature. Note that the barrier height is influenced by the magnitude of local electric field which results in image-

charge effect and a nonlinear exponential dependence of the current density on the applied voltage. This thermionic emission can be described using the Schottky-Richardson relation. Finally a summary of these conduction mechanism is given in Table 1.3.1.

1.3.2. Transition Voltage Spectroscopy

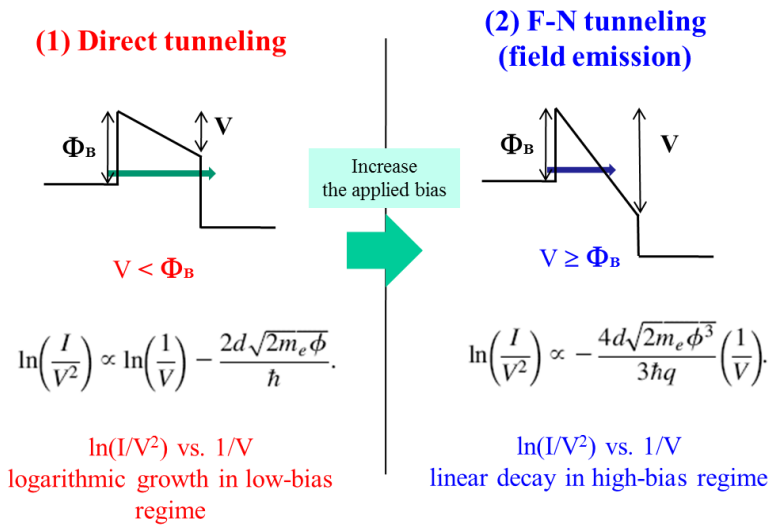

Figure 1.3.1. A schematic illustration of the TVS analysis**.**

TVS represents appealing spectroscopic tool for molecular electronic. The main concept of TVS starts with analyzing the tunneling transport with a conventional energy band model. In the tunneling transport, charge transport is governed by direct tunneling when the applied bias between the electrodes is less than the barrier height ($V < \Phi_B/e$), and the barrier shape appears as a trapezoidal shape. However, when the applied bias exceeds the barrier height ($V > \Phi_B/e$), the electron conduction is changed into the field emission (or Fowler-Nordheim) tunneling, and the barrier shape appears as a triangular shape.[44] The important point is that the transition of the charge transport from direct tunneling to field emission tunneling accompanies an inflection in a Fowler-Nordheim plot ($\ln(I/V^2)$ versus

(1/V)). This inflection point is called the transition voltage (V_{trans}) and by finding this value, one can estimate relative barrier height of molecular junctions. Therefore, the TVS can provide useful information about the location of the frontier molecular orbital with respect to the Fermi level of the electrodes. A schematic illustration of the TVS analysis is given in Figure 1.3.1. However, contrary to the initial claim, transition voltage is not related to a "transition" in a conventional sense which means V_{trans} is not identical to Φ_B; rather, the "transition" is from a linear response regime to a significant nonlinear regime which is related to the tail of molecular frontier orbital. Also, asymmetric coupling effect of metal-electrodes contact should be considered for more detailed examination.[119,120]

1.3.3. Multibarrier Tunneling Model

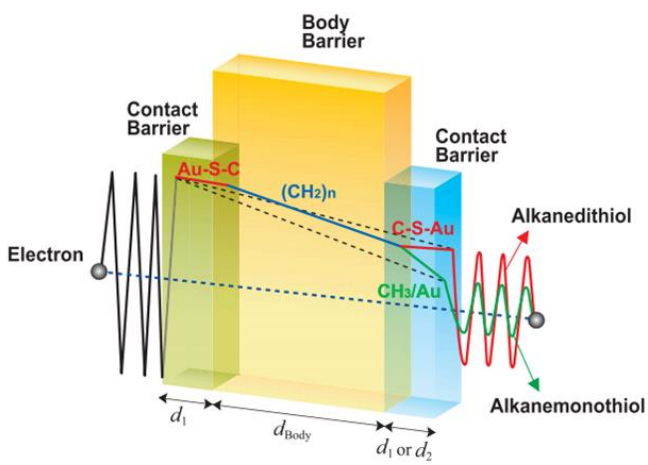

Figure 1.3.2. Schematic illustration of the MBT model.

The concept of multibarrier tunneling (MBT) phenomenon is proposed for investigating a possibility to boost the density and performance of non-volatile memory cells which is called a MBT device.[121] This model adopts sequential stacking of rectangular tunneling barriers between electrodes which enables a simple analytic

investigation of tunneling parameters without complicated approximations. The first study to apply the MBT model to molecular electronic junction is conducted by Wang et al.[11] In this study, they have generalized the Simmons tunneling model, a widely used model for describing a rectangular tunneling barrier in metal-alkanethiolate-metal junctions. The molecules were divided into three parts: a molecular-chain body and metal-molecule contacts, represented as three individual rectangular tunneling barriers, as schematically illustrated in Figure 1.3.2. Then it is possible to describe the overall tunneling parameters, for example, decay coefficient as a combination of the parameters from individual tunneling barriers. This approach of separation of the metal-molecule contact and the molecular body from alkanethiolate molecular junction is reasonable since hybridization of the metal-molecule wave function decays rapidly into the junction for alkanethiolate molecular devices.[122] Also because of the separation, the results can be applied to similar molecular junction systems which are slightly different from reference system.

1.3.4. Inelastic Electron Tunneling Spectroscopy

IETS is an experimental spectroscopy tool for characterizing vibrational modes of molecular adsorbates between metal electrodes (metal-molecule-metal junction). The advantage of IETS is that it can yields vibrational modes of the molecules with high resolution (< 0.5 meV) and high sensitivity ($< 10^{13}$ molecules, even the modes can be detected in single molecule junction).[123] Also the molecular vibration modes which are optically forbidden transitions can be detected as well.[124] Figures 1.3.3(a) and 1.3.3(b) are well-known diagrams for IETS characteristics. Figure 1.3.3(a) is an energy band diagram of a molecular tunnel junction with a vibrational mode of frequency ω localized in the junction due to the specific molecular vibration. Figure 1.3.3(b) presents schematic

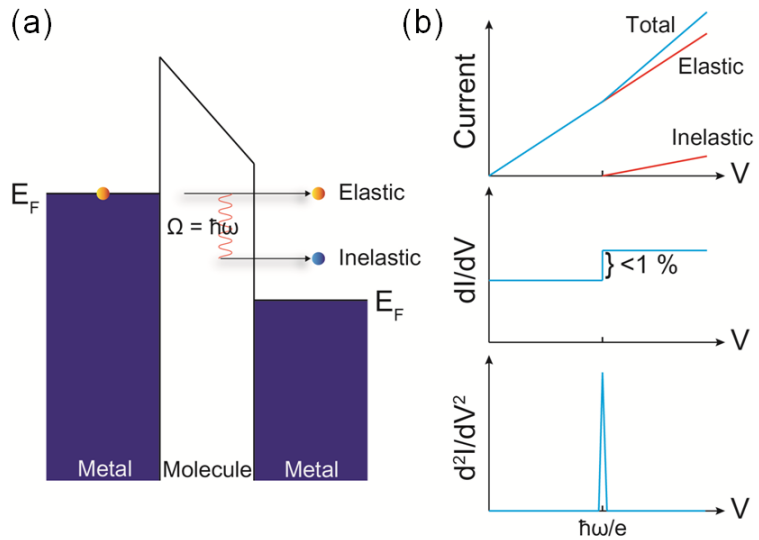

Figure 1.3.3. (a) Energy band diagram of a molecular tunnel junction with a vibrational mode of frequency ω localized inside the barrier. (b) Corresponding schematic I-V, dI/dV, d^2I/dV^2 characteristics.

current-voltage (I-V), differential conductance (dI/dV), and second derivative (d^2I/dV^2) curves, indicating the coupling feature of inelastically tunneling electrons with molecular vibration specified with frequency ω. When a negative bias voltage is applied to the left metal electrode, the Fermi level of the left electrode is lifted (Figure 1.3.3 (a)). An electron on an occupied state of the left electrode can tunnel onto an empty state of the right electrode with its energy conserved. This process is the elastic tunneling process where the current increases with the applied low bias. However, if there is a vibration mode in a chemical bonding of molecules with a characteristic phonon frequency ω, then when the applied bias is large enough to excite this vibration mode such that $eV > \hbar\omega$, the electron can lose its energy with the amount of quantum energy of ħω through the interaction with the molecular vibration mode. Then, an electron can also tunnel into an additional empty energy state of the right electrode, which opens an inelastic tunneling channel for the

electron, and the overall tunneling probability is increased. In this case, the total tunneling current increases more as a function of the applied bias over the bias of $V = \hbar\omega/e$, which becomes a step in the differential conductance (dI/dV) plot and a peak in the d^2I/dV^2 plot (Figure 1.3.3(b)).[125] Usually because the inelastic portion of the tunneling current is very small compared to elastic tunneling current (~ 0.1 %), low signal detection technology which incorporates lock-in amplifier based AC modulation method is applied under extreamly low cryogenic temperature environment (@ 4.2 K using liquid helium). When utilizing this technique, variations in the spectral feature is highly influenced by magnitude of the AC modulation voltage and the cryogenic temperature.

1.4. Functional Molecular Electronic Junctions

For the development of this emerging technology, the fundamental physics governing the basis of charge transport must be thoroughly investigated to make significant progress. For this purpose, alkanethiolates, adopted from a pioneering study by Mann and Kuhn,[126] become a standard benchmark for various experimental testbeds in molecular electronics.[7] The alkanethiolate SAMs are known to form a well-ordered, densely packed molecular layer on a metal electrode. In addition, due to a large highest occupied molecular orbital (HOMO)-lowest unoccupied molecular orbital (LUMO) gap of approximately 8-10 eV,[122] these molecules can be regarded as insulating molecules. Consequently, the main transport mechanism is coherent tunneling, in which the tunneling current decreases exponentially as molecular length increases. Therefore, they can provide a fundamental basis for understanding the underlying physics in molecular charge transport. On the other

hands, these molecules contain no special electronic functionality in their molecular structure that can be applied to practical electronic device applications. In this context, with functional molecules containing the desired functionality in the molecular structure, active research on high-yield functional molecular devices seeking potential electronic device applications has been ongoing. Although it remains a distant goal, achieving commercially available molecular electronics is the subject of accelerated, intriguing research. These kinds of examples of functional molecular electronic devices can be molecular diodes, molecular photoswitches, molecular transistors, molecular memories, flexible molecule devices, molecular plasmonic devices, etc.[127] Here, we briefly mention some of these applications focusing on a form of the high-yield ensemble molecular junction system.

1.4.1. Molecular Diodes

The diode or rectifier, which conducts a much larger current in one biased polarity (forward) than the other (reverse), is one of key components in modern integrated electronic circuits. In conventional semiconductor-based electronics, this feature can usually be implemented by joining oppositely doped (p-type and n-type) semiconductors to each other.[128] The first theoretical proposal regarding the use of a single molecule as part of a molecular rectifier was introduced by Aviram and Ratner in the 1970s.[3] In their proposal, the basic principle to facilitate the rectifying features is borrowed from the conventional semiconductor diode, in which the organic molecule contains an electron-donating moiety (donor) and an electron-withdrawing moiety (acceptor) joined by the σ bridge that electrically separates each part. Since then, tremendous experimental efforts to realize the unique features in the 2-terminal molecular junctions have been pursued.[90,129,130] Most of these studies have been conducted primarily on single molecule junctions for a deeper

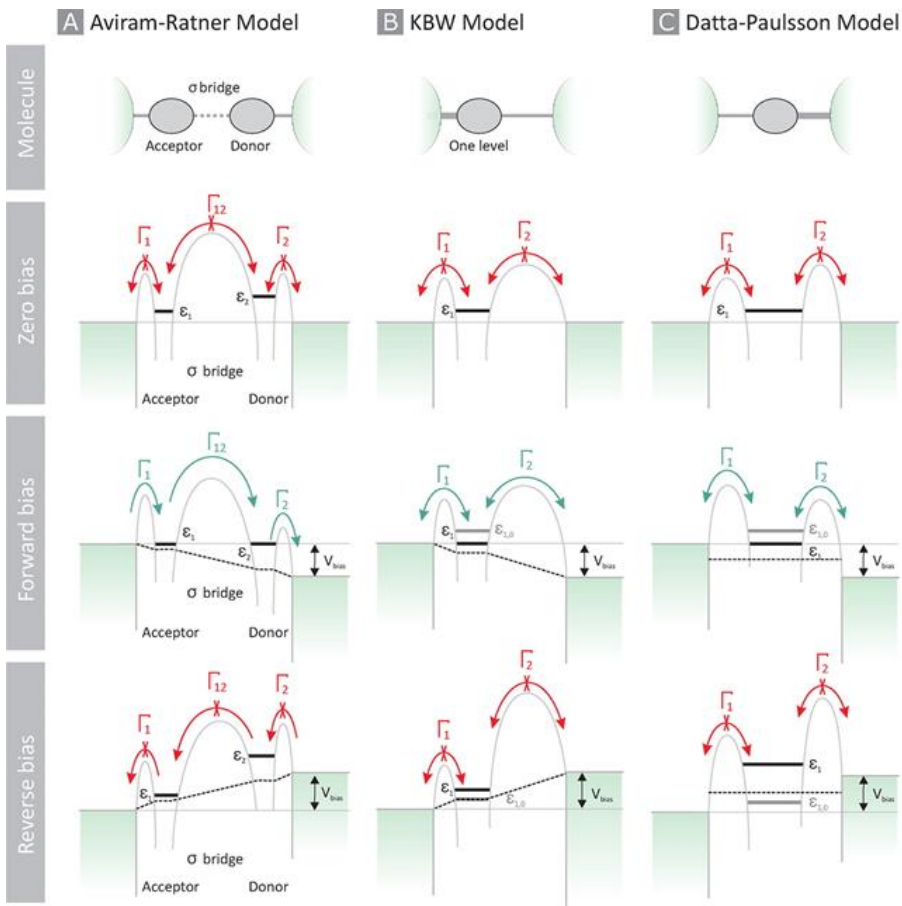

Figure 1.4.1. Comparison of models for molecular diodes. (A) Aviram-Ratner proposal with molecule levels shifting through the applied electric field. The different level spacings for donor and acceptor moieties, in combination with the large electrical spacer separating the two moieties, finally leads to a difference in the current onset. (B) Simplified model as proposed by Kornilovitch-Bratkovsky-Williams with one level. The level is shifted with respect to applied electric field. (C) Considering the charging of the energy levels (proposed by Datta and Paulsson) can also lead to diode behavior, even without level shifting by an electric field. Reproduced from Ref. [131].

understanding of the charge transport characteristics of the molecular diodes rather than for practical applications. In addition to the experimental efforts, there were further theoretical investigations of the rectification mechanism in the molecular junctions that could be classified as three mechanisms, that is, the Aviram-Ratner model,[3] Kornilovitch-

Bratkovsky-Williams model,[132] and Datta-Paulsson model [133] as show in Figure 1.4.1.[131] Those theoretical investigations usually incorporate with an asymmetric structure in a molecular backbone which eventually results in asymmetries in energetic parameters of the molecular junctions such as molecular orbital energy states and couplings. One of examples of these molecules can be ferrocene-alkanethiolate. In this sense, rational design of molecular species can even exhibit rectification ratio of ~10^5.[134]

1.4.2. Molecular Photoswitches

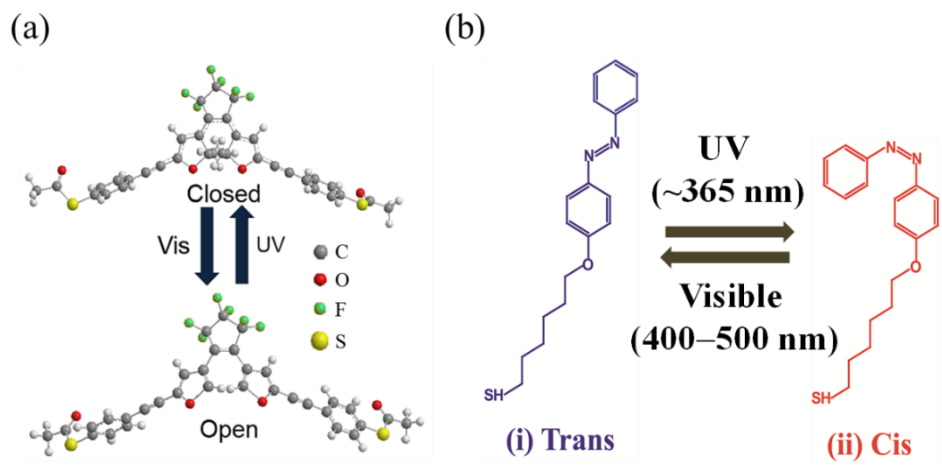

Figure 1.4.2. Examples of photoswitching molecules. (a) Diarylethene-derivative, (b) Azobenzene-derivative. Reproduced from Ref. [77,78,115].

An electronic switch device, in which the conductance is controllably tuned on and off by external stimuli (e.g., electric, magnetic field, light, or heat, among others), is a key component of modern computer circuits because the fundamental operation is based on digital processing. In recent years, a large amount of studies has been conducted to address the molecular switching phenomenon stimulated by electric field,[6,63,79] magnetic field,[135] photon,[115,136] or chemical processes.[137,138] To exploit this property, the

molecules should have at least two stable isomer states between which transition is allowed. Molecular photoswitches exhibit such a switching phenomenon by using a photochromic molecule with a moiety that reacts with a specific light and changes the isomer states which is called photoisomerization process.

Among various photochromic molecules, azobenzene- and diarylethene-derivative molecules are the most frequently studied candidates for photoswitching molecular junctions as shown in Figure 1.4.2. Azobenzene is composed of two phenyl rings linked by a N=N double bond, in which the photoisomerization of trans and cis isomers is possible when light of particular wavelengths is shed: ultraviolet light, which corresponds to the energy gap of the π-π* (S2 state) transition, for trans-to-cis conversion, and blue light, which is equivalent to that of the n-π* (S1 state) transition, for cis-to-trans isomerization.[139] Due to physical and chemical changes resulting from photoisomerization, the electronic characteristics of the azobenzene-derivatives may also change in response to light illumination. For example, Kim et al. reported the conductance switching properties of azobenzene-derivative ((4-(phenylazo)phenoxy)hexane-1-thiol) molecular junctions in terms of their molecular configurations with a high-yield vertical junction structure as solid-state device platform.[115] These azobenzene-derivative molecules have two distinct isomers: a trans- (extended form) and a cis-isomer (compact form), depending on the wavelength of irradiating light (365/400~500 nm for cis/trans), as shown in Figure 1.4.2(b). Generally, this kind of transition can be characterized by two distinct band peaks consisting of an intense band peak near 350 nm and a weak band peak between 400 and 450 nm in the UV-Vis absorption spectrum.[140] In their research, they could observe a transition of the absorption spectra and water contact angle on the Au surface from each isomer state. Another well-known class of photochromic molecules is

diarylethene-derivatives.[141,142] These molecular switches have two distinct isomers like the azobenzene-derivatives: the ring-closed form is conjugated, and the ring-open form is non-conjugated as shown in Figure 1.4.2(a). The ring-closed form of the diarylethene derivatives is achieved under irradiation in the UV region (λ = 300-350 nm), and the ring-open form is under irradiation in the visible region (λ = 500-600 nm). It is expected that both isomers show different conductance because the conjugation is changed.[136,142] This is a somewhat different type of photoisomerization process compared with the azobenzene-derivatives because the main origin of the different conductance for trans- and cis- isomers of azobenzene derivatives is usually attributed to the different tunneling distance. The implementation of molecular photoswitches processed by conventional fabrication techniques shows clear progress towards functional molecular electronic applications and circuit integration.

1.4.3. Molecular Memories

Molecular memory is a data storage device that uses molecular species as the data storage element performed by any of several mechanisms, including charge storage, photochromism, or changes in conductance.[143] In principle, the fabrication of this molecular memory junction requires the integration of molecular switches, in which the intrinsic properties of the molecular layer transform in response to external stimuli because independently stable states can encode the information as “ON” and “OFF”.[144] However, an additional feature that should be possessed by molecular memories for real implementation is that these independent states should retain their information without spontaneous degradation, especially while reading the information. To achieve this goal, the rational design of molecular species and suitable choices of junction structure and

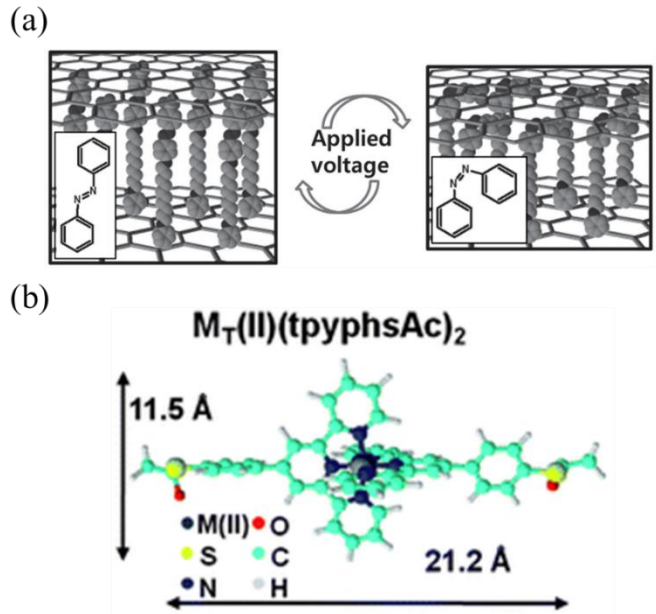

Figure 1.4.3. (a) Illustration of voltage-induced conductance switching between the two conductance states of the conformational isomers of the azobenzene (PhC10AB) molecules in a monolayer. (b) Structure of transition metal(II) bis-acetylthiophenylterpyridine (i.e., $M_T^{II}(tpyphs)_2$) complexes. Reproduced from Ref. [79,145].

materials are critical to achieve stable and high-yield ensemble molecular layer-based nonvolatile memories. Moreover, in terms of practical applications of molecular memories, the 2-dimensional array or crossbar geometry is a promising architecture for the nanoelectric circuitry for several reasons:[146,147] (i) due to the simple 2-dimensional structure, crossbars may be fabricated using a wide variety of techniques including conventional lithography,[148,148] (ii) it can exhibit excellent scaling and integration density depending on the wire configuration,[150] and (iii) the crossbar structure is defect-tolerant. Thus, the crossbar-type molecular memories may be served as a primary prototype of the molecular memory architecture. For example, nanoscale molecular random access memory composed of a [2]rotaxane monolayer with a crossbar architecture have been

reported as a prototype of molecular memory.[151] For example, Min et al. proposed the solution-processed fabrication of an azobenzene derivative (PhC10AB) molecular layer-based nonvolatile memory device on a reduced graphene oxide (rGO) electrode with the crossbar structure.[79] The molecule exhibits voltage-induced trans-cis isomerization, in which a specific bias voltage applied between two electrodes in a molecular junction can allow the transition of the isomer states by electron transmission between an electrode and molecules.[152] In the previous section, the authors showed that reversible voltage-controlled isomerization of azobenzene-derivatives is available with a change in the junction distance in rGO-PhC10AB//rGO devices that will lead to a rewritable nonvolatile memory effect. In contrast to trans-cis photoisomerization of azobenzene derivatives in monolayers or in solution, this electric field (or electron)-induced isomerization occurs in a few seconds,[152] which takes from a few to several tens of minutes in the case of photoisomerization.[153] Rather than utilizing an isomerization process in a molecule, a redox-active molecule, with reversible electron transfer behavior, in the metal complex by oxidation and reduction processes, involves an attractive feature that shows hysteric electrical characteristics, which can be used for nonvolatile memory applications.[154,155] Lee et al. reported a nonvolatile memory effect in ensemble molecular junctions using alkylthiolates with Ru^{II} terpyridine complexes. In the negatively biased region when the top electrode was biased, reproducible hysteric J-V characteristics were observed, in which charging/uncharging of the Ru^{II} complexes in the SAMs were attributed to represent the origin of the hysteresis.[156] The molecular structures of such molecules are presented in Figure 1.4.3.

1.4.4. Molecular Flexible Devices

Recently, flexible electronics, which is an emerging technology for fabricating electronic circuits on flexible plastic substrates, such as polyimide (PI), polyethylene terephthalate (PET), and polyethylene naphthalate (PEN), has attracted great attention from many research groups due to its potential applicability to wearable electronics.[157,158] Based on a rapid advance in materials for flexible circuit applications, various electronic applications have been developed, such as light-emitting diodes,[159] electronic circuits,[160,161] memory devices,[162] sensors,[163,164] displays,[165,166] solar cells,[167] and bioelectronic devices.[168] One of the most noticeable advantages of using molecular layers as an active device component for electronic devices is that ultimate scaling is feasible because the molecular layers can be considered as extremely thin organic films. This thin film property also makes the molecular layers a suitable channel material for flexible electronics applications.[169] Thus, with an adequate selection of materials and architectures for molecular junctions, high-yield flexible molecular devices may provide a clear example for practical applications of the molecular junctions.

1.4.5. Other Applications of Functional Molecular Devices

Another kind of functional molecular device could be a molecular optoelectronic device. Nijhuis group have extensively studied the potential applicability of molecular optoelectronic devices.[170] Surface plasmon polaritons (SPPs) are confined and enhanced local electromagnetic waves at infrared or visible frequencies that propagate along a metal-dielectric interface, thereby providing a new nanofabricated system for optoelectronic circuit applications.[171] To excite the surface plasmons, external light sources are usually utilized for this purpose.[172] Instead of the light-driven excitation of the surface plasmons, tunneling electrons in metal-insulator-metal junctions can also directly excite the surface

plasmons in a manner such that the tunneling electrons inelastically couple to a plasmon mode.[173] The tunneling electron-driven plasmonic source is attractive because there is no interference by background light and the response is fast. Especially in molecular electronic junctions, tunneling behavior can be carefully controlled by tuning the chemistry of the molecule, which enables adjustment of the properties of the plasmons. In addition, due to an ultimately miniaturized scale of the molecular length, the molecular electronic plasmon sources are smaller than the conventional plasmon sources. Using these properties, high-performance and ultimately miniaturized molecular plasmonic source could be realized.

The major goal of molecular electronics is to combine the different types of functional molecules into integrated circuits through an autonomous self-assembly process.[68] One of the most remarkable advantage of the massively parallel lithographic fabrication of high-yield molecular junctions is that it may allow molecular junctions to be integrated with commercially viable microelectronics.[174] The integration of individual molecular junctions, however, requires additional processes like wiring interconnects, which may be limited depending on the molecular junctions architecture or processing window.[68] Thus, reliable, stable and high-yield molecular junctions with a suitable junction architecture are accompanied for integrated molecular circuits. For example, Hal et al.[68] demonstrated the integration of large-area molecular junctions in strings where up to 200 devices are connected in series.

To the best of our knowledge, the first practical application for the commercial production of large-area molecular junctions was introduced by Bergren et al. as a discrete component in analog clipping circuit.[91] The audio clipping circuits often utilize electronic components with non-linear current-voltage characteristics (e.g., semiconductor

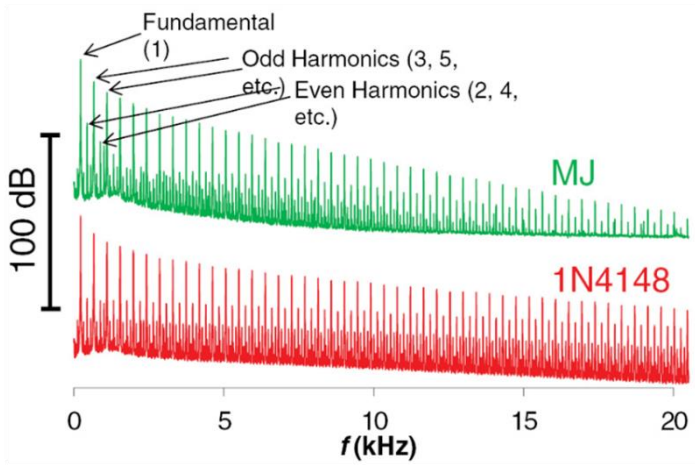

Figure 1.4.4. The power spectra for the Si and molecular junction waveforms with odd and even harmonics labeled. Reproduced from Ref. [91].

diodes) to distort the input signal waveforms. A common analog distortion circuit that utilizes voltage waveform clipping using the operational amplifier. Feedback clipping operates to distort the input signal using a feedback component with non-linear current voltage characteristics. Therefore, because the molecular junctions exhibit unique and tunable non-linear electrical characteristics, differences in the electrical performance of the molecular junctions enables the wide range of sounds in electronic music. Power spectra for the clipped waveforms are shown in Figure 1.4.4, which depict the distribution of the harmonics. The molecular junctions provided a different power response in comparison to the Si diode clippers, and they could be tuned by adjusting molecular layer thickness resulting in different non-linear current-voltage characteristics. Finally, this fascinating study presented a representative example of a real-world application of high-yield functional molecular junctions and the feasibility of manufacturing molecular junctions for use in commercial applications.

1.5. Outline of This Thesis

This thesis mainly focuses on the electrical characterization of high-yield rectifying molecular junctions using ferrocene-alkanehiolate SAMs and the development of a fabrication method for high-yield, reliable M-M-M junction in solid-state device platform. In chapter 2, I discuss (1) redox-induced abnormal temperature dependent charge transport characteristics of ferrocene-alkanethiolate molecular junctions fabricated on rigid and flexible substrates, which is closely related to redox-induced conformational change of the molecules, (2) an in-depth study of this redox-induced conformational changes of the molecules using temperature-dependent transition voltage spectroscopy analysis. In chapter 3, I discuss (1) a new approach for obtaining high-yield, vertically structured M-M-M junctions in which the top metal electrodes are formed on alkanethiolate SAMs by a direct metal transfer (DMT) method without the use of any additional protecting interlayers in the junctions, (2) measurements of the IETS characteristics of alkanethiolate SAMs based molecular junctions fabricated using DMT method, (3) analysis of the electrical transport characteristics of the molecular junctions that were statistically collected and examination of the statistical variations in the length-dependent electrical characteristics, especially the Gaussian standard deviation σ of the current density histogram. Finally, chapter 4 summaries this thesis and suggests some future directions.

References

[1] *Single-Molecule Electronics: An Introduction to Synthesis, Measurement and Theory* Kiguchi, M. Ed., Springer **2016**.

[2] *Organic Electronics: Materials, Manufacturing and Applications* Klauk, H. Ed., Wiley-VCH **2006**.

[3] Aviram, A.; Ratner, M. A. Molecular Rectifiers. *Chem. Phys. Lett.* **1974,** *29*, 277-283.

[4] Reed, M. A.; Zhou, C.; Muller, C. J.; Burgin, T. P.; Tour, J. M. *Science* **1997,** *278*, 252-254.

[5] Nitzan, A.; Ratner, M. A. *Science* **2003,** *300*, 1384-1389.

[6] Collier, C. P.; Wong, E. W.; Belohradský, M.; Raymo, F. M.; Stoddart, J. F.; Kuekes, P. J.; Williams, R. S.; Heath, J. R. *Science* **1999,** *285*, 391-394.

[7] Love, J. C.; Estroff, L. A.; Kriebel, J. K.; Nuzzo, R. G.; Whitesides, G. M. *Chem. Rev.* **2005,** *105*, 1103-1169.

[8] Metzger, R. M.; Chen, B.; Höpfner, U.; Lakshmikantham, M. V.; Vuillaume, D.; Kawai, T.; Wu, X.; Tachibana, H.; Hughes, T. V.; Sakurai, H.; Baldwin, J. W.; Hosch, C.; Cava, M. P.; Brehmer, L.; Ashwell, G. J. *J. Am. Chem. Soc.* **1997,** *119*, 10455-10466.

[9] Xiang, D.; Wang, X.; Jia, C.; Lee, T.; Guo, X. *Chem. Rev.* **2016,** *116*, 4318-4440.

[10] Wang, W. Y.; Lee, T.; Reed, M. A. *Phys. Rev. B* **2003,** *68*, 035416.

[11] Wang, G.; Kim, T. W.; Lee, H.; Lee, T. *Phys. Rev. B* **2007,** *76*, 205320.

[12] Kushmerick, J. G.; Naciri, J.; Yang, J. C.; Shashidhar, R. *Nano Lett.* **2003,** *3*, 897-900.

[13] Chabinyc, M. L.; Chen, X. X.; Holmlin, R. E.; Jacobs, H.; Skulason, H.; Frisbie, C. D.; Mujica, V.; Ratner, M. A.; Rampi, M. A.; Whitesides, G. M. *J. Am. Chem. Soc.* **2002,** *124*, 11730-11736.

[14] Fracasso, D.; Valkenier, H.; Hummelen, J. C.; Solomon, G. C.; Chiechi, R. C. *J. Am. Chem. Soc.* **2011,** *133*, 9556-9563.

[15] Zhou, C.; Deshpande, M. R.; Reed, M. A.; Jones, L.; Tour, J. M. *Appl. Phys. Lett.* **1997,** *71*, 611-613.

[16] Majumdar, N.; Gergel, N.; Routenberg, D.; Bean, J. C.; Harriott, L. R.; Li, B.; Pu,

L.; Yao, Y.; Tour, J. M. *J. Vac. Sci. Technol., B: Microelectron. Nanometer Struct.-Process., Meas., Phenom.* **2005,** *23*, 1417-1421.

[17] Wang, W. Y.; Lee, T.; Reed, M. A. *Phys. E* **2003,** *19*, 117-125.

[18] Wang, W. Y.; Lee, T.; Kretzschmar, I.; Reed, M. A. *Nano Lett.* **2004,** *4*, 643-646.

[19] Wang, W. Y.; Lee, T.; Reed, M. A. *Rep. Prog. Phys.* **2005,** *68*, 523-544.

[20] Hwang, G. J.; Jeng, P. R.; Lien, C.; Chen, C. S.; Tsao, Y. S.; Hwang, H. S.; Xu, S. Q.; Hong, T. M.; Chou, Y. C. *Appl. Phys. Lett.* **2006,** *89*, 133120.

[21] Wang, W.; Lee, T.; Kamdar, M.; Reed, M. A.; Stewart, M. P.; Hwang, J. J.; Tour, J. M. *Superlattices Microstruct.* **2003,** *33*, 217-226.

[22] Song, H.; Lee, T.; Choi, N. J.; Lee, H. *Appl. Phys. Lett.* **2007,** *91*, 253116.

[23] Kim, T. W.; Wang, G. N.; Lee, H.; Lee, T. *Nanotechnology* **2007,** *18*, 315204.

[24] Kim, T. W.; Wang, G.; Lee, T. *IEEE Trans. Nanotechnol.* **2008,** *7*, 140-144.

[25] Wang, G.; Kim, T. W.; Jang, Y. H.; Lee, T. *J. Phys. Chem. C* **2008,** *112*, 13010-13016.

[26] Haick, H.; Cahen, D. *Acc. Chem. Res.* **2008,** *41*, 359-366.

[27] Fisher, G. L.; Walker, A. V.; Hooper, A. E.; Tighe, T. B.; Bahnck, K. B.; Skriba, H. T.; Reinard, M. D.; Haynie, B. C.; Opila, R. L.; Winograd, N.; Allara, D. L. *J. Am. Chem. Soc.* **2002,** *124*, 5528-5541.

[28] Haynie, B. C.; Walker, A. V.; Tighe, T. B.; Allara, D. L.; Winograd, N. *Appl. Surf. Sci.* **2003,** *203*, 433-436.

[29] de Boer, B.; Frank, M. M.; Chabal, Y. J.; Jiang, W. R.; Garfunkel, E.; Bao, Z. *Langmuir* **2004,** *20*, 1539-1542.

[30] Walker, A. V.; Tighe, T. B.; Cabarcos, O. M.; Reinard, M. D.; Haynie, B. C.; Uppili, S.; Winograd, N.; Allara, D. L. *J. Am. Chem. Soc.* **2004,** *126*, 3954-3963.

[31] Haick, H.; Ghabboun, J.; Cahen, D. *Appl. Phys. Lett.* **2005,** *86*, 042113.

[32] Haick, H.; Niitsoo, O.; Ghabboun, J.; Cahen, D. *J. Phys. Chem. C* **2007,** *111*, 2318-2329.

[33] Chen, J.; Reed, M. A.; Rawlett, A. M.; Tour, J. M. *Science* **1999,** *286*, 1550-1552.

[34] Xu, T.; Morris, T. A.; Szulczewski, G. J.; Metzger, R. M.; Szablewski, M. *J. Mater. Chem.* **2002,** *12*, 3167-3171.

[35] Bolotin, K. I.; Kuemmeth, F.; Pasupathy, A. N.; Ralph, D. C. *Appl. Phys. Lett.* **2004,**

84, 3154-3156.

[36] Amlani, I.; Rawlett, A. M.; Nagahara, L. A.; Tsui, R. K. *Appl. Phys. Lett.* **2002,** *80*, 2761-2763.

[37] Chu, C. W.; Na, J. S.; Parsons, G. N. *J. Am. Chem. Soc.* **2007,** *129*, 2287-2296.

[38] Long, D. P.; Patterson, C. H.; Moore, M. H.; Seferos, D. S.; Bazan, G. C.; Kushmerick, J. G. *Appl. Phys. Lett.* **2005,** *86*.

[39] Long, D. P.; Lazorcik, J. L.; Mantooth, B. A.; Moore, M. H.; Ratner, M. A.; Troisi, A.; Yao, Y.; Ciszek, J. W.; Tour, J. M.; Shashidhar, R. *Nat. Mater.* **2006,** *5*, 901-908.

[40] Kushmerick, J. G.; Allara, D. L.; Mallouk, T. E.; Mayer, T. S. *MRS Bull.* **2004,** *29*, 396-402.

[41] Kushmerick, J. G.; Holt, D. B.; Pollack, S. K.; Ratner, M. A.; Yang, J. C.; Schull, T. L.; Naciri, J.; Moore, M. H.; Shashidhar, R. *J. Am. Chem. Soc.* **2002,** *124*, 10654-10655.

[42] Kushmerick, J. G.; Holt, D. B.; Yang, J. C.; Naciri, J.; Moore, M. H.; Shashidhar, R. *Phys. Rev. Lett.* **2002,** *89*, 086802.

[43] Kushmerick, J. G.; Whitaker, C. M.; Pollack, S. K.; Schull, T. L.; Shashidhar, R. *Nanotechnology* **2004,** *15*, S489-S493.

[44] Beebe, J. M.; Kim, B.; Gadzuk, J. W.; Frisbie, C. D.; Kushmerick, J. G. *Phys. Rev. Lett.* **2006,** *97*, 026801.

[45] Race, H. H.; Reynolds, S. I. *J. Am. Chem. Soc.* **1939,** *61*, 1425-1432.

[46] Rampi, M. A.; Whitesides, G. M. *Chem. Phys.* **2002,** *281*, 373-391.

[47] Weiss, E. A.; Chiechi, R. C.; Kaufman, G. K.; Kriebel, J. K.; Li, Z. F.; Duati, M.; Rampi, M. A.; Whitesides, G. M. *J. Am. Chem. Soc.* **2007,** *129*, 4336-4349.

[48] Chiechi, R. C.; Weiss, E. A.; Dickey, M. D.; Whitesides, G. M. *Angew. Chem., Int. Ed.* **2008,** *47*, 142-144.

[49] Ghosh, S.; Halimun, H.; Mahapatro, A. K.; Choi, J.; Lodha, S.; Janes, D. *Appl. Phys. Lett.* **2005,** *87*, 233509.

[50] Sordan, R.; Balasubramanian, K.; Burghard, M.; Kern, K. *Appl. Phys. Lett.* **2005,** *87*, 013106.

[51] Trouwborst, M. L.; van der Molen, S. J.; van Wees, B. J. *J. Appl. Phys.* **2006,** *99*, 114316.

[52] Heersche, H. B.; Lientschnig, G.; O'Neill, K.; van der Zant, H. S. J. *Appl. Phys. Lett.* **2007,** *91*, 072107.

[53] Dickey, M. D.; Chiechi, R. C.; Larsen, R. J.; Weiss, E. A.; Weitz, D. A.; Whitesides, G. M. *Adv. Funct. Mater.* **2008,** *18*, 1097-1104.

[54] Thuo, M. M.; Reus, W. F.; Nijhuis, C. A.; Barber, J. R.; Kim, C.; Schulz, M. D.; Whitesides, G. M. *J. Am. Chem. Soc.* **2011,** *133*, 2962-2975.

[55] Cademartiri, L.; Thuo, M. M.; Nijhuis, C. A.; Reus, W. F.; Tricard, S.; Barber, J. R.; Sodhi, R. N. S.; Brodersen, P.; Kim, C.; Chiechi, R. C.; Whitesides, G. M. *J. Phys. Chem. C* **2012,** *116*, 10848-10860.

[56] Reus, W. F.; Thuo, M. M.; Shapiro, N. D.; Nijhuis, C. A.; Whitesides, G. M. *ACS Nano* **2012,** *6*, 4806-4822.

[57] Krapchetov, D. A.; Ma, H.; Jen, A. K. Y.; Fischer, D. A.; Loo, Y. L. *Langmuir* **2005,** *21*, 5887-5893.

[58] Wan, A.; Jiang, L.; Sangeeth, C. S. S.; Nijhuis, C. A. *Adv. Funct. Mater.* **2014,** *24*, 4442-4456.

[59] Mbindyo, J. K. N.; Mallouk, T. E.; Mattzela, J. B.; Kratochvilova, I.; Razavi, B.; Jackson, T. N.; Mayer, T. S. *J. Am. Chem. Soc.* **2002,** *124*, 4020-4026.

[60] Akkerman, H. B.; Blom, P. W. M.; de Leeuw, D. M.; de Boer, B. *Nature (London, U. K.)* **2006,** *441*, 69-72.

[61] Neuhausen, A. B.; Hosseini, A.; Sulpizio, J. A.; Chidsey, C. E. D.; Goldhaber-Gordon, D. *ACS Nano* **2012,** *6*, 9920-9931.

[62] Wang, G.; Kim, Y.; Choe, M.; Kim, T. W.; Lee, T. *Adv. Mater.* **2011,** *23*, 755-760.

[63] Seo, S.; Min, M.; Lee, J.; Lee, T.; Choi, S. Y.; Lee, H. *Angew. Chem., Int. Ed.* **2012,** *51*, 108-112.

[64] Najarian, A. M.; Szeto, B.; Tefashe, U. M.; McCreery, R. L. *ACS Nano* **2016,** *10*, 8918-8928.

[65] Akkerman, H. B.; de Boer, B. *J. Phys.: Condens. Matter* **2008,** *20*, 013001.

[66] Akkerman, H. B.; Naber, R. C. G.; Jongbloed, B.; van Hal, P. A.; Blom, P. W. M.; de Leeuw, D. M.; de Boer, B. *Proc. Natl. Acad. Sci. U. S. A.* **2007,** *104*, 11161-11166.

[67] Akkerman, H. B.; Kronemeijer, A. J.; van Hal, P. A.; de Leeuw, D. M.; Blom, P. W.

M.; de Boer, B. *Small* **2008,** *4*, 100-104.

[68] Van Hal, P. A.; Smits, E. C. P.; Geuns, T. C. T.; Akkerman, H. B.; De Brito, B. C.; Perissinotto, S.; Lanzani, G.; Kronemeijer, A. J.; Geskin, V.; Cornil, J.; Blom, P. W. M.; De Boer, B.; De Leeuw, D. M. *Nat. Nanotechnol.* **2008,** *3*, 749-754.

[69] Wang, G.; Yoo, H.; Na, S. I.; Kim, T. W.; Cho, B.; Kim, D. Y.; Lee, T. *Thin Solid Films* **2009,** *518*, 824-828.

[70] Pandolfo, A. G.; Hollenkamp, A. F. *J. Power Sources* **2006,** *157*, 11-27.

[71] Frackowiak, E. *Phys. Chem. Chem. Phys.* **2007,** *9*, 1774-1785.

[72] Zhang, L. L.; Zhao, X. S. *Chem. Soc. Rev.* **2009,** *38*, 2520-2531.

[73] Geim, A. K.; Novoselov, K. S. *Nat. Mater.* **2007,** *6*, 183-191.

[74] Castro Neto, A. H.; Guinea, F.; Peres, N. M. R.; Novoselov, K. S.; Geim, A. K. *Rev. Mod. Phys.* **2009,** *81*, 109-162.

[75] Huang, X.; Yin, Z. Y.; Wu, S. X.; Qi, X. Y.; He, Q. Y.; Zhang, Q. C.; Yan, Q. Y.; Boey, F.; Zhang, H. *Small* **2011,** *7*, 1876-1902.

[76] Georgakilas, V.; Otyepka, M.; Bourlinos, A. B.; Chandra, V.; Kim, N.; Kemp, K. C.; Hobza, P.; Zboril, R.; Kim, K. S. *Chem. Rev.* **2012,** *112*, 6156-6214.

[77] Kim, D.; Jeong, H.; Lee, H.; Hwang, W. T.; Wolf, J.; Scheer, E.; Huhn, T.; Jeong, H.; Lee, T. *Adv. Mater.* **2014,** *26*, 3968-3973.

[78] Kim, D.; Jeong, H.; Hwang, W. T.; Jang, Y.; Sysoiev, D.; Scheer, E.; Huhn, T.; Min, M.; Lee, H.; Lee, T. *Adv. Funct. Mater.* **2015,** *25*, 5918-5923.

[79] Min, M.; Seo, S.; Lee, S. M.; Lee, H. *Adv. Mater.* **2013,** *25*, 7045-7050.

[80] Park, S.; An, J. H.; Jung, I. W.; Piner, R. D.; An, S. J.; Li, X. S.; Velamakanni, A.; Ruoff, R. S. *Nano Lett.* **2009,** *9*, 1593-1597.

[81] Zhu, Y. W.; Murali, S.; Cai, W. W.; Li, X. S.; Suk, J. W.; Potts, J. R.; Ruoff, R. S. *Adv. Mater.* **2010,** *22*, 3906-3924.

[82] Skakalova, V.; Kaiser, A. B.; Dettlaff-Weglikowska, U.; Hrncarikova, K.; Roth, S. *J. Phys. Chem. B* **2005,** *109*, 7174-7181.

[83] Li, D.; Muller, M. B.; Gilje, S.; Kaner, R. B.; Wallace, G. G. *Nat. Nanotechnol.* **2008,** *3*, 101-105.

[84] Mattevi, C.; Eda, G.; Agnoli, S.; Miller, S.; Mkhoyan, K. A.; Celik, O.; Mastrogiovanni, D.; Granozzi, G.; Garfunkel, E.; Chhowalla, M. *Adv. Funct. Mater.*

2009, *19*, 2577-2583.

[85] Eda, G.; Chhowalla, M. *Adv. Mater.* **2010,** *22*, 2392-2415.

[86] Eda, G.; Chhowalla, M. *Nano Lett.* **2009,** *9*, 814-818.

[87] Moon, I. K.; Lee, J.; Ruoff, R. S.; Lee, H. *Nat. Commun.* **2010,** *1*, 73.

[88] Yan, H. J.; Bergren, A. J.; McCreery, R. L. *J. Am. Chem. Soc.* **2011,** *133*, 19168-19177.

[89] Sayed, S. Y.; Bayat, A.; Kondratenko, M.; Leroux, Y.; Hapiot, P.; McCreery, R. L. *J. Am. Chem. Soc.* **2013,** *135*, 12972-12975.

[90] Bayat, A.; Lacroix, J. C.; McCreery, R. L. *J. Am. Chem. Soc.* **2016,** *138*, 12287-12296.

[91] Bergren, A. J.; Zeer-Wanklyn, L.; Semple, M.; Pekas, N.; Szeto, B.; McCreery, R. L. *J. Phys.: Condens. Matter* **2016,** *28*, 094011.

[92] Ivashenko, O.; Bergren, A. J.; McCreery, R. L. *Adv. Electron. Mater.* **2016,** *2*, 1600351.

[93] Ivashenko, O.; Bergren, A. J.; McCreery, R. L. *J. Am. Chem. Soc.* **2016,** *138*, 722-725.

[94] Ranganathan, S.; McCreery, R. L.; Majji, S. M.; Madou, M. *J. Electrochem. Soc.* **2000,** *147*, 277-282.

[95] Ranganathan, S.; McCreery, R. L. *Anal. Chem.* **2001,** *73*, 893-900.

[96] Loo, Y. L.; Lang, D. V.; Rogers, J. A.; Hsu, J. W. P. *Nano Lett.* **2003,** *3*, 913-917.

[97] Jeong, H.; Kim, D.; Kim, P.; Cho, M. R.; Hwang, W. T.; Jang, Y.; Cho, K.; Min, M.; Xiang, D.; Park, Y. D.; Jeong, H.; Lee, T. *Nanotechnology* **2015,** *26*, 025601.

[98] Nijhuis, C. A.; Reus, W. F.; Barber, J. R.; Dickey, M. D.; Whitesides, G. M. *Nano Lett.* **2010,** *10*, 3611-3619.

[99] Bonifas, A. P.; McCreery, R. L. *Nano Lett.* **2011,** *11*, 4725-4729.

[100] Loo, Y. L.; Willett, R. L.; Baldwin, K. W.; Rogers, J. A. *Appl. Phys. Lett.* **2002,** *81*, 562-564.

[101] Xia, Y. N.; Whitesides, G. M. *Angew. Chem., Int. Ed.* **1998,** *37*, 550-575.

[102] Gates, B. D.; Xu, Q. B.; Stewart, M.; Ryan, D.; Willson, C. G.; Whitesides, G. M. *Chem. Rev.* **2005,** *105*, 1171-1196.

[103] Cui, X. D.; Primak, A.; Zarate, X.; Tomfohr, J.; Sankey, O. F.; Moore, A. L.; Moore,

T. A.; Gust, D.; Harris, G.; Lindsay, S. M. *Science* **2001,** *294*, 571-574.

[104] Losic, D.; Shapter, J. G.; Gooding, J. J. *Langmuir* **2001,** *17*, 3307-3316.

[105] Xu, B. Q.; Tao, N. J. *Science* **2003,** *301*, 1221-1223.

[106] Hallback, A. S.; Oncel, N.; Huskens, J.; Zandvliet, H. J. W.; Poelsema, B. *Nano Lett.* **2004,** *4*, 2393-2395.

[107] Kaun, C. C.; Guo, H. *Nano Lett.* **2003,** *3*, 1521-1525.

[108] Seminario, J. M.; Yan, L. M. *Int. J. Quantum Chem.* **2005,** *102*, 711-723.

[109] Shimizu, K. T.; Fabbri, J. D.; Jelincic, J. J.; Melosh, N. A. *Adv. Mater.* **2006,** *18*, 1499-1504.

[110] Jeong, H.; Hwang, W. T.; Kim, P.; Kim, D.; Jang, Y.; Min, M.; Xiang, D.; Song, H.; Park, Y. D.; Jeong, H.; Lee, T. *Appl. Phys. Lett.* **2015,** *106*, 063110.

[111] Nijhuis, C. A.; Reus, W. F.; Barber, J. R.; Whitesides, G. M. *J. Phys. Chem. C* **2012,** *116*, 14139-14150.

[112] Wan, A.; Sangeeth, C. S. S.; Wang, L. J.; Yuan, L.; Jiang, L.; Nijhuis, C. A. *Nanoscale* **2015,** *7*, 19547-19556.

[113] McDonald, J. C.; Whitesides, G. M. *Acc. Chem. Res.* **2002,** *35*, 491-499.

[114] Bonifas, A. P.; McCreery, R. L. *Nat. Nanotechnol.* **2010,** *5*, 612-617.

[115] Kim, Y.; Wang, G.; Choe, M.; Kim, J.; Lee, S.; Park, S.; Kim, D. Y.; Lee, B. H.; Lee, T. *Org. Electron.* **2011,** *12*, 2144-2150.

[116] Jeong, H.; Jang, Y.; Kim, D.; Hwang, W. T.; Kim, J. W.; Lee, T. *J. Phys. Chem. C* **2016,** *120*, 3564-3572.

[117] Karthäuser, S. *J. Phys.: Condens. Matter* **2010**, *23*, 013001.

[118] McCreery, R. L. *Chem. Mater.* **2004,** *16*, 4477-4496.

[119] Wang, G.; Kim, Y.; Na, S. I.; Kahng, Y. H.; Ku, J.; Park, S.; Jang, Y. H.; Kim, D. Y.; Lee, T. *J. Phys. Chem. C* **2011,** *115*, 17979-17985.

[120] Jang, Y.; Kwon, S. J.; Shin, J.; Jeong, H.; Hwang, W. T.; Kim, J. W.; Koo, J.; Ko, T. Y.; Ryu, S.; Wang, G.; Lee, T. W.; Lee, T. W.; Lee, T. *ACS Appl. Mater. Interfaces* **2017**, *9*, 42043-42049.

[121] Gehring, A.; Grasser, T.; Cheong, B. -H.; Selberherr, S. *Solid State Electron.* **2002**, *46*, 1545-1551.

[122] Salomon, A.; Cahen, D.; Lindsay, S.; Tomfohr, J.; Engelkes, V. B.; Frisbie, C. D.

Adv. Mater. **2003,** *15*, 1881-1890.

[123] Langan, J.; Hansma, P. *Surf. Sci.* **1975**, *52*, 211.

[124] *Inelastic Electron Tunneling Spectroscopy, Handbook of Vibrational Spectroscopy* Hipps, K. W.; Mazur, U. Ed., Wiley-VCH **2001**.

[125] Lambe, J.; Jaklevic, R. C. *Phys. Rev.* **1968**, *165*, 821.

[126] Mann, B.; Kuhn, H. *J. Appl. Phys.* **1971,** *42*, 4398-4405.

[127] Jeong, H.; Kim, D.; Xiang, D.; Lee, T. *ACS Nano* **2017**, *11*, 6511-6548.

[128] *Physics of Semiconductor Devices* Sze S. M.; Ng K. K. Ed., John Wiley & Sons, Inc **2007**.

[129] Nijhuis, C. A.; Reus, W. F.; Whitesides, G. M. *J. Am. Chem. Soc.* **2010,** *132*, 18386-18401.

[130] Capozzi, B.; Xia, J.; Adak, O.; Dell, E. J.; Liu, Z. F.; Taylor, J. C.; Neaton, J. B.; Campos, L. M.; Venkataraman, L. *Nat. Nanotechnol.* **2015**, *10*, 522-527.

[131] Lörtscher, E.; Gotsmann, B.; Lee, Y.; Yu, L.; Rettner, C.; Riel, H. *ACS Nano* **2012,** *6*, 4931-4939.

[132] Kornilovitch, P. E.; Bratkovsky, A. M.; Williams, R. S. *Phys. Rev. B* **2002,** *66*, 165436.

[133] Zahid, F.; Ghosh, A. W.; Paulsson, M.; Polizzi, E.; Datta, S. *Phys. Rev. B* **2004,** *70*, 1-5.

[134] Chen, X.; Roemer, M.; Yuan, L.; Du, W.; Thompson, D.; Del Barco, E.; Nijhuis, C. A. *Nat. Nanotechnol.* **2017**, *12*, 797-803.

[135] Sanvito, S. *Chem. Soc. Rev.* **2011,** *40*, 3336-3355.

[136] Kronemeijer, A. J.; Akkerman, H. B.; Kudernac, T.; Van Wees, B. J.; Feringa, B. L.; Blom, P. W. M.; De Boer, B. *Adv. Mater.* **2008,** *20*, 1467-1473.

[137] Darwish, N.; Díez-Pérez, I.; Da Silva, P.; Tao, N.; Gooding, J. J.; Paddon-Row, M. N. *Angew. Chem., Int. Ed.* **2012,** *51*, 3203-3206.

[138] Kay, N. J.; Higgins, S. J.; Jeppesen, J. O.; Leary, E.; Lycoops, J.; Ulstrup, J.; Nichols, R. J. *J. Am. Chem. Soc.* **2012,** *134*, 16817-16826.

[139] Henzl, J.; Mehlhorn M.; Gawronski, H.; Rieder, K.; Morgenstern, K. *Angew. Chem., Int. Ed.* **2006**, *45*, 603-606.

[140] Saremi, F.; Tieke, B. *Adv. Mater.* **1998,** *10*, 388-391.

[141] Kim, Y.; Hellmuth, T. J.; Sysoiev, D.; Pauly, F.; Pietsch, T.; Wolf, J.; Erbe, A.; Huhn, T.; Groth, U.; Steiner, U. E.; Scheer, E. *Nano Lett.* **2012,** *12*, 3736-3742.

[142] Dulić, D.; Van Der Molen, S. J.; Kudernac, T.; Jonkman, H. T.; De Jong, J. J. D.; Bowden, T. N.; Van Esch, J.; Feringa, B. L.; Van Wees, B. J. *Phys. Rev. Lett.* **2003,** *91*, 207402.

[143] *Molecular Memory and Processing Devices in Solution and on Surfaces. In Molecular Machines and Motors* Shipway, A. N.; Katz, E.; Willner, I. Ed., Springer **2001**.

[144] Green, J. E.; Wook Choi, J.; Boukai, A.; Bunimovich, Y.; Johnston-Halperin, E.; Deionno, E.; Luo, Y.; Sheriff, B. A.; Xu, K.; Shik Shin, Y.; Tseng, H. R.; Stoddart, J. F.; Heath, J. R. *Nature* **2007,** *445*, 414-417.

[145] Lee, J.; Chang, H.; Kim, S.; Bang, G. S.; Lee, H. *Angew. Chem., Int. Ed.* **2009,** *48*, 8501-8504.

[146] Stan, M. R.; Franzon, P. D.; Goldstein, S. C.; Lach, J. C.; Ziegler, M. M. *Proc. IEEE* **2003,** *91*, 1940-1957.

[147] Lee, M. H.; Kim, Y. K.; Choi, Y. H. *IEEE Trans. Nanotechnol.* **2004,** *3*, 152-157.

[148] Messer, B.; Song, J. H.; Yang, P. *J. Am. Chem. Soc.* **2000,** *122*, 10232-10233.

[149] Martin, B. R.; Furnange, D. C.; Jackson, T. N.; Mallouk, T. E.; Mayer, T. S. *Adv. Funct. Mater.* **2001,** *11*, 381-386.

[150] Kuekes, P. J.; Williams, R. S. *US Patent* 6256767, **2001**.

[151] Chen, Y.; Jung, G. Y.; Ohlberg, D. A. A.; Li, X.; Stewart, D. R.; Jeppesen, J. O.; Nielsen, K. A.; Stoddart, J. F.; Williams, R. S. *Nanotechnology* **2003,** *14*, 462-468.

[152] Choi, B. Y.; Kahng, S. J.; Kim, S.; Kim, H.; Kim, H. W.; Song, Y. J.; Ihm, J.; Kuk, Y. *Phys. Rev. Lett.* **2006,** *96*, 156106.

[153] Ferri, V.; Elbing, M.; Pace, G.; Dickey, M. D.; Zharnikov, M.; Samor, P.; Mayor, M.; Rampi, M. A. *Angew. Chem., Int. Ed.* **2008,** *47*, 3407-3409.

[154] Mahapatro, A. K.; Ying, J.; Ren, T.; Janes, D. B. *Nano Lett.* **2008,** *8*, 2131-2136.

[155] Pradhan, B.; Das, S. *Chem. Mater.* **2008,** *20*, 1209-1211.

[156] Seo, K.; Konchenko, A. V.; Lee, J.; Gyeong, S. B.; Lee, H. *J. Am. Chem. Soc.* **2008,** *130*, 2553-2559.

[157] Kim, D. H.; Lu, N.; Ma, R.; Kim, Y. S.; Kim, R. H.; Wang, S.; Wu, J.; Won, S. M.;

Tao, H.; Islam, A.; Yu, K. J.; Kim, T. I.; Chowdhury, R.; Ying, M.; Xu, L.; Li, M.; Chung, H. J.; Keum, H.; McCormick, M.; Liu, P.; Zhang, Y. W.; Omenetto, F. G.; Huang, Y.; Coleman, T.; Rogers, J. A. *Science* **2011,** *333*, 838-843.

[158] Akinwande, D.; Petrone, N.; Hone, J. *Nat. Commun.* **2014,** *5*, 5678.

[159] Gustafsson, G.; Cao, Y.; Treacy, G. M.; Klavetter, F.; Colaneri, N.; Heeger, A. J. *Nature* **1992,** *357*, 477-479.

[160] Klauk, H.; Zschieschang, U.; Pflaum, J.; Halik, M. *Nature* **2007,** *445*, 745-748.

[161] Sekitani, T.; Zschieschang, U.; Klauk, H.; Someya, T. *Nat. Mater.* **2010,** *9*, 1015-1022.

[162] Kim, S. J.; Lee, J. S. *Nano Lett.* **2010,** *10*, 2884-2890.

[163] Sekitani, T.; Yokota, T.; Zschieschang, U.; Klauk, H.; Bauer, S.; Takeuchi, K.; Takamiya, M.; Sakurai, T.; Someya, T. *Science* **2009,** *326*, 1516-1519.

[164] Mannsfeld, S. C. B.; Tee, B. C. K.; Stoltenberg, R. M.; Chen, C. V. H. H.; Barman, S.; Muir, B. V. O.; Sokolov, A. N.; Reese, C.; Bao, Z. *Nat. Mater.* **2010,** *9*, 859-864.

[165] Gelinck, G. H.; Huitema, H. E. A.; Veenendaal, E. V.; Cantatore, E.; Schrijnemakers, L.; Van Der Putten, J. B. P. H.; Geuns, T. C. T.; Beenhakkers, M.; Giesbers, J. B.; Huisman, B. H.; Meijer, E. J.; Benito, E. M.; Touwslager, F. J.; Marsman, A. W.; Van Rens, B. J. E.; De Leeuw, D. M. *Nat. Mater.* **2004,** *3*, 106-110.

[166] Sekitani, T.; Nakajima, H.; Maeda, H.; Fukushima, T.; Aida, T.; Hata, K.; Someya, T. *Nat. Mater.* **2009,** *8*, 494-499.

[167] Gomez De Arco, L.; Zhang, Y.; Schlenker, C. W.; Ryu, K.; Thompson, M. E.; Zhou, C. *ACS Nano* **2010,** *4*, 2865-2873.

[168] Kim, D. H.; Viventi, J.; Amsden, J. J.; Xiao, J.; Vigeland, L.; Kim, Y. S.; Blanco, J. A.; Panilaitis, B.; Frechette, E. S.; Contreras, D.; Kaplan, D. L.; Omenetto, F. G.; Huang, Y.; Hwang, K. C.; Zakin, M. R.; Litt, B.; Rogers, J. A. *Nat. Mater.* **2010,** *9*, 511-517.

[169] Park, S.; Wang, G.; Cho, B.; Kim, Y.; Song, S.; Ji, Y.; Yoon, M. H.; Lee, T. *Nat. Nanotechnol.* **2012,** *7*, 438-442.

[170] Wang, T.; Nijhuis, C. A. *Appl. Mater. Today* **2016,** *3*, 73-86.

[171] Barnes, W. L.; Dereux, A.; Ebbesen, T. W. *Nature* **2003,** *424*, 824-830.

[172] Koller, D. M.; Hohenau, A.; Ditlbacher, H.; Galler, N.; Reil, F.; Aussenegg, F. R.;

Leitner, A.; List, E. J. W.; Krenn, J. R. *Nat. Photonics* **2008,** *2*, 684-687.

[173] Lambe, J.; McCarthy, S. L. *Phys. Rev. Lett.* **1976,** *37*, 923-925.

[174] McCreery, R. L.; Bergren, A. J. *Adv. Mater.* **2009,** *21*, 4303-4322.

Chapter 2. Functional Molecular Electronic Junctions: Rectifying Molecules (Ferrocene-Alkanethiolate)

2.1. Redox-Induced Abnormal Temperature Dependent Charge Transport Characteristics of Ferrocene-Alkanethiolate Molecular Junctions on Rigid and Flexible Substrates

In this chapter, we will discuss about the electrical characterization of ferrocene-alkanethiolate self-assembled monolayers (SAMs) on a high yield solid-state device structure. The devices were fabricated using a conductive polymer poly(3,4-ethylene-dioxythiophene) stabilized with poly(4-styrenesulphonic acid) (PEDOT:PSS) interlayer between the top electrode and the SAMs on both silicon-based rigid substrates and polyimide (PI)-based flexible substrates. We observed asymmetric electrical transport characteristics that originated from the ferrocene moieties. In particular, we found an abnormal temperature dependence of the current (i.e., a decrease in current density as temperature increases) at a high reverse bias, which is associated with the redox reaction of ferrocenium groups in the molecular junction. We further demonstrated that the molecular devices could function on flexible substrates under various mechanical stress configurations with consistent electrical characteristics which represents robust mechanical stability of the molecular devices. Our study would enhance the understanding of asymmetric charge transport characteristics in molecular junctions and may lead to the development of functional molecular electronic devices on both rigid and flexible substrates.

2.1.1. Introduction

The study of molecular electronic devices that utilize single molecules or molecular

monolayers as active electronic channels is important in understanding the electronic transport properties of molecules and developing miniaturized electronic devices for real-world applications.[1-3] Significant progress has been made towards understanding the charge transport characteristics of various molecular systems,[4-7] and molecular junctions displaying unique electrical properties have been investigated for use in a wide range of applications including diodes, switches, memory, and transistors.[8-14] However, many challenges remain in making molecular electronics a viable technology.

A primary obstacle in the development of molecular electronics is the lack of an accurate understanding of molecular reactions in the active electronic channels. For example, recently various types of molecular reactions such as change of chemical bonding, redox process, photo- or charge-induced conformal change, phase transition in molecular electronic devices have been widely investigated in order to enlarge the knowledge of intrinsic molecular properties.[12,15-21] However, these kinds of molecular reactions in molecular electronic devices are subjects still under debate due to a difficulty of precise characterizations. The absence of reliable and high-yield device platforms for testing molecular junctions that exhibit the unique and intrinsic functional properties of their component molecules is also one of the most common issues. In this context, various reliable and high-yield device platforms which utilize various types of interlayer materials such as graphene, PEDOT:PSS are proposed and investigated even under unconventional environments.[22-25] However, most of those efforts have been concentrated on insulating molecules which have no special intrinsic functionality of molecules.

Meanwhile, the diode, which conducts a much larger current in one biased polarity (forward) than the other (reverse), is one of key components in modern integrated electronic circuits. In conventional semiconductor-based electronics, this feature can usually be

implemented by joining oppositely doped (p-type and n-type) semiconductors to each other.[26] The first theoretical proposal regarding the use of a single molecule as part of a molecular diode was introduced by Aviram and Ratner in the 1970s.[1] In their proposal, the basic principle to facilitate the rectifying features is borrowed from the conventional semiconductor diode, in which the organic molecule contains an electron-donating moiety (donor) and an electron-withdrawing moiety (acceptor) joined by the σ bridge that electrically separates each part. Since then, tremendous experimental efforts to realize the distinctive features in the 2-terminal molecular junctions have been pursued.[27-29] Most of these studies have been conducted primarily on single molecule junctions for a deeper understanding of the charge transport characteristics of the molecular diodes rather than for practical applications. Therefore, in this context, it is valuable to develop high-yield functional molecular diode focusing on their practical applicability.

Here, we reported the electrical characteristics of molecular junctions composed of ferrocene-alkanethiolate functional molecules as a high-yield solid-state device structure. The devices were fabricated using the conductive polymer PEDOT:PSS as a conducting interlayer electrode.[12,22,23] Interestingly, we observed an abnormal temperature dependence of the junction current density; that is, the current decreased with increasing temperature at temperatures with a threshold bias voltage upon an applied bias polarity. This is in contrast to the typical behavior for thermally activated charge transport, in which current increases with increasing temperature. We proposed that this unique behavior can be attributed to the redox process of ferrocenium groups in the molecular junctions. In addition, we demonstrated that the molecular devices could be fabricated on flexible substrates as well, exhibiting consistent charge transport properties as rigid substrates even under severely bent conditions. This study suggests the understanding of the intrinsic

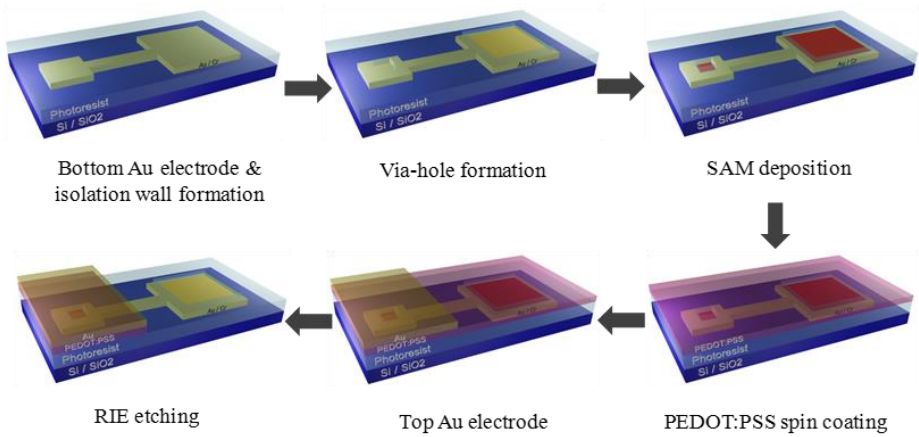

Figure 2.1.1. Device fabrication procedure.

molecular reactions is important when we apply functional molecules to molecular and organic electronic devices. Furthermore this study will lead to the further development of functional molecular electronic devices with flexible configurations.

2.1.2. Experimental

Figure 2.1.1 shows device fabrication procedure. The fabrication process consists of six steps: (1) Using conventional optical lithography and shadow mask, the bottom Au (50 nm)/Cr (10 nm) electrodes were made on rigid (Si/SiO_2) or plastic (PI) substrates. The metal layer was deposited using an e-beam evaporator at a slow deposition rate of ~0.1 Å/s to obtain a smooth electrode surface. The root mean square (RMS) roughness of the Au electrode surface was determined to be ~0.194 nm using atomic force microscopy (AFM) images with a scan size of 1 μm × 1 μm (NX-100, Park systems) as shown in Figure 2.1.2. After the formation of the bottom electrode, photoresist (Az5214E, purchased from Az Electronic Materials) was spin-coated (4000 rpm, 1 minute) on substrates to create isolation wall. (2) The via-hole for SAMs was made using optical lithography, followed by a hard-

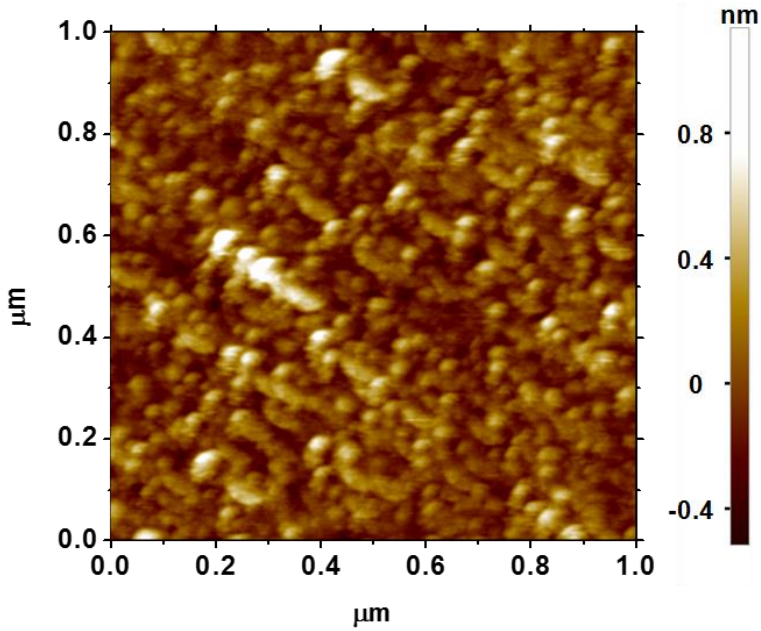

Figure 2.1.2. Topographic image of the bottom Au/Cr electrode.

bake process of the photoresist in order to avoid the isolation wall from being soluble in molecular solution at 190 °C for 2 h. (3) Following film formation, SAMs composed of an alkanethiolate with a terminal ferrocene moiety were allowed to assemble on the bottom electrode surface. And the SAMs were deposited on bottom Au electrodes by dipping the substrates in the molecular solution (~3 mM in anhydrous ethanol) in N_2-filled glove box for ~1 day. After deposition of SAMs, the substrates were rinsed with anhydrous ethanol to remove the physically unbound molecules and then dried by N_2 stream in N_2-filled glove box for ~2 h. (4) Conducting polymer PEDOT:PSS (PH1000, purchased from Clevios™) interlayer doped with dimethyl sulfoxide (DMSO) and surfactant (Triton-X100 purchased from Sigma-Aldrich) was spin-coated (3500 rpm, 30 seconds) on the SAMs-deposited substrates to avoid electrical short problem.[22,23,25] (5) The top Au (50 nm thick) electrodes were formed with shadow mask. (6) Finally, with reactive ion etching (RIE) process (using O_2 gas, 11 sccm, 50 W), residual PEDOT:PSS was removed to prevent the

formation of direct current pathway between top and bottom electrodes. The electrical characteristics of the devices were measured with a semiconductor parameter analyzer (Keithley 4200 SCS) and a probe station system (JANIS Model ST-500) under room/low temperature using liquid nitrogen.

2.1.3. Results and Discussion

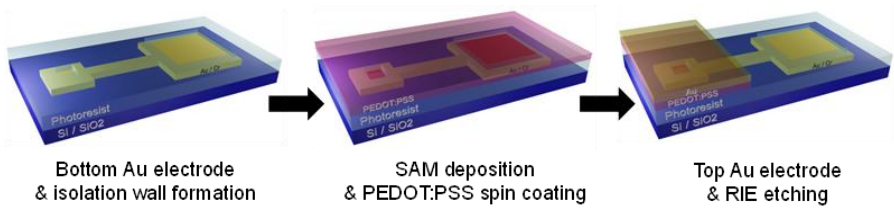

Figure 2.1.3. The molecular device fabrication processes on a rigid substrate.

Figure 2.1.3 summaries a schematic of the fabrication procedure for the molecular devices developed in this study. To be brief, first, the bottom electrode (Au (50 nm) and Cr (10 nm)) was prepared by photolithography and e-beam evaporator. Following film formation, self-assembled monolayers (SAMs) composed of three molecules ferrocene-alkanethiolate molecules (6-(ferrocenyl)hexanethiol, 8-(ferrocenyl)octanethiol, and 11-(ferrocenyl)undecanethiol which are denoted as FcC6, FcC8, and FcC11, respectively) were allowed to assemble on the film surface. The chemical structures of the molecules are shown in Figure 2.1.4. The molecules varied in length depending on the number of alkyl chains present ($(CH_2)_N$, where N = 6, 8, and 11; FcC6 and FcC11 are available from Sigma-Aldrich Co. and FcC8 is available from Dojindo Molecular Technologies, Inc.). The electrical characteristics of alkanethiolate molecular junctions have been widely studied, and tunneling has been demonstrated as the main conduction mechanism.[13,22,24,30-38] When a ferrocene moiety was attached to the head group of these alkanethiols, the overall

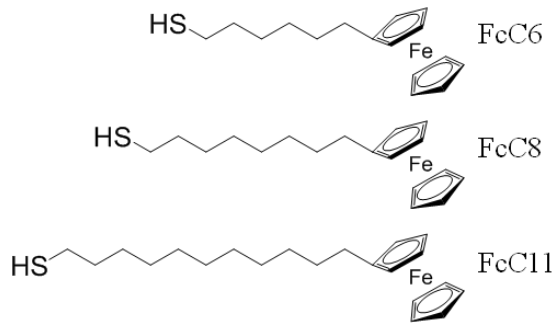

Figure 2.1.4. The chemical structures of the molecules.

molecular junctions exhibited an asymmetric electrical characteristics.[14,28,39-42] Due to its attractive property of these molecules, there have been many studies to investigate the characteristics of the molecular system, for example, (i) the even-odd effect,[41] (ii) role of a binding group and purity of the precursors, and surface topology of bottom electrodes in the performance of molecular diodes,[43,44] and (iii) enhancement of the rectification ratio by rational design of the molecule.[45] In our study, SAMs were deposited by immersing the samples for 1-2 days in a dilute ethanolic solution of the desired

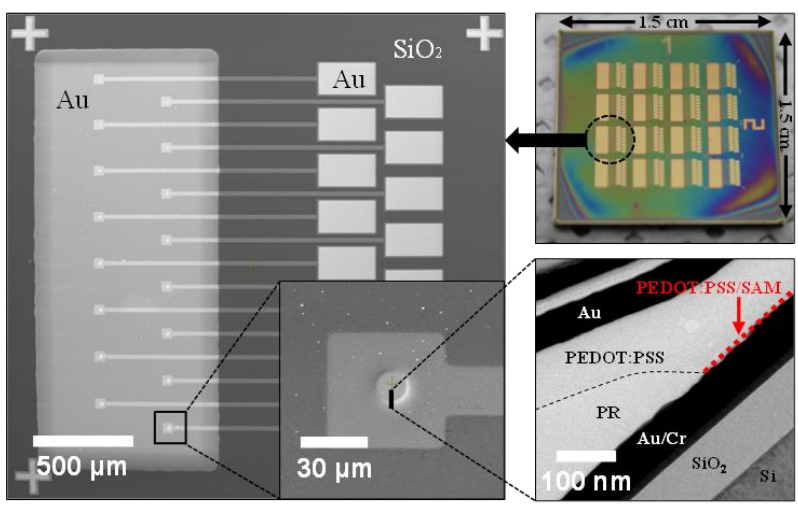

Figure 2.1.5. Optical, SEM, and cross-sectional TEM images of the molecular devices. The molecular junctions are circular with radii of 7, 8, and 9 μm.

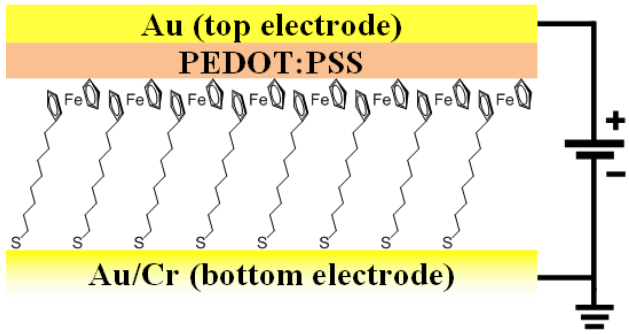

Figure 2.1.6. The schematic of the molecular device measurement configuration.

molecule in a N_2-filled glove box. The thiol moieties bond strongly to the bottom electrode (Au surface), while the ferrocene moieties make contact with the top electrode.

The previously reported vertical metal-molecule-metal junctions are prone to electrical shorting due to the penetration of the top metal through the SAMs during metal evaporation, which creates conducting paths between the bottom and top electrodes.[36,46-49] To resolve the issue, an intermediate protective layer such as a conducting polymer[22,25,50] or carbon film[24,51,52] can be introduced between the top electrode and the SAMs. In our study, we used a method reported by Akkerman et al. in which a highly conductive polymer, PEDOT:PSS doped with DMSO for enhancing electrical conductance, was used as a conducting interlayer.[22,25] This fabrication technique was used to improve the device yield,[53] and the reliability of molecular-scale electronic devices under mechanically deformed configurations was also demonstrated.[25] In this study, prior to depositing the top electrode, we spin-coated a PEDOT:PSS interlayer of 100 nm thickness, as determined using cross-sectional transmission electron microscopy (TEM) (Figure 2.1.5). Subsequently, a 50 nm Au film was deposited on the PEDOT:PSS layer (Figure 2.1.6). By using this PEDOT:PSS-interlayer fabrication method, we improved the

Molecules	# of fabricated devices	Fab. failure	Short	Open	Non-working	Working	Device yield
FcC6	96 (100.0%)	23 (24.0%)	0 (0.0%)	12 (12.5%)	12 (12.5%)	49 (51.0%)	
FcC8	96 (100.0%)	22 (22.9%)	1 (1.0%)	20 (20.8%)	8 (8.3%)	45 (46.9%)	**140 (48.6%)**
FcC11	96 (100.0%)	36 (37.5%)	0 (0.0%)	11 (11.5%)	3 (3.1%)	46 (47.9%)	

Table 2.1.1. Statistical data of device yield for the FcC6, FcC8, and FcC11 molecular devices fabricated on rigid substrates.

device yield to near ~50 %. In comparison, the device yield of simple metal-molecule-metal junctions without interlayers is typically ~1 %.[36,54] Table 2.1.1 shows the statistical data of device yield for the FcC6, FcC8, and FcC11 molecular devices fabricated on rigid substrates. Here, the total number of fabricated devices is 96 for each length of molecule (total 288 devices) on a single substrate (1.5 cm × 1.5 cm). The failed devices (e.g. unusual isolation wall formation, failure on bottom Au/Cr electrode etc.) were defined as fabrication failed devices. To define the working devices, we followed the analogy proposed in previous report.[36,55] To do this, we plotted the histogram of logarithmic current density at fixed bias (±1 V) and performed Gaussian distribution fitting on the histograms. From the fitted Gaussian distribution, we estimated the average values (m) of the logarithmic current densities and standard deviations (σ). Then, we defined the working devices as the ones which the logarithmic current densities were located in a defined range (from m-3σ to m+3σ) corresponding to ~99.7 % of the distributions. Following this criteria, the estimated device yield was found to be ~49 %. The junctions were circular, with radii of 7, 8, and 9 μm. Scanning electron microscopy (SEM), transmission electron microscopy (TEM), and optical microscopy images of the fabricated devices are shown in Figure 2.1.5.

Figure 2.1.7 shows the representative current density–voltage (J–V) behavior of the

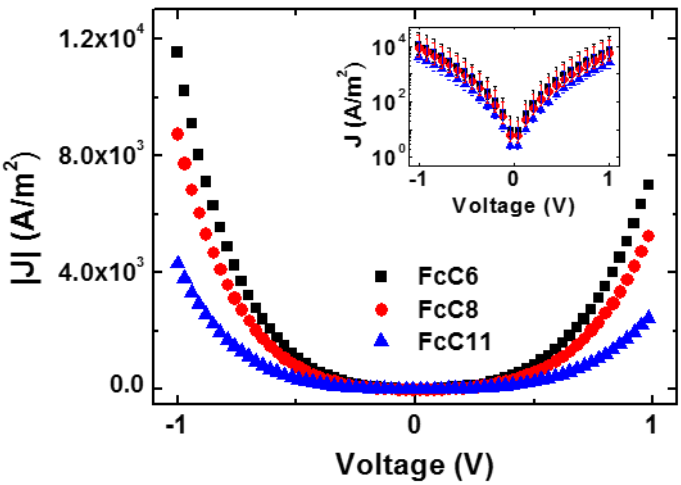

Figure 2.1.7. J-V characteristics for FcC6, FcC8 and FcC11 molecular devices. The inset shows a semi-log plot of the J-V characteristics with error bars determined from the standard deviation of all the measured devices (140 devices).

three molecules of varying length used in our study. In this plot, the current density values at negative (forward) a bias were converted to positive values for easy comparison with those at a positive bias. The inset plot displays statistical J-V data from ~50 measured devices for each molecular length. The error bars depict the standard deviation of the current density values measured from all of the working devices (~140 devices, see Table 2.1.1). Alkyl molecules with ferrocene moieties have previously exhibited asymmetric electrical properties, in which SAMs of these molecules were sandwiched between a Ag bottom electrode and a top electrode comprising eutectic Ga and In (EGaIn).[14,28,39-41] In this structure, rectification occurred because the highest occupied molecular orbital (HOMO) of the ferrocene moiety participated in charge transport under negative bias only. At a negative bias, the HOMO of ferrocene is located between the Fermi levels of the two electrodes and contributes to charge transport, whereas at a positive bias the HOMO of ferrocene is below the Fermi levels of both electrodes and therefore cannot contribute to

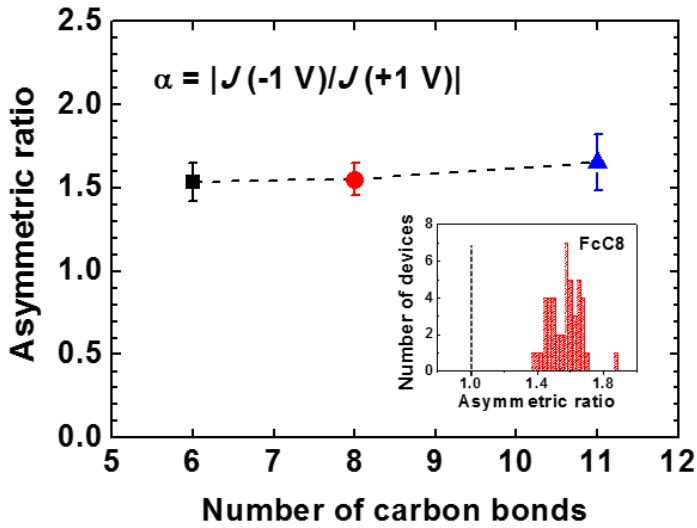

Figure 2.1.8. Asymmetric ratio for FcC6, FcC8 and FcC11 molecular devices. Inset shows the histograms of the asymmetric ratios for FcC8.

charge transport.[28,39] We observed similar asymmetric electrical characteristics in our study but with somewhat lower asymmetric ratios. The asymmetric ratio (α), which is defined as α = | J(-1 V)/J(+1 V) |, where J(+1 V) is the current density measured at +1 V, was lower (α = ~1.6) in our study. The summarized asymmetric ratios for different molecules are presented in Figure 2.1.8 with the statistical histogram of distribution in the inset. The observed low asymmetric ratio is due to the different junction structures employed, particularly for the top electrode material. The greater detail regarding the origin of this effect and conditions for improvement of the asymmetric ratio will be explained in below (Figure 2.1.9). And to ensure that the off unity asymmetric ratio is truly attributed to the ferrocene moiety, we could find from our previous reports that the estimated asymmetric ratio is clearly ~1 when the deposited molecules are lacking the ferrocene moiety but under same device configurations.[25,53] Also from our freshly characterized results, we confirmed that similar tendency was repeatedly observed (Figures 2.1.10(a) and

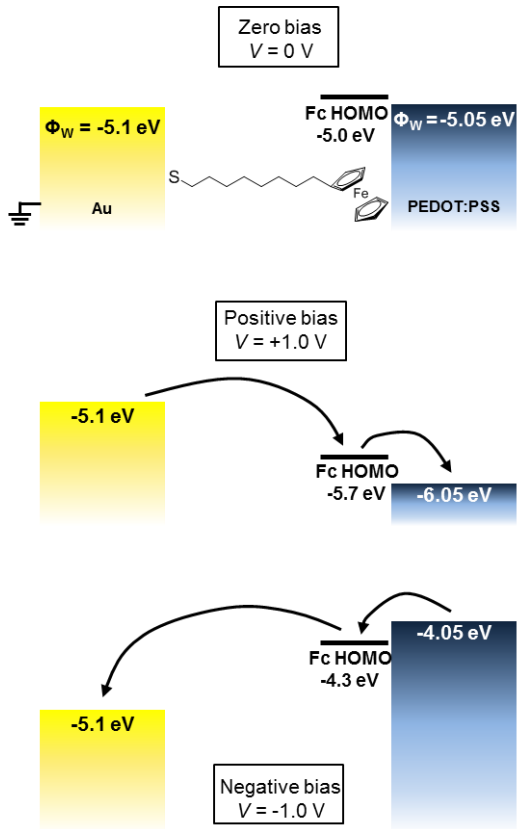

Figure 2.1.9. The proposed energy band diagram for the molecular junctions at three bias conditions (0, +1, and -1 V). Arrows depict the charge conduction through the molecular junction. The HOMO of ferrocene and the Fermi level of Au were adopted from the literature, while the Fermi level of PEDOT:PSS was measured by Kelvin Probe measurements.

2.1.10(b)). Therefore, the off unity asymmetric ratio evidently originates from the ferrocene moiety. And unlike the previous report by Nerngchamnong et al.,[41] we did not observe the odd/even effect in the asymmetric ratio using three different lengths of ferrocene-alkanethiolates (FcCn, n = 6, 8, 11). We think that the absence of the odd/even effect in this study is caused by un-flatness of the bottom electrodes and the non-uniform contact between ferrocene moieties and the PEDOT:PSS interlayer.

Figure 2.1.11(a), 2.1.11(b) and 2.1.11(c) depict the statistical histograms of the

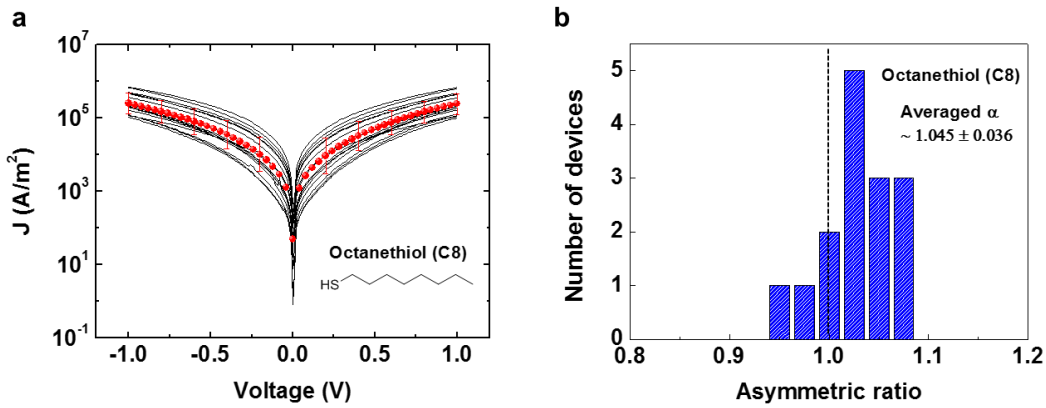

Figure 2.1.10. (a) The J-V characteristics of Au/PEDOT: PSS/C8/Au junctions. (b) Histogram of asymmetric ratios for C8 devices.

distribution of logarithmic current densities measured at ±1 V for our FcC6, FcC8 and FcC11 molecular devices. The arrows indicate representative values of each molecular devices. The logarithmic distribution of current density arises from variations in the linear distance between the top and bottom electrodes because the overall current, and the tunneling current in particular, depends exponentially on the gap distance between the two electrodes.[36,55] From this histogram, one can see that our devices exhibit asymmetric electrical characteristics, with the current at a negative bias (forward bias) statistically higher than that at a positive bias (reverse bias), which is regardless of molecular length.

To understand the origin of asymmetric electrical characteristics, Figure 2.1.9 shows the energy band diagrams of our molecular junctions. The work function of Au is ~5.1 eV. The work function of PEDOT:PSS was determined to be ~5.05 eV using a Kelvin probe measurement. The HOMO of the ferrocene moiety is ~ -5.0 eV (i.e., 5.0 V below the vacuum level).[14,28,39-41] With these values, the energy band diagram at zero bias can be depicted as shown in the top schematic in Figure 3d. The middle and bottom schematics depict the energy band diagram when +1 V and -1 V are applied to the PEDOT:PSS side,

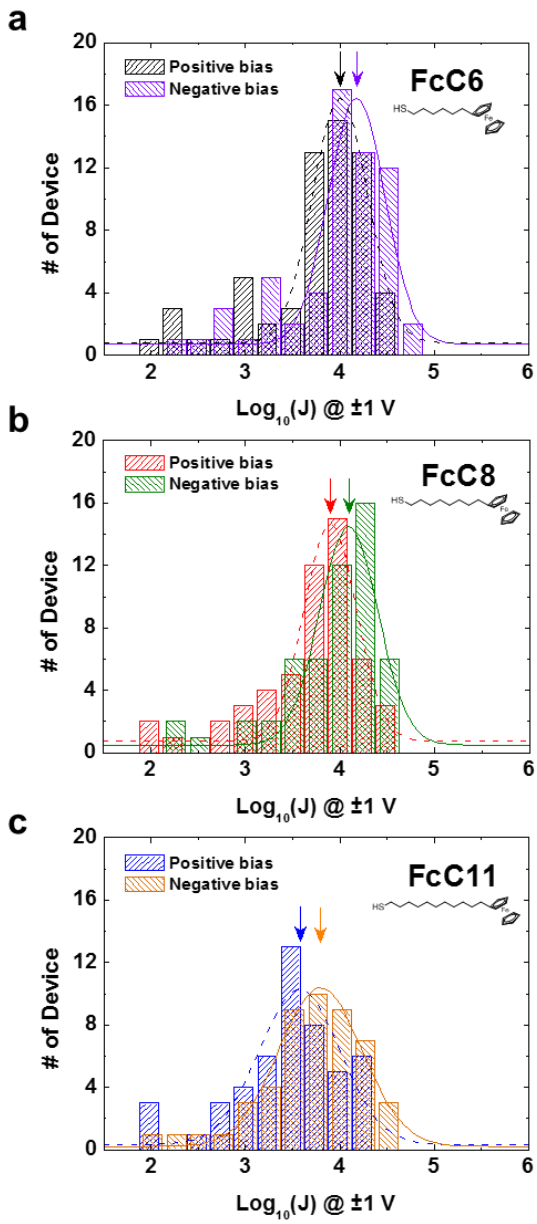

Figure 2.1.11. (a, b, c) Histograms of the logarithmic current densities measured at ±1 V for FcC6, FcC8 and FcC11 molecular devices. The arrows indicate the mean value of the logarithmic current density of the each molecular device at both bias polarities.

respectively. For these diagrams we assumed that the ferrocene moiety formed van der Waals contacts with the PEDOT:PSS, resulting in a potential drop of 0.3 V, as described in

previous reports.[14,28,39-41] Therefore, when +1 V is applied the HOMO of ferrocene decreases to -5.7 eV, whereas an applied bias of -1 V increases the HOMO to - 4.3 eV. To achieve a high asymmetric ratio, the HOMO of the ferrocene moiety should lie between the bias window between the two electrodes' Fermi levels under one bias polarity (forward bias) but lie below the bias window between the Fermi levels of both electrodes at the other bias polarity (reverse bias). These conditions enable a high asymmetric ratio because a HOMO that lies between the Fermi levels at the forward bias condition can act as a resonant energy state for charge transport.[14,28,39-42] However, in our study, the HOMO of ferrocene is located between the Fermi levels of each electrode (PEDOT:PSS and Au) at both bias polarities considering work functions of each electrode (5.05 eV for PEDOT:PSS and 5.1 eV for Au). Thus, the HOMO of the ferrocene can participate in charge transport at both bias polarity conditions, resulting in the low asymmetric ratio (~1.6) observed in our study (Figures 2.1.8).

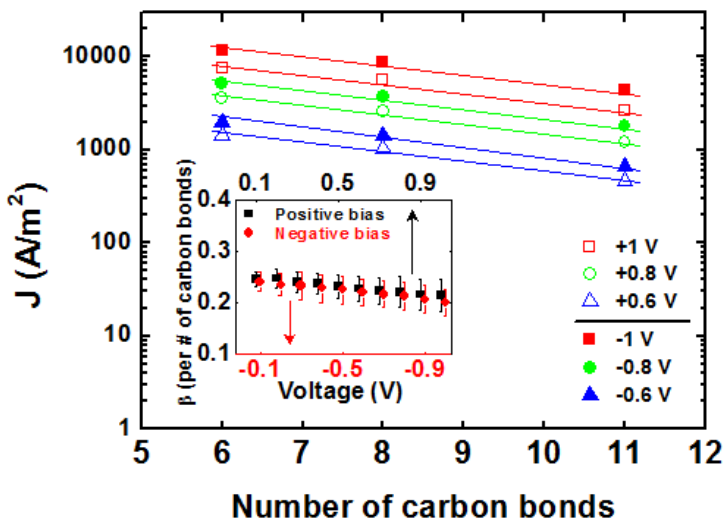

Figure 2.1.12. A semi-log plot of the current density as a function of the number of carbon bonds (i.e., the length of the alkyl chains). The lines through the data points represent the exponential fits. The inset displays the estimated decay coefficients at each bias.

As depicted in Figure 2.1.7, the current density of each molecule decreases as the number of alkyl chains increases (N = 6, 8, 11). Longer molecular lengths lead to larger effective tunneling barrier widths, which results in a decrease in the tunneling current that displays an exponential dependence described by $J \sim \exp(-\beta d)$ (Figure 2.1.12), where β is the decay coefficient and d is the gap distance. The decay coefficient β can be deduced from the slope of the linear fitting of current density along the number of carbon bonds at a fixed bias, which obeys the exponential dependence as $J \sim \exp(-\beta d)$. The determined β values are shown in the inset of Figure 2.1.12. The β values were found to range from 0.20 to 0.25 per carbon bond for both positive and negative biases. The β values observed in our study are smaller than those previously reported for alkyl molecular junctions (0.7-1.2 per carbon bond).[24,31,33,34,36,56-59] We previously reported the β values of pure alkyl molecules to be ~1.0 per carbon bond (corresponding to ~0.8 /Å), which differs from the lower values for ferrocene-alkanethiolate molecules in our current study.[36,54,60] This is probably due to the ferrocene moiety at the molecule which dominates charge transport characteristics of the molecular junction, but, further study seems to be needed.

To understand the electronic transport properties of our molecular junctions, we performed temperature-variable current-voltage (I-V-T) measurements while the temperature was varied from 80 to 300 K in increments of 20 K. Figures 2.1.13(a) and 2.1.13(b) present Arrhenius plots (ln(J) versus 1/T) of a FcC11 device at negative and positive bias, respectively (see Figure 2.1.14). The currents were nearly bias-independent at lower temperatures, indicating that tunneling is the dominant conduction mechanism at this temperature range. However, at high temperatures (> ~220 K), there is a distinction in the behavior between the two bias polarities. At a negative bias, weak thermal activation occurs at the high temperature range (Figure 2.1.13(a)). This thermal activation could be

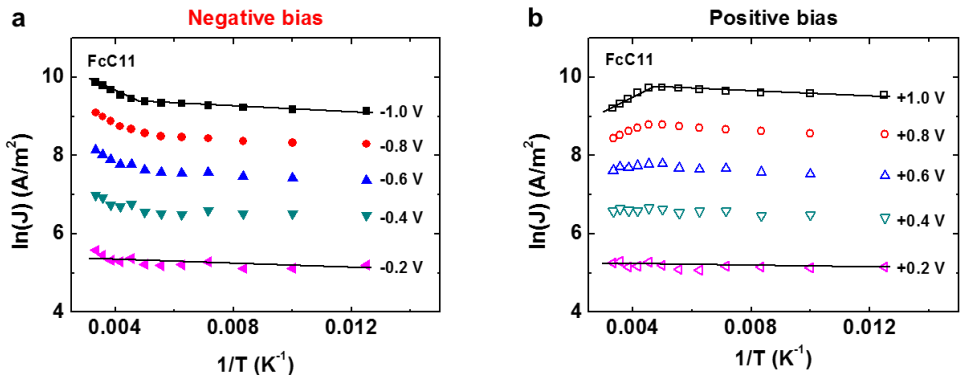

Figure 2.1.13. Arrhenius plots of ln(J) versus 1/T for an FcC11 molecular device at different (a) negative and (b) positive biases.

interpreted as weak hopping conduction (not thermionic conduction, detailed analysis is not provided here). More importantly, an interesting feature was observed at the positive bias polarity. As shown in Figure 2.1.13(b), at the low temperature range the conduction is dominated by tunneling. However, at the high temperature range (> ~220 K) and at high biases (e.g., the 0.6, 0.8, and 1.0 V conditions in Figure 2.1.13(b)), the current decreased with increasing temperature. Normally, current through a molecular junction (or other types of junctions) is either independent of temperature when a tunneling is dominating, or dependent on temperature such a way that current increases as the increasing temperature when a thermionic conduction or defect-mediate conduction mechanisms are dominating. On the contrary, we observed an opposite temperature dependent conduction characteristics in our study, which is that current decreased as the increasing temperature.

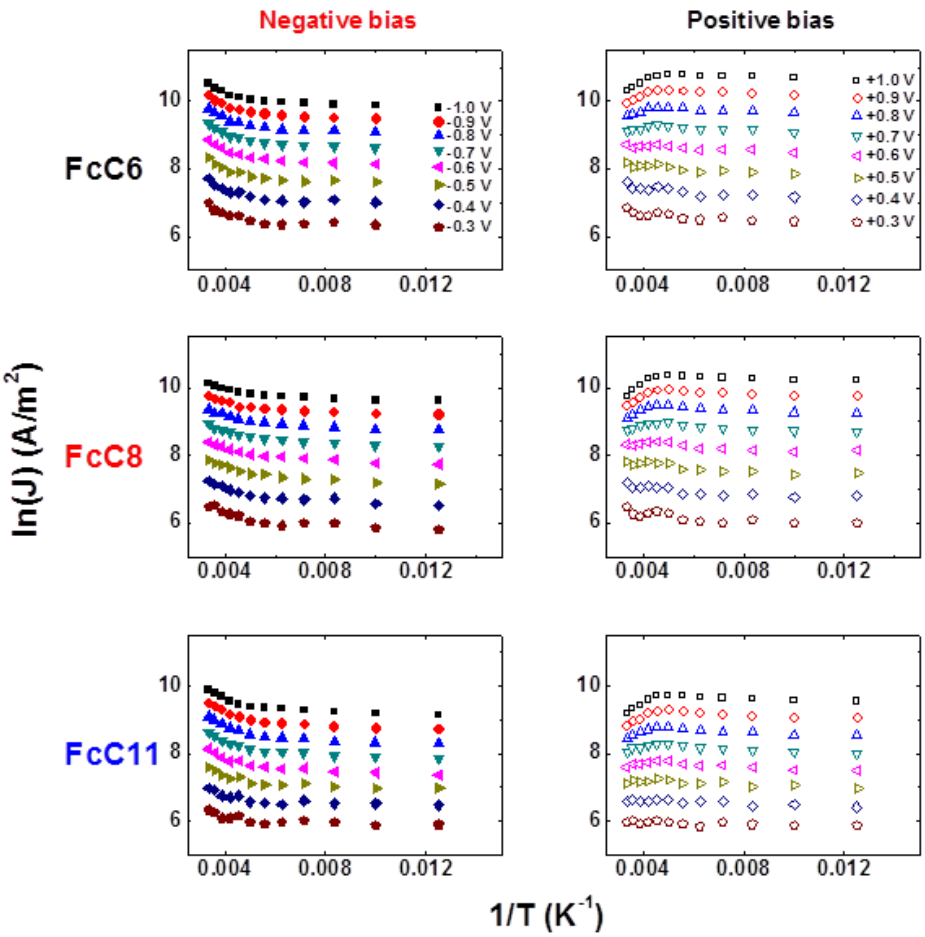

Figure 2.1.14. Arrhenius plots for FcC6, FcC8, and FcC11 molecular devices at different biases.

This unique feature, in which current decreases with increasing temperature at a positive bias, can be more clearly observed when the currents measured at +1 V are plotted together as a function of temperature, as shown in Figure 2.1.15(a). We can deduce that this feature is a molecular effect because typical metallic behavior was observed over the entire temperature range (i.e., current decreased with increasing temperature) for molecule-free Au/PEDOT:PSS/Au junctions, without the appearance of any unusual behavior at 220 K

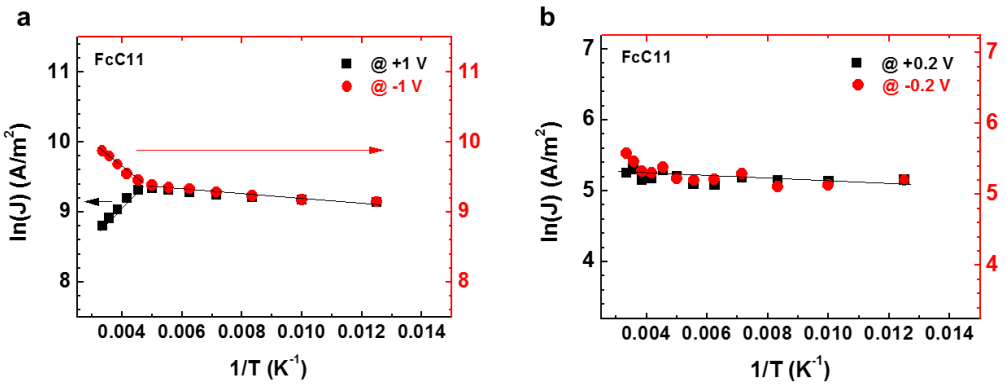

Figure 2.1.15. Arrhenius plot of the data measured at (a) ±1 V and (b) ±0.2 V from Figure 2.1.13(a) and 2.1.13(b), respectively.

(see Figure 2.1.16(b)). Also Figure 2.1.16(a) represents current J-V characteristics of a Au/PEDOT: PSS/Au junction without molecules. The current density is linear on the applied bias (i.e., Ohmic behavior), and the current density level is higher than ~10^7 A/m^2 at ±1 V, as similar to previous reports.[12,23,25,61,62] Note that this unique feature was observed only at high positive biases (higher than ~0.6 V) and did not occur at low positive biases (see Figures 2.1.14 and 2.1.15). Combining these I-V-T results, we also plotted the asymmetric ratios as a function of temperature, as shown in Figures 2.1.17. At temperatures of up to ~220 K, the asymmetric ratio was nearly constant. At higher temperatures (> ~220 K), the asymmetric ratio increased due to the different I-V-T behaviors at negative and positive biases. This unique behavior was consistently observed for many of the other devices, regardless of molecule length (see Figures 2.1.17). We also found that this behavior was seen in six different devices for each molecular length (total of 18 devices), all of which exhibited similar behaviors (See Figure A1 in Appendix A).

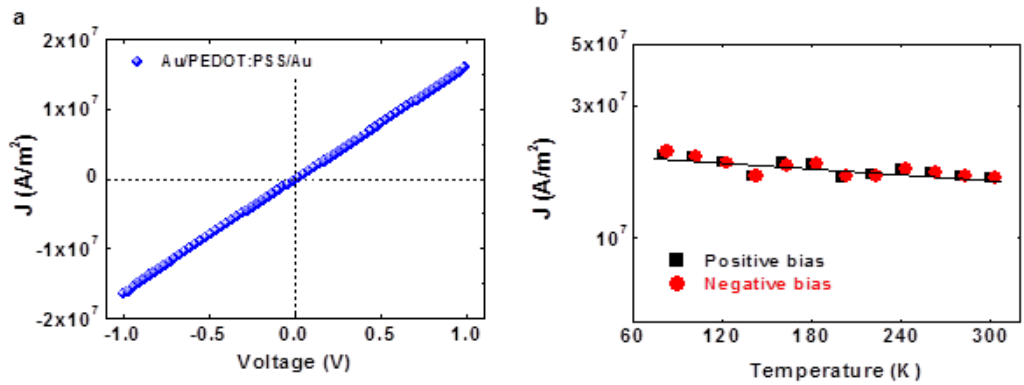

Figure 2.1.16. Electrical characteristics of Au/PEDOT:PSS/Au junction. (a) J-V characteristics of Au/PEDOT:PSS/Au junction. (b) Plot of the current densities as a function of temperature for a molecule-free Au/PEDOT:PSS/Au junction.

One possible mechanism for our observation can be the redox-induced conformational change of ferrocene-alkanethiolate.[63] It has also been reported that the environmental effects such as surface coverage can make an influence on the orientation change by theoretical and experimental studies.[64-66] From these reports (Ref. [64-66]), we can expect that the orientation change of the ferrocene-alkanethiolates can be induced by the redox process of the ferrocene moieties. Ferrocene-alkanethiolate can be reversibly oxidized under relatively small applied biases due to the presence of strongly electron-donating ferrocene terminal groups,[67] whose oxidation peaks have been observed near +0.6 V with respect to a Au electrode using cyclic voltammetry.[63,68] Even in solid state junctions, this kind of redox process is shown to be available due to the charge injection to a special molecule with relevant molecular orbitals and metal complexes which can be regarded as a parallel capacitor.[69-72] When ferrocenes are oxidized (to ferricenium cations) by applied biases higher than ~+0.6 V, the positively charged ferrocene terminal

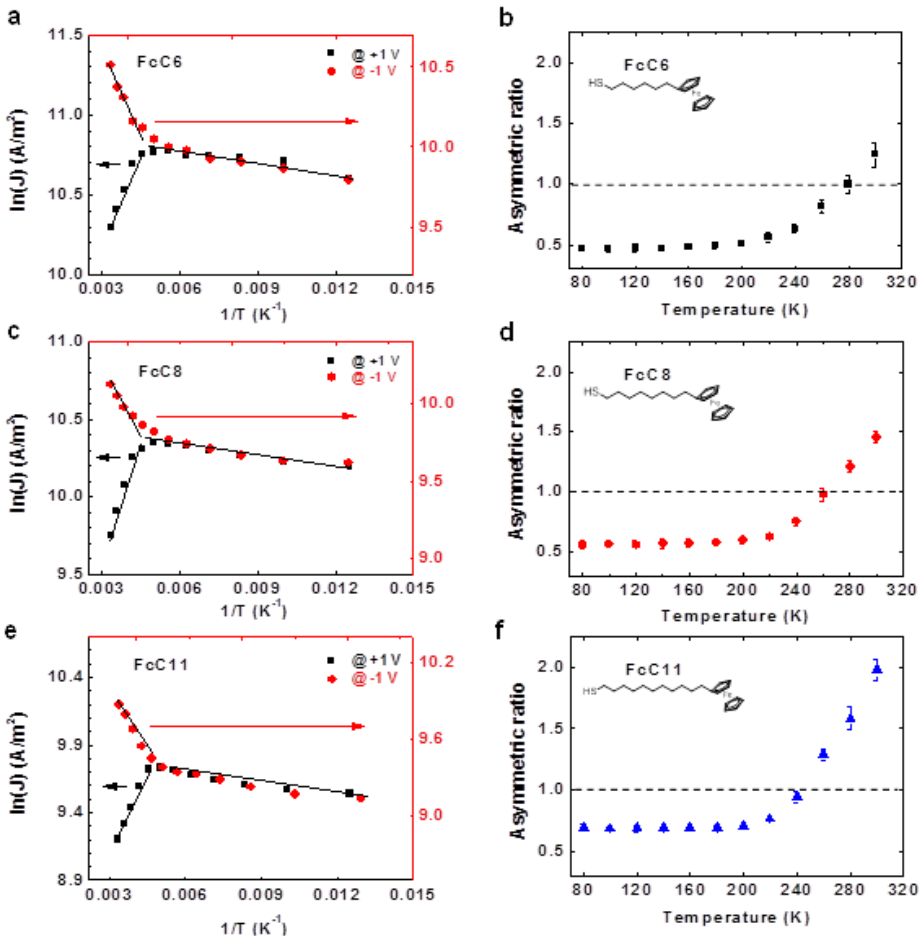

Figure 2.1.17. (a, c, e) The Arrhenius plots of the current densities at ±1 V for a FcC6, FcC8, FcC11 molecular device, respectively. The black solid lines represent the linear fittings of the curves. (b, d, f) Asymmetric ratio versus temperature for FcC6, FcC8, FcC11 molecular device, respectively.

groups in the SAMs will exert a lateral repulsive force on the neighboring molecules.[63] This repulsion can be alleviated by increasing the distance between the oxidized ferrocenes. One way to achieve this is to orient the molecules perpendicular to the electrode surface as shown in Figure 2.1.18(a),[63] leading to an increase in the distance between the two electrodes and a decrease in the current density between them. This type of SAMs rearrangement would require an energy input, and a current density dependence on

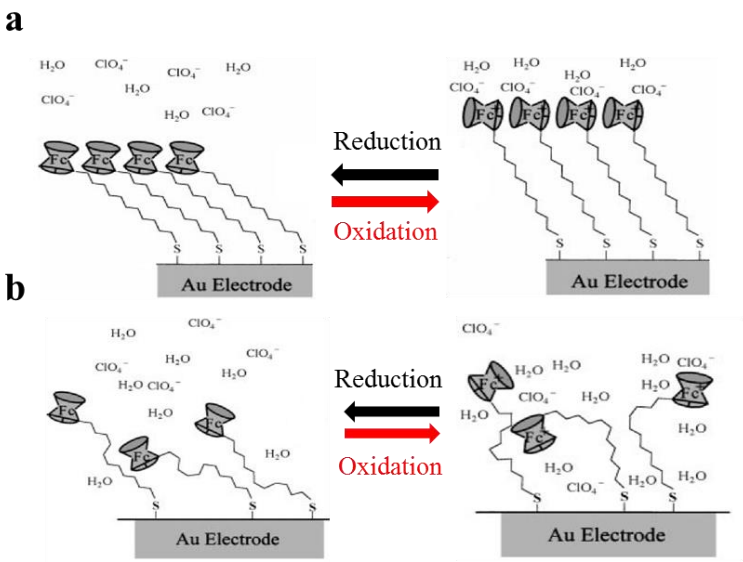

Figure 2.1.18. Proposed redox-induced conformational change of the SAMs of ferrocene-alkanethiolate molecules, (a) Raising up effect, (b) disordering effect. Reproduced from Ref. [73].

orientation would therefore appear at high temperatures (> ~220 K in this work). From our data in Figure 2.1.15 and the estimated decay coefficient (β) value from Figure 2.1.12, we estimated that the current decrease from 220 to 300 K corresponds to a change of ~2 Å in the distance between the two electrodes which is a reasonable value as the conformational change. Another possible mechanism is disordering in the SAMs as shown in Figure 2.1.18(b) due to electrostatic repulsions between the oxidized ferrocene moieties. Disordering would prevent the ferrocene moieties from making good contact with the PEDOT:PSS layer and reduce the current. Indeed, the disordering of SAMs of ferrocene-alkanethiolate has been described in a previous report.[41] In our molecular junctions, both of these mechanisms may be at work. Even so, further evidence is needed to fully understand our observation. As a control group, when the molecules had no ferrocene moieties but only the alkyl chain, there were no distinctive behaviors in the electrical

characteristics at different temperatures.[25] Therefore, the electroactive nature of the ferrocene moieties is truly the origin of the distinctive temperature dependent behaviors observed in this study. Note that the device cyclability was maintained under several measurements without losing its own characteristics. Also the temperature sweep direction (i.e. high temperature to low temperature and low temperature to high temperature) did not influence on the manifestation of the distinctive temperature dependency. We expect the reason for the stability in spite of the dynamic process is that the degree of configuration change of the monolayer is fairly small compared to the length of the molecules. Guojon et al. has reported that the molecular orientation change due to the oxidation of the ferrocene is mainly observed in the random system (i.e., ferrocene-alkanethiolates diluted with alkanethiolates) whereas it is less pronounced in the cluster system (i.e., pure ferrocene-alkanethiolates).[64] Interestingly, we also observed this unique feature in the molecular junctions on flexible substrate structures, as explained in the following. But to understand the influence of the temperature on the distinctive electrical characteristics precisely, it is expected that the more delicate study should be progressed. In this sense, to confirm the validity of the mechanisms, we performed a temperature-dependent transition voltage spectroscopy (TVS) analysis based on a multibarrier tunneling (MBT) model that will be discussed in detail following chapter. In this analysis, the two possible conformational changes of the ferrocene-alkanethiolate were confirmed as a barrier-raising effect of both the alkyl chain and ferrocene.

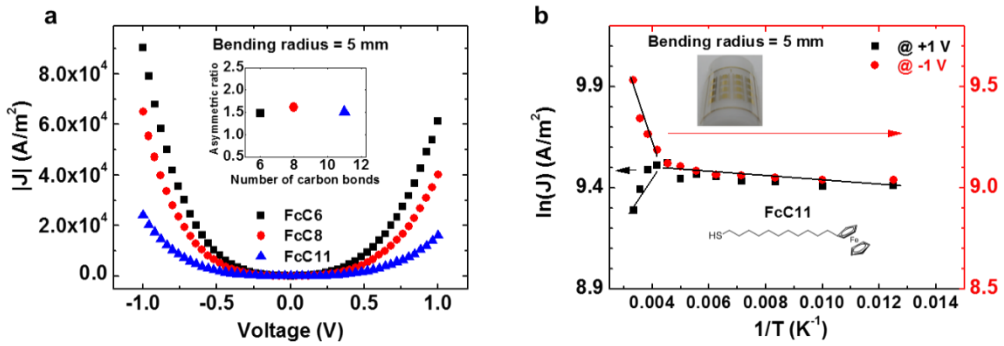

Figure 2.1.19. (a) J-V characteristics of FcC6, FcC8 and FcC11 molecular devices fabricated on flexible substrates. The data were measured under bending conditions with a bending radius of 5 mm. The inset displays the asymmetric ratios of the devices under the same bending conditions. (b) Arrhenius plot for a flexible FcC11 molecular device under bending conditions with a bending radius of 5 mm.

The ferrocene-alkanethiolate SAMs were also fabricated and characterized on a polyimide (PI) flexible substrate. The device fabrication procedure was similar to that used for the rigid device (Figure 2.1.1 and Figure 2.1.3), with the exception of the use of a PI substrate (Neopulim L-3430 purchased from Mitsubishi Gas Chemical Co., Inc.). Because the PI substrate can endure high temperature annealing process while we performed to make the PR insulating wall insoluble in the SAMs solution, we chose the PI substrate instead of other conventional plastic substrates such as a polyethylene terephthalate (PET) and polyethylene naphthalate (PEN) substrate. The junction area on the flexible devices measured 30 μm by 30 μm with a rectangular shape. Figure 2.1.19(a) presents the representative J-V characteristics of FcC6, FcC8, and FcC11 flexible molecular devices fabricated on PI substrates under flat conditions (defined as bending radius = ∞). The current densities of the flexible devices were similar to those of the rigid devices (Figure 2.1.7) within the error bar range. The asymmetric ratios (shown in the inset of Figure 2.1.19(a)) were also similar to those of the rigid devices (Figure 2.1.8). Subsequently, we

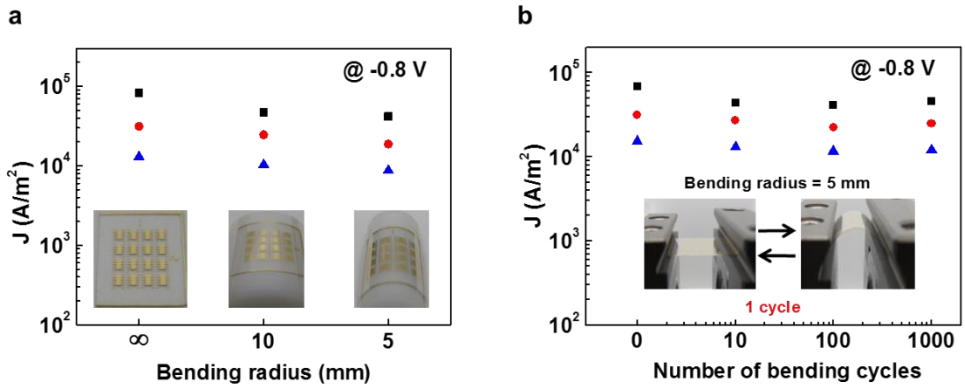

Figure 2.1.20. (a) The current density (J) values measured at −0.8 V for FcC6, FcC8, and FcC11 flexible molecular devices under various bending radius conditions (∞, 10 mm, and 5 mm). (b) The current density (J) values measured at −0.8 V for FcC6, FcC8, and FcC11 flexible molecular devices under repeated bending cycles (0, 10, 100, and 1000 times; bending radius = 5 mm).

examined the mechanical stability of these flexible molecular devices under various bending conditions. Figure 2.1.20(a) shows the current densities measured for the FcC6, FcC8, and FcC11 flexible molecular devices under different bending radius conditions (bending radius = ∞, 10 mm, and 5 mm). Figure 2.1.20(b) presents the current densities for these flexible devices after repeated bending cycles (10, 100, and 1000 times) at a bending radius of 5 mm. These results demonstrate that the electrical properties of our flexible molecular devices were well preserved under various mechanical bending conditions. The flexible devices were also tested under severe bending conditions with a bending radius of 1 mm, yet still maintained their electrical characteristics, as shown in Figure 2.1.21. We further performed I-V-T measurements for our flexible molecular devices under a bent configuration with a bending radius of 5 mm, and the results are shown in Figure 2.1.19(b). The unique feature (the decrease of current with increasing temperature at positive biases) that was observed for the rigid devices (Figure 2.1.19(a)) was also observed in the flexible devices under a bent configuration, confirming that this

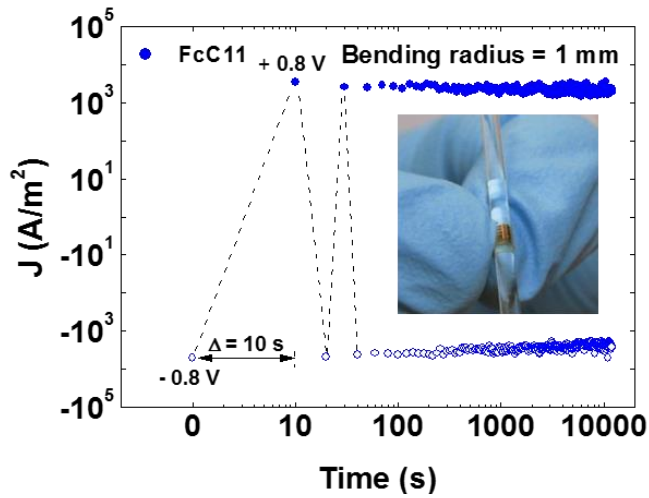

Figure 2.1.21. A retention plot showing that the measured J values at ±0.8 V for 10^4 s (time interval Δt = 10 s) of an FcC11 flexible molecular device under extreme bending conditions (a thin cylindrical glass rod with radius = 1 mm).

characteristic is reproducible in both rigid and flexible devices and under both flat and bending conditions. This results represent the distinctive electrical characteristics are intrinsic molecular properties irrelevant to external conditions such as substrate type or mechanical stress. Remarkably, our thin molecular layer devices on flexible substrates are able to maintain their molecular conductance characteristics under bending conditions due to the dominant through-bond pathways of molecular junctions.[25]

2.1.4. Chapter Summary

Conclusively in this chapter, we studied the redox-induced electronic transport properties of ferrocene-alkanethiolate molecules using a conducting polymer-interlayer device structure. We observed asymmetric electrical transport properties, which arise due to the existence of ferrocene moiety. In particular, we observed distinctive electrical characteristics that the current in the junction decreased with increasing temperature at high

temperatures (> ~220 K) and when a large positive bias (> ~0.6 V) was applied to the ferrocene end-group side. This behavior is attributed to the redox process of the ferrocene moiety in the molecular junction. We also fabricated the same molecular junctions on flexible device substrates and demonstrated consistent electrical characteristics (i.e., asymmetric current-voltage characteristics and distinctive temperature dependence) under various bending configurations. This ensures that the unique feature originated from the intrinsic molecular reactions but not from the effect of substrates or device configuration. This study suggests the importance of consideration of intrinsic molecular reactions especially redox process when one applies molecules to the robust functional molecular devices. And this work also provides a route toward the practical implementation of functional molecular devices with unconventional flexible configurations.

References

[1] Aviram, A.; Ratner, M. A. *Chem. Phys. Lett.* **1974,** *29*, 277.

[2] Aviram, A.; Ratner, M. A. *Science* **2003,** *300*, 1384.

[3] *Molecular Electronics: An Introduction to Theory and Experiment* Cuevas, J. C.; Scheer, E. Ed., World Scientific Publishing Co. Pte. Ltd. **2010**.

[4] Reed, M. A.; Zhou, C.; Muller, C. J.; Burgin, T. P.; Tour, J. M. *Science* **1997,** *278*, 252.

[5] Venkataraman, L.; Klare, J. E.; Nuckolls, C.; Hybertsen, M. S.; Steigerwald, M. L. *Nature* **2006,** *442*, 904.

[6] Galperin, M.; Ratner, M. A.; Nitzan, A.; Troisi, A. *Science* **2008,** *319*, 1056.

[7] Lafferentz, L.; Ample, F.; Yu, H.; Hecht, S.; Joachim, C.; Grill, L. *Science* **2009,** *323*, 1193.

[8] Chen, J.; Reed, M. A.; Rawlett, A. M.; Tour, J. M. *Science* **1999,** *286*, 1550.

[9] Liang, W. J.; Shores, M. P.; Bockrath, M.; Long, J. R.; Park, H. *Nature* **2002,** *417*, 725.

[10] Park, J.; Pasupathy, A. N.; Goldsmith, J. I.; Chang, C.; Yaish, Y.; Petta, J. R.; Rinkoski, M.; Sethna, J. P.; Abruna, H. D.; McEuen, P. L.; Ralph, D. C. *Nature* **2002,** *417*, 722.

[11] Green, J. E.; Choi, J. W.; Boukai, A.; Bunimovich, Y.; Johnston-Halperin, E.; DeIonno, E.; Luo, Y.; Sheriff, B. A.; Xu, K.; Shin, Y. S.; Tseng, H. R.; Stoddart, J. F.; Heath, J. R. *Nature* **2007,** *445*, 414.

[12] Kronemeijer, A. J.; Akkerman, H. B.; Kudernac, T.; van Wees, B. J.; Feringa, B. L.; Blom, P. W. M.; de Boer, B. *Adv. Mater.* **2008,** *20*, 1467.

[13] Song, H.; Kim, Y.; Jang, Y. H.; Jeong, H.; Reed, M. A.; Lee, T. *Nature* **2009,** *462*, 1039.

[14] Nijhuis, C. A.; Reus, W. F.; Siegel, A. C.; Whitesides, G. M. *J. Am. Chem. Soc.* **2011,** *133*, 15397.

[15] Derosa, P. A.; Guda, S.; Seminario, J. M. *J. Am. Chem. Soc.* **2003**, *125*, 14240.

[16] Gorman, C. B.; Carroll, R. L.; Fuierer, R. R. *Langmuir* **2001**, *17*, 6923.

[17] Jung, U.; Filinova, O.; Kuhn, S.; Zargarani, D.; Bornholdt, C.; Herges, R.; Magnussen, O. *Langmuir* **2010**, *26*, 13913.

[18] Kim, Y.; Hellmuth, T. J.; Sysoiev, D.; Pauly, F.; Pietsch, T.; Wolf, J.; Erbe, A.; Huhn, T.; Groth, U.; Steiner, U. E.; Scheer, E. *Nano Lett.* **2012**, *12*, 3736.

[19] McCreery, R.; Dieringer, J.; Solak, A. O.; Snyder, B.; Nowak, A. M.; McGovern, W. R.; DuVall, S. *J. Am. Chem. Soc.* **2003**, *125*, 10748.

[20] McCreery, R. L.; Wu, J.; Kalakodimi, R. P. *Phys. Chem. Chem. Phys.* **2006**, *8*, 2572.

[21] Russew, M. M.; Hecht, S. *Adv. Mater.* **2010**, *22*, 3348.

[22] Akkerman, H. B.; Blom, P. W. M.; de Leeuw, D. M.; de Boer, B. *Nature* **2006,** *441*, 69.

[23] Van Hal, P. A.; Smits, E. C. P.; Geuns, T. C. T.; Akkerman, H. B.; De Brito, B. C.; Perissinotto, S.; Lanzani, G.; Kronemeijer, A. J.; Geskin, V.; Cornil, J.; Blom, P. W. M.; De Boer, B.; De Leeuw, D. M. *Nat. Nanotechnol.* **2008,** *3*, 749.

[24] Wang, G.; Kim, Y.; Choe, M.; Kim, T. W.; Lee, T. *Adv. Mater.* **2011,** *23*, 755.

[25] Park, S.; Wang, G.; Cho, B.; Kim, Y.; Song, S.; Ji, Y.; Yoon, M. H.; Lee, T. *Nat. Nanotechnol.* **2012,** *7*, 438.

[26] *Physics of Semiconductor Devices* Sze S. M.; Ng K. K. Ed., John Wiley & Sons, Inc **2007**.

[27] Bayat, A.; Lacroix, J. C.; McCreery, R. L. *J. Am. Chem. Soc.* **2016,** *138*, 12287-12296.

[28] Nijhuis, C. A.; Reus, W. F.; Whitesides, G. M. *J. Am. Chem. Soc.* **2010,** *132*, 18386-18401.

[29] Capozzi, B.; Xia, J.; Adak, O.; Dell, E. J.; Liu, Z. F.; Taylor, J. C.; Neaton, J. B.; Campos, L. M.; Venkataraman, L. *Nat. Nanotechnol.* **2015**, *10*, 522-527.

[30] Wold, D. J.; Frisbie, C. D. *J. Am. Chem. Soc.* **2001,** *123*, 5549.

[31] Cui, X. D.; Zarate, X.; Tomfohr, J.; Sankey, O. F.; Primak, A.; Moore, A. L.; Moore, T. A.; Gust, D.; Harris, G.; Lindsay, S. M. *Nanotechnology* **2002,** *13*, 5.

[32] Rampi, M. A.; Whitesides, G. M. *Chem. Phys.* **2002,** *281*, 373.

[33] Wang, W. Y.; Lee, T.; Reed, M. A.; *Phys. Rev. B* **2003,** *68*, 035416.

[34] Engelkes, V. B.; Beebe, J. M.; Frisbie, C. D. *J. Am. Chem. Soc.* **2004,** *126*, 14287.

[35] Wang, W. Y.; Lee, T.; Kretzschmar, I.; Reed, M. A. *Nano Lett.* **2004,** *4*, 643.

[36] Kim, T. W.; Wang, G. N.; Lee, H.; Lee, T. *Nanotechnology* **2007,** *18*, 315204.

[37] Beebe, J. M.; Kim, B.; Frisbie, C. D.; Kushmerick, J. G. *ACS Nano* **2008,** *2*, 827.

[38] Kim, Y.; Song, H.; Strigl, F.; Pernau, H. F.; Lee, T.; Scheer, E. *Phys. Rev. Lett.* **2011,** *106*, 196804.

[39] Nijhuis, C. A.; Reus, W. F.; Whitesides, G. M. *J. Am. Chem. Soc.* **2009**, *131*, 17814.

[40] Nijhuis, C. A.; Reus, W. F.; Barber, J. R.; Dickey, M. D.; Whitesides, G. M. *Nano Lett.* **2010**, *10*, 3611.

[41] Nerngchamnong, N.; Yuan, L.; Qi, D. C.; Li, J.; Thompson, D.; Nijhuis, C. A. *Nat. Nanotechnol.* **2013**, *8*, 113.

[42] Liu, Y. Q.; Offenhausser, A.; Mayer, D. *Phys. Status Solidi A* **2010**, *207*, 891.

[43] Jiang, L.; Yuan, L.; Cao, L.; Nijhuis, C. A. *J. Am. Chem. Soc.* **2014,** *136*, 1982-1991.

[44] Yuan, L.; Jiang, L.; Thompson, D.; Nijhuis, C. A. *J. Am. Chem. Soc.* **2014,** *136*, 6554-6557.

[45] Yuan, L.; Breuer, R.; Jiang, L.; Schmittel, M.; Nijhuis, C. A. *Nano Lett.* **2015,** *15*, 5506-5512.

[46] Fisher, G. L.; Walker, A. V.; Hooper, A. E.; Tighe, T. B.; Bahnck, K. B.; Skriba, H. T.; Reinard, M. D.; Haynie, B. C.; Opila, R. L.; Winograd, N.; Allara, D. L. *J. Am. Chem. Soc.* **2002,** *124*, 5528.

[47] de Boer, B.; Frank, M. M.; Chabal, Y. J.; Jiang, W. R.; Garfunkel, E.; Bao, Z. *Langmuir* **2004,** *20*, 1539.

[48] Walker, A. V.; Tighe, T. B.; Cabarcos, O. M.; Reinard, M. D.; Haynie, B. C.; Uppili, S.; Winograd, N.; Allara, D. L. *J. Am. Chem. Soc.* **2004,** *126*, 3954.

[49] Haick, H.; Cahen, D. *Accounts Chem. Res.* **2008,** *41*, 359.

[50] Neuhausen, A. B.; Hosseini, A.; Sulpizio, J. A.; Chidsey, C. E. D. *ACS Nano* **2012,** *6*, 9920.

[51] Seo, S.; Min, M.; Lee, J.; Lee, T.; Choi, S. Y.; Lee, H. *Angew. Chem. Int. Edit.* **2012,** *51*, 108.

[52] Najarian, A. M.; Szeto, B.; Tefashe, U. M.; McCreery, R. L. *ACS Nano* **2016,** *10*, 8918-8928.

[53] Wang, G.; Yoo, H.; Na, S. I.; Kim, T. W.; Cho, B.; Kim, D. Y.; Lee, T. *Thin Solid Films* **2009,** *518*, 824.

[54] Wang, G.; Kim, T. W. Lee, H.; Lee, T. *Phys. Rev. B* **2007,** *76*, 205320.

[55] Reus, W. F.; Nijhuis, C. A.; Barber, J. R.; Thuo, M. M.; Tricard, S.; Whitesides, G. M. *J. Phys. Chem. C* **2012**, *116*, 6714.

[56] Cui, X. D.; Primak, A.; Zarate, X.; Tomfohr, J.; Sankey, O. F.; Moore, A. L.; Moore, T. A.; Gust, D.; Harris, G.; Lindsay, S. M. *Science* **2001,** *294*, 571.

[57] Holmlin, R. E.; Haag, R.; Chabinyc, M. L.; Ismagilov, R. F.; Cohen, A. E.; Terfort, A.; Rampi, M. A.; Whitesides, G. M. *J. Am. Chem. Soc.* **2001,** *123*, 5075.

[58] Wold, D. J.; Haag, R.; Rampi, M. A.; Frisbie, C. D. *J. Phys. Chem. B* **2002,** *106*, 2813.

[59] Akkerman, H. B.; Kronemeijer, A. J.; van Hal, P. A.; de Leeuw, D. M.; Blom, P. W. M.; de Boer, B. *Small* **2008,** *4*, 100.

[60] Song, H.; Lee, T.; Choi, N. J.; Lee, H. *J. Vac. Sci. Technol. B* **2008,** *26*, 904.

[61] Kim, Y.; Wang, G.; Choe, M.; Kim, J.; Lee, S.; Park, S.; Kim, D. Y.; Lee, B. H.; Lee, T. *Org. Electron.* **2011,** *12*, 2144-2150.

[62] Wang, G.; Na, S. I.; Kim, T. W.; Kim, Y.; Park, S.; Lee, T. *Org. Electron.* **2012**, *13*, 771.

[63] Ye, S.; Sato, Y.; Uosaki, K. *Langmuir* **1997,** *13*, 3157.

[64] Goujon, F.; Bonal, C.; Limoges, B.; Malfreyt, P. *J. Phys. Chem. B* **2010**, *114*, 6447

[65] Filippini, G.; Israeli, Y.; Goujon, F.; Limoges, B.; Bonal, C.; Malfreyt, P. *J. Phys. Chem. B* **2011**, *115*, 11678

[66] Lee, L. Y. S.; Sutherland, T. C.; Rucareanu, S.; Lennox, R. B. *Langmuir* **2006**, *22*, 4438

[67] Tivanski, A. V.; Walker, G. C. *J. Am. Chem. Soc.* **2005,** *127*, 7647.

[68] Xiao, X. Y.; Brune, D.; He, J.; Lindsay, S.; Gorman, C. B.; Tao, N. J. *Chem. Phys.* **2006,** *326*, 138.

[69] Migliore, A.; Nitzan, A. *ACS Nano* **2011**, *5*, 6669.

[70] Chen, C. -P.; Luo, W. -R.; Chen, C. -N.; Wu, S. -M.; Hsieh, S.; Chiang, C. -M.; Dong, T. -Y. *Langmuir* **2013**, *29*, 3106.

[71] Seo, K.; Konchenko, A. V.; Lee, J.; Bang, G. S.; Lee, H. *J. Mater. Chem.* **2009**, *19*, 7617.

[72] Kiehl, R. A.; Le, J. D.; Candra, P.; Hoye, R. C.; Hoye, T. R. *Appl. Phys. Lett.* **2006**, *88*, 172102.

[73] Ye, S.; Haba, T.; Sato, Y.; Shimazu, K.; Uosaki, K. *Phys. Chem. Chem. Phys.* **1999**, *1*, 3653.

Chapter 2.2. An In-Depth Study of Redox-Induced Conformational Changes in Charge Transport Characteristics of a Ferrocene-Alkanethiolate Molecular Electronic Junction: Temperature-Dependent Transition Voltage Spectroscopy Analysis

In this chapter, we studied the temperature dependent electrical properties of ferrocene-alkanethiolate molecular electronic junctions fabricated by a conventional solid-state device technique using a PEDOT:PSS interlayer. In previous chapter, we had observed unusual temperature dependent electrical characteristics at a voltage polarity larger than +0.6 V and at temperatures higher than ~220 K. The origin of this distinctive behavior was ascribed to redox-induced conformational changes of the ferrocene-alkanethiolate molecules. To investigate the validity of this claim, we performed temperature dependent transition voltage spectroscopy (TVS) analysis based on the multibarrier tunneling (MBT) model to support the proposed redox-induced conformational changes observed in the ferrocene-alkanethiolate molecular junctions. The obtained results were consistent with the unusual thermal characteristics of the ferrocene-alkanethiolate molecular junctions predicted by the proposed redox-induced conformational changes of the molecules.

2.2.1. Introduction

The ultimate aim of molecular electronics is to overcome the limit of the conventional silicon based solid-state electronics by utilizing either single molecules or a bundle of molecules as an active electronic device component. Since the first conceptual molecular diode theoretically proposed by Aviram and Ratner in 1974, the research field of molecular electronics has been widened and deepened by many research groups.[1-8] Although many issues must still be resolved to enable practical applications of molecular

electronics, a large amount of comprehensive studies of the fundamental transport characteristics of molecular junctions and also of a wide range of potential device applications such as those for diodes, memory, transistors, and switches have been performed by these groups.[9-13] Recently, in an attempt to develop a reliable electronic device component, molecular diodes have gained increasing attention from researchers. Molecular diodes can be applied even in a single molecule junction by adopting various approaches that are able to engineer molecular junction parameters such as the molecular structure, electrodes, and their electronic coupling characteristics.[12,14-19] For example, Nijhuis et al. recently reported a robust molecular diode using ferrocene-alkanethiolate SAMs and EGaIn electrodes.[12,16,20] They demonstrated a large rectification ratio of up to ~1000 and reported that the strong asymmetric electrical characteristics could be interpreted by hopping assisted tunneling transport arising from the ferrocene-alkanethiolates and the electrodes. Similar to these studies, we have also examined the possibility of the electronic device application by fabricating a large number of molecular devices based on ferrocene-alkanethiolate (denoted as FcC in this thesis) SAMs using a conventional solid-state device fabrication technique both on rigid and flexible substrates in previous chapter. In this previous study, we could only obtain a relatively small rectification ratio (~1.6) mainly due to the improper choice of the electrodes. Nevertheless, we observed a distinctive temperature dependence on the electrical characteristics; that is, the current density decreased as the temperature increased in a certain temperature range when a sufficient voltage was applied with a certain voltage polarity (i.e., when a large enough positive voltage was applied to ferrocene group side of the FcC molecular junction). This behavior was in contrast to the usually expected thermally activated charge transport in the molecular device junction or other device junctions in which, most times, the current

density increases as the temperature increases. In that study,[21] we suggested the unusual thermal characteristics are probably due to the redox-induced conformational changes of the ferrocene-alkanethiolates in the molecular junctions. While the analysis was quite reasonable and consistent with the experimental results, further evidence was needed to support our suggested explanation.

Here, thus, we report the temperature dependent electrical characteristics of the FcC molecular junctions fabricated by a conventional solid-state device technique using a PEDOT:PSS interlayer. We have observed unusual temperature dependent electrical characteristics at voltage polarities larger than +0.6 V and at temperatures higher than ~220 K. The origin of this distinctive behavior was ascribed to redox-induced conformational changes of the ferrocene-alkanethiolate molecules. The analysis of the results of the temperature dependent TVS based on a MBT model supports the occurrence of the proposed redox-induced conformational changes in the ferrocene-alkanethiolate molecular junctions.

2.2.2. Experimental

To fabricate the molecular junctions, we followed the same fabrication process reported in chapter 2.1. The electrical characteristics of the FcC molecular junctions were measured using a temperature variable probe station system (ST-500 purchased from Janis Research Company, Inc.) and a semiconductor parameter analyzer (Keithley 4200SCS). We applied the voltage to the top electrodes while the bottom electrodes were grounded as shown in Figure 2.1.6. The voltage was swept from -1 to +1 V. For temperature variable characterizations, we used liquid nitrogen and a feedback looped heat generator to adjust the samples' temperature. The temperature was varied from 80 to 300 K at intervals of 20

K. Additionally, the measurements at the low temperatures were performed by raising the temperature and vice versa. The obtained results were consistent with each other.

2.2.3. Results and Discussion

In the field of molecular electronics, TVS has been found to be a promising tool for understanding the charge transport mechanism through molecular junctions, especially for the tunneling transport involving frontier molecular orbitals and the Fermi level of the electrodes.[22-24] Based on the fact that the effective tunneling barrier shape can be modulated by the applied voltage on the sandwiched molecules between the electrodes, the examination of the Fowler-Nordheim plot (F-N plot; $\ln(J/V^2)$ versus $1/V$) can provide general insight into the energy offset between the frontier molecular orbital and the Fermi level of the electrodes.[22-24] The advantage of the TVS analysis is that, because it does not depend on a detailed microscopic model, it can be applied to various molecular systems to extract the energy level alignment.[25,26] Since Beebe et al. first proposed this technique to investigate the transport properties of molecular junctions, TVS has been widely adopted by many research groups and has been developed both theoretically and experimentally to consider the more subtle features of molecular junctions such as an asymmetric coupling effect.[27,28] Here, we applied this technique to investigate our molecular junctions. As mentioned above, according to the temperature dependence analysis, tunneling transport is the dominant transport mechanism in our FcC molecular junctions. Although the weak hopping transport mediated by the HOMO of the ferrocene moiety also influenced the charge transport characteristics, this effect may be too weak to dominate the entire charge transport characteristics due to the large barrier height of the long alkyl chains. In this case, we could assume that the energy band diagram of our molecular junctions is represented

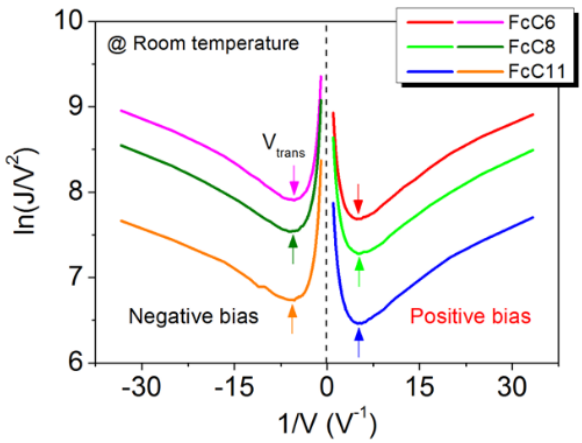

Figure 2.2.1. Fowler-Nordheim plots of representative FcC molecular devices at room temperature (300 K) under each voltage polarity. Arrows depict inflection points of the plots that represent V_{trans} values.

by an effective single barrier model by considering the energetic contact between the ferrocene moieties and the PEDOT:PSS layer as an individual barrier. This idea is based on the MBT model, previously reported by our group.[29] The main concept of the MBT model is the generalization of the Simmons tunneling model by dividing a single rectangular tunneling barrier of the molecule into the set of individual barriers such as the molecular-chain body barrier and the metal-molecule contact barriers.[29] More detailed introduction of MBT model is given in chapter 1. Based on this model, we could consider our FcC molecular junctions as an effective tunneling barrier replaced with a set of individual tunneling barriers: the alkyl chains and ferrocene moiety-PEDOT:PSS layer contact. Figure 2.2.1 presents the F-N plots of representative FcC molecular devices at room temperature (300 K) under each voltage polarity. In a F-N plot, the transition voltage (V_{trans}) is determined by the inflection point ($d(\ln(J/V^2)/d(1/V) = 0$) that eventually becomes the same as the minimum point of the plot. In Figure 2.2.2, the minimum points of each plot that represent V_{trans} of each representative molecular device are marked. To extract the

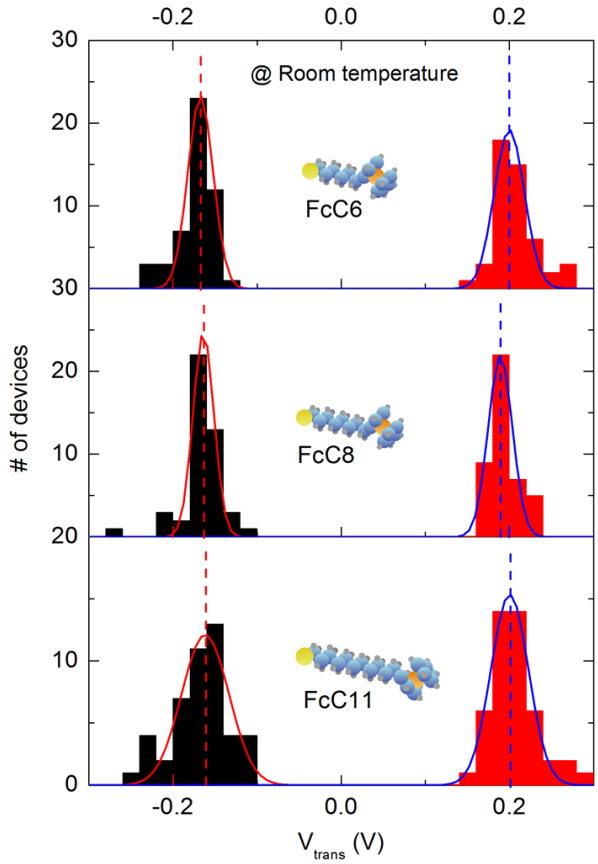

Figure 2.2.2. Statistical histograms of the V_{trans} values of each representative molecular junction at both voltage polarities. Fitting curves using a normal distribution function are also depicted.

most probable V_{trans} values, we characterized the V_{trans} values of each set of ~50 FcC molecular devices. Figures 2.2.2 and 2.2.3 show the statistical histograms and the obtained results for the V_{trans} values at room temperature. We plotted the fitting curves using a normal distribution function and their averages as dotted lines. Based on these histograms, it was statistically determined that the averaged V_{trans} values were -0.183 ± 0.021 V, -0.176 ± 0.025 V, and -0.177 ± 0.035 V for the FcC6, FcC8, and FcC11 devices, respectively, at the negative voltage polarity and 0.201 ± 0.032 V, 0.190 ± 0.030 V, and 0.195 ± 0.029 V at the positive voltage polarity. These results suggest three features: (1) the V_{trans} values at the

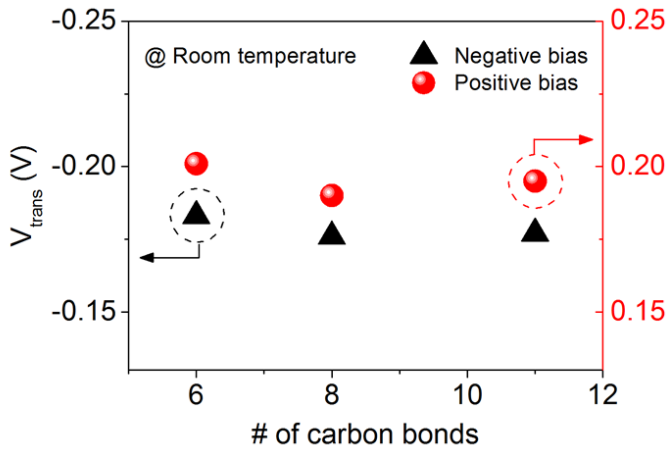

Figure 2.2.3. Averaged V_{trans} values at each voltage polarity.

positive voltage (i.e., the effective barrier height at the positive voltage) are larger than those at the negative voltage for each molecule, in agreement with the asymmetric I-V characteristics shown in Figure 2.1.7 (i.e., the current densities were higher at the negative voltage than at the positive voltage). This type of difference between the V_{trans} values at each voltage polarity can be easily found in many molecular systems when the electronic coupling strength between the molecules and the electrodes differ at the two sides.[28-30] However, here, it should be noted that the V_{trans} values may not be identical to the effective barrier heights.[22,23,25,26] Therefore, we cannot compare the absolute barrier height magnitudes; we can compare only their differences. (2) The V_{trans} values show values that are much different than those of the molecular junctions using the usual alkanethiolates that do not contain the ferrocene end group (i.e., ~1.2 V for the Au/alkanethiolate-PEDOT:PSS/Au junction).[29,31] This indicates that the introduction of the ferrocene end-group does influence the charge transport characteristics. However, it should again be noted that this cannot be used for evaluation of how much the effective barrier height has been changed. (3) Regardless of the number of alkyl chains, the V_{trans} data showed similar values

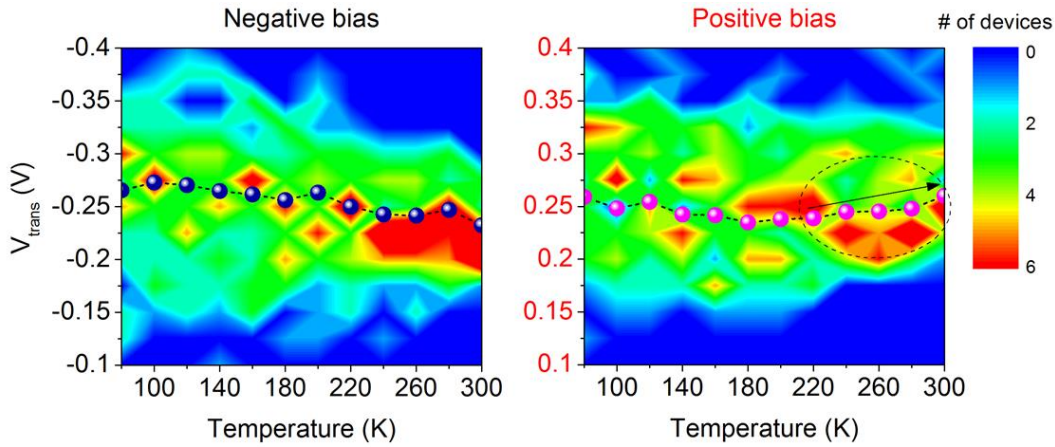

Figure 2.2.4. Contour plots of statistical histograms of the V_{trans} values versus the temperatures at each voltage polarity. In the plots, the averaged values are depicted as data points and dotted lines.

within the error range. This can be expected due to the fact that the dominant charge transport mechanism through the ferrocene-alkanethiolates is tunneling via the long alkyl chains and their HOMO-LUMO gap remains effectively constant as the number of alkyl chains changes.[32-34] These findings agreed well with the investigation of the basic transport characteristics at room temperature described in the previous chapter.

Furthermore, following this analysis, we investigated the temperature dependent charge transport characteristics and especially the unexpected feature at the positive voltage. Figure 2.2.4 shows the contour plots of statistical histograms of the V_{trans} values versus the temperatures at each voltage polarity. For example, Figure 2.2.5 shows three representative V_{trans} values under temperature variation at both bias polarity. Here, we characterized a total of ~25 working molecular devices and depicted their averaged values as data points and dotted lines in the plots. Examination of the statistical results shows that V_{trans} values remained almost constant as the temperature changed and showed similar values at both voltage polarities. However, at temperatures higher than ~220 K, they showed slightly different properties at each voltage, i.e., the V_{trans} values slightly increased at the positive

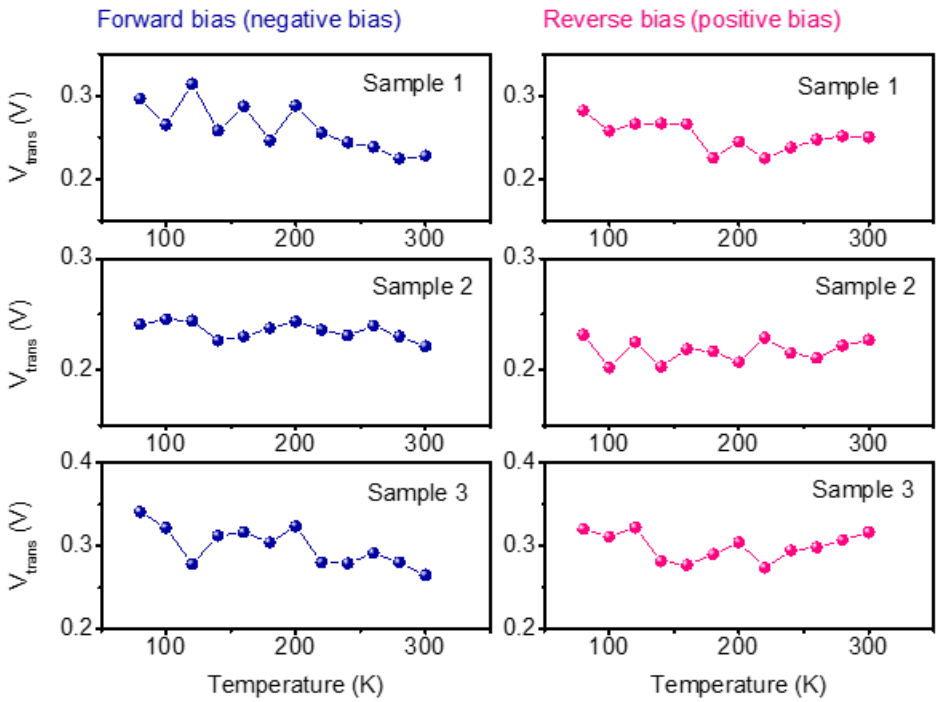

Figure 2.2.5. Three representative V_{trans} values under temperature variation at both bias polarity.

voltage in contrast to the behavior at the negative voltage; this implies that the effective barrier height increased. To visualize this more clearly, we individually replotted the averaged V_{trans} values versus the temperatures, as shown in Figure 2.2.6. Examination of the plot shows that the V_{trans} values at the positive voltage started to increase at temperatures higher than ~220 K, unlike the case at the negative voltage. This subtle distinction at the positive voltage can be explained consistently by the redox-induced conformational changes of the ferrocene-alkanethiolates, as mentioned above. In the molecular systems, the charge transport through the molecules can be strongly influenced by the molecular conformations, which may lead to the change of the transition voltage due to conformational changes.[35] Figures 2.2.7(a) and 2.2.7(b) show schematic illustrations of two possible redox-induced conformational changes of the ferrocene-alkanethiolates at the positive voltage. When the ferrocene moieties are oxidized by the positively applied

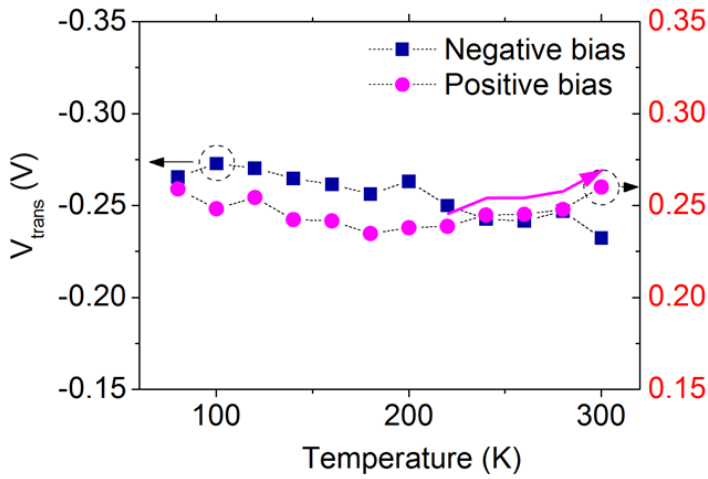

Figure 2.2.6. Averaged V_{trans} values are re-depicted for clear identification.

voltage, the SAMs are reoriented to be more perpendicular with the bottom Au electrodes, i.e., the tilt angle decreases as shown in Figure 2.2.7(a).[36] As the molecular tilt angle decreases, the chain-to-chain tunneling (i.e., through-space tunneling) between the adjacent alkyl chains becomes less significant in addition to the already existing through-bond tunneling.[37,38] This results in the reduction of the strength of the field emission by the reduction of electric field, leading to a weakening of the electric field induced barrier lowering effect and thus appearing as a barrier raising effect.[38] In Figure 2.2.8(a), this effect is schematically presented based on the MBT model. On the other hand, the coupling strength between the molecules and the electrodes on each side, i.e., the contact properties, can also influence the contact barrier height based on the MBT model.[29,39] Usually poor contact causes an increase in the contact barrier height due to poor charge transfer efficiency between the molecules and the electrodes.[29,39] For example, we previously reported that the difference in the specific bonding nature of alkanethiolates to the top electrodes (physical bond) could result in the increase of contact barrier height.[29] In this report, the deduced contact barrier height of the poor physical contact (methyl-Au) has been

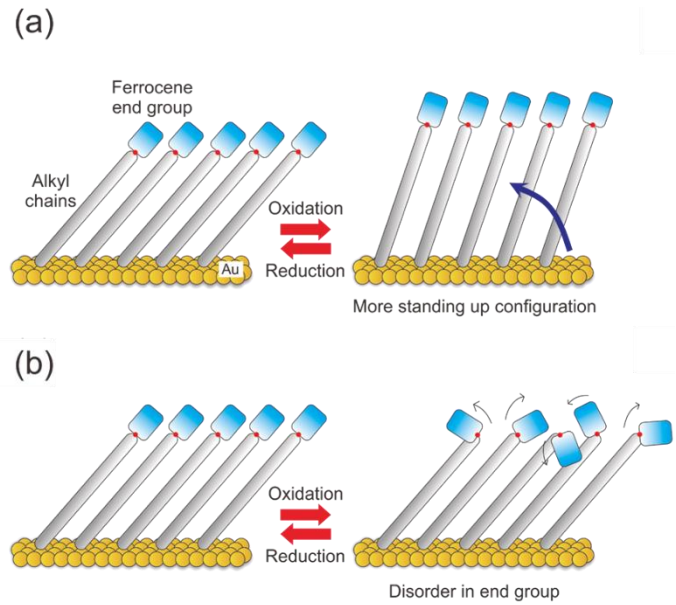

Figure 2.2.7. Schematic illustrations of proposed redox-induced conformational changes of the ferrocene-alkanethiolates and their corresponding barrier raising effect based on the MBT model. (a) More standing up configuration of the alkyl chain body and (b) Disorder in the ferrocene end-group.

found to be higher than that of the good chemical contact (thiol-Au). In our case, the repulsive force between each individual ferrocenium cation could weak the electron overlapping (hybridization) of neighboring ferrocenium molecular orbitals or atomic orbitals of the top metal electrodes because the valence electrons are missing. Therefore, this effect could reduce the molecular electron transfer rates between them, which can be considered as poor physisorbed contact. Therefore, we can expect that the disorder in the ferrocene end-group induced by the redox process of the ferrocene-alkanethiolates leads to poor physisorbed contact with the PEDOT:PSS layer, causing an increase in the contact barrier height. Figure 2.2.8(b) schematically presents this effect based on the MBT model. Here, we considered these two effects based on the MBT model, but both effects can lead

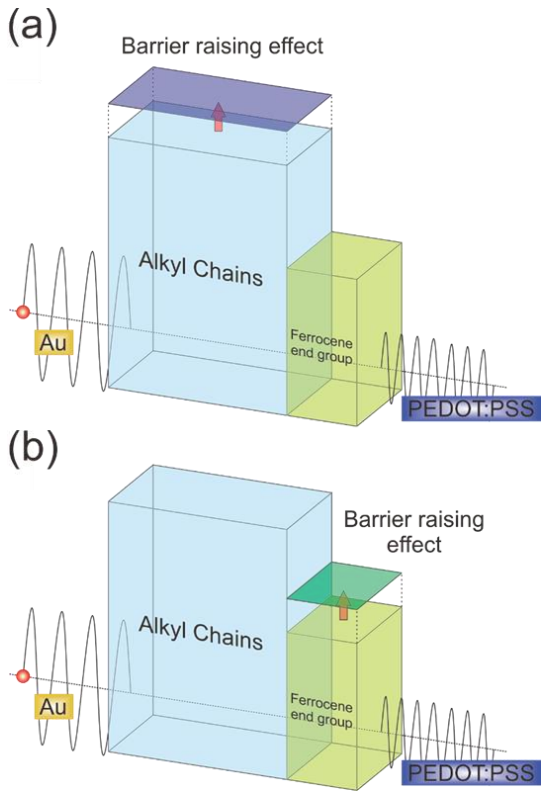

Figure 2.2.8. Schematic illustrations of increase of effective barrier height effect. (a) Increase of the barrier height of the alkyl chain body due to more standing up configuration of the alkyl chain body. (b) Increase of the barrier height of the ferrocene end-group due to disorder in the ferrocene end-group.

to the increase in the total effective barrier height, which will consequently result in an increase of the V_{trans} values at a positive voltage. Based on this analysis, we can conclude that the unusual I-V-T characteristics at positive voltages are supported by the redox-induced conformational changes of the ferrocene-alkanethiolates that are consistent with temperature dependent TVS results. Nevertheless, we emphasize here that a more careful and direct verification of this type of conformational change must be obtained in order to strengthen our analysis and fully understand the nature of this effect in future studies. For example, asymmetric coupling effect between molecular species and electrodes can be

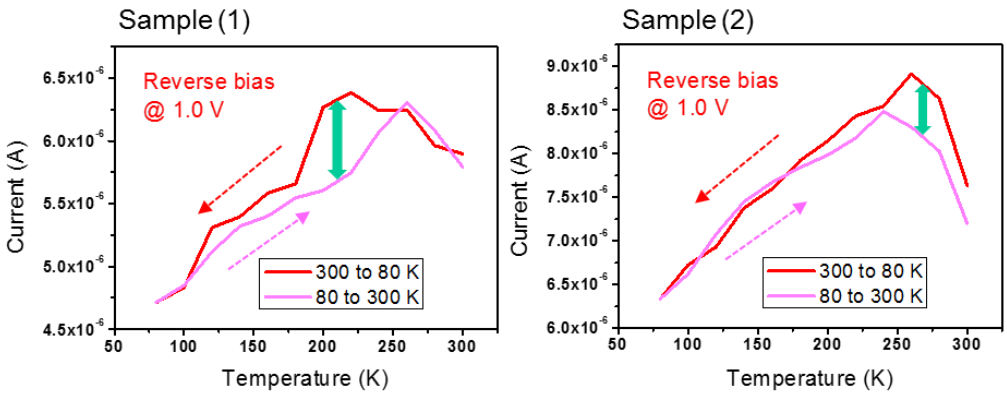

Figure 2.2.9. Two representative plots of temperature dependent current density at +1 V depending on temperature sweep direction which show different behaviors respectively.

accounted for better understanding of temperature dependent TVS analysis results.[27,40]

As one of future studies, we investigated reversibility of the abnormal temperature dependence of electrical characteristics of ferrocene-alkanethiolate molecular junctions. Because the disordering of ferrocenium moiety in molecular species is thermodynamically irreversible process that cannot be inversed once the effect happens, the validity of the disordering effect can be identified by investigating the electrical characteristics of our molecular junctions under different temperature sweep direction. To be more specific, if the temperature dependent electrical characteristics at positive bias change with temperature sweep direction, it means that the intrinsic molecular conformational change is irreversible. Therefore, the disordering effect can be valid. For example, Figure 2.2.9 shows current density at positive +1 V bias versus temperature with different sweep direction of two individual device. As shown in this plot, the current density shows different behavior with different temperature sweep direction around ~220 K even though the general trajectory exhibits similar tendency. On the other hands, however, Figure 2.2.10 shows a similar current density dependency with different temperature sweep direction

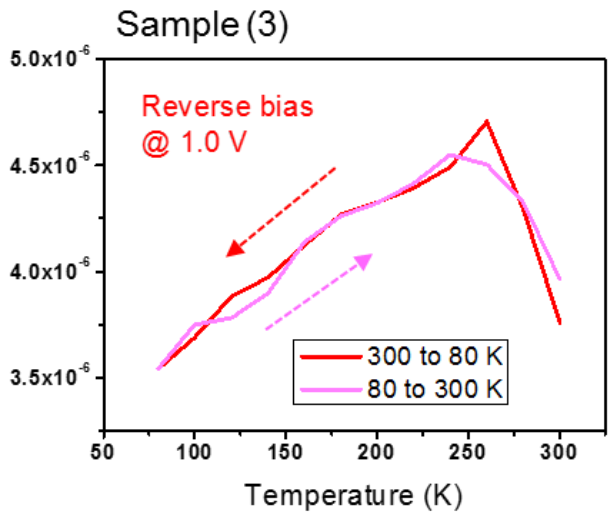

Figure 2.2.10. Another plot of temperature dependent current density at +1 V depending on temperature sweep direction which shows similar behaviors respectively.

which represents device to device variation. Therefore, here we couldn't verify whether the disordering effect is valid or not, and we expect that as a result, the alkyl chain body effect is more dominant in this case. More detailed discussion regarding this analysis and charge transport phenomena in ferrocene-alkanethiolate molecular junctions are presented in Appendix B.

2.2.4. Chapter Summary

In summary of this chapter, we investigated the temperature dependent electrical characteristics of the ferrocene-alkanethiolate molecular junctions using the PEDOT:PSS interlayer. We fabricated and analyzed a statistically sufficient number of devices to ensure the reliability of the data. In particular, we consistently observed unusual temperature dependent electrical characteristics at a voltage polarity larger than +0.6 V and at

temperatures higher than ~220 K. The origin of this distinctive behavior was attributed to the redox-induced conformational changes of the ferrocene-alkanethiolate molecules. We used the TVS analysis to understand the electrical characteristics of these molecular junctions. From the analysis, we found that the obtained TVS results were consistent and in good agreement with the measured electrical characteristics. Additionally, we performed a temperature dependent TVS analysis based on the multibarrier tunneling model to support the proposed redox-induced conformational changes of the molecules. Our study suggests the significance of the consideration of the macroscopic structural organization of the molecular junction as well as the intrinsic molecular properties, which includes the redox processes or molecular conformations, to understand the charge transport characteristics of the molecular junctions.

References

[1] Reed, M. A.; Zhou, C.; Muller, C. J.; Burgin, T. P.; Tour, J. M. *Science* **1997**, *278*, 252-254.

[2] Joachim, C.; Gimzewski, J. K.; Aviram, A. *Nature* **2000**, *408*, 541-548.

[3] Nitzan, A.; Ratner, M. A. *Science* **2003**, *300*, 1384-1389.

[4] McCreery, R. L. *Chem. Mater.* **2004**, *16*, 4477-4496.

[5] Love, J. C.; Estroff, L. A.; Kriebel, J. K.; Nuzzo, R. G.; Whitesides, G. M. *Chem. Rev.* **2005**, *105*, 1103-1169.

[6] Akkerman, H. B.; Blom, P. W. M.; de Leeuw, D. M.; de Boer, B. *Nature* **2006**, *441*, 69-72.

[7] Song, H.; Reed, M. A.; Lee, T. *Adv. Mater.* **2011**, *23*, 1583-1608.

[8] Wang, G.; Kim, T.-W.; Lee, T. *J. Mater. Chem.* **2011**, *21*, 18117-18136.

[9] Park, H.; Park, J.; Lim, A. K. L.; Anderson, E. H.; Alivisatos, A. P.; McEuen, P. L. *Nature* **2000**, *407*, 57-60.

[10] Green, J. E., et al. *Nature* **2007**, *445*, 414-417.

[11] Kronemeijer, A. J.; Akkerman, H. B.; Kudernac, T.; van Wees, B. J.; Feringa, B. L.; Blom, P. W. M.; de Boer, B. *Adv. Mater.* **2008**, *20*, 1467-1473.

[12] Nijhuis, C. A.; Reus, W. F.; Whitesides, G. M. *J. Am. Chem. Soc.* **2009**, *131*, 17814-17827.

[13] Quek, S. Y.; Kamenetska, M.; Steigerwald, M. L.; Choi, H. J.; Louie, S. G.; Hybertsen, M. S.; Neaton, J. B.; Venkataraman, L. *Nat. Nanotechnol.* **2009**, *4*, 230-234.

[14] Kornilovitch, P. E.; Bratkovsky, A. M.; Williams, R. S. *Phys. Rev. B* **2002**, *66*, 165436.

[15] Diez-Perez, I.; Hihath, J.; Lee, Y.; Yu, L.; Adamska, L.; Kozhushner, M. A.; Oleynik, I. I.; Tao, N. *Nat. Chem.* **2009**, *1*, 635-641.

[16] Nijhuis, C. A.; Reus, W. F.; Siegel, A. C.; Whitesides, G. M. *J. Am. Chem. Soc.* **2011**, *133*, 15397-15411.

[17] Loertscher, E.; Gotsmann, B.; Lee, Y.; Yu, L.; Rettner, C.; Riel, H. *ACS Nano* **2012**, *6*, 4931-4939.

[18] Yoon, H. J.; Liao, K.-C.; Lockett, M. R.; Kwok, S. W.; Baghbanzadeh, M.; Whitesides, G. M. *J. Am. Chem. Soc.* **2014**, *136*, 17155-17162.

[19] Capozzi, B.; Xia, J.; Adak, O.; Dell, E. J.; Liu, Z.-F.; Taylor, J. C.; Neaton, J. B.; Campos, L. M.; Venkataraman, L. *Nat. Nanotechnol.* **2015**, *10*, 522-527.

[20] Yuan, L.; Breuer, R.; Jiang, L.; Schmittel, M.; Nijhuis, C. A. *Nano Lett.* **2015**, *15*, 5506-5512.

[21] Jeong, H., et al. *Adv. Funct. Mater.* **2014**, *24*, 2472-2480.

[22] Beebe, J. M.; Kim, B.; Gadzuk, J. W.; Frisbie, C. D.; Kushmerick, J. G. *Phys. Rev. Lett.* **2006**, *97*, 026801.

[23] Beebe, J. M.; Kim, B.; Frisbie, C. D.; Kushmerick, J. G. *ACS Nano* **2008**, *2*, 827-832.

[24] Bennett, N.; Xu, G.; Esdaile, L. J.; Anderson, H. L.; Macdonald, J. E.; Elliott, M. *Small* **2010**, *6*, 2604-2611.

[25] Huisman, E. H.; Guedon, C. M.; van Wees, B. J.; van der Molen, S. J. *Nano Lett.* **2009**, *9*, 3909-3913.

[26] Markussen, T.; Chen, J.; Thygesen, K. S. *Phys. Rev. B* **2011**, *83*, 155407.

[27] Wang, G.; Kim, Y.; Na, S.-I.; Kahng, Y. H.; Ku, J.; Park, S.; Jang, Y. H.; Kim, D.-Y.; Lee, T. *J. Phys. Chem. C* **2011**, *115*, 17979-17985.

[28] Baldea, I. *Phys. Rev. B* **2012**, *85*, 035442.

[29] Wang, G.; Kim, T.-W.; Lee, H.; Lee, T. *Phys. Rev. B* **2007**, *76*, 205320.

[30] Guo, S.; Hihath, J.; Diez-Perez, I.; Tao, N. *J. Am. Chem. Soc.* **2011**, *133*, 19189-19197.

[31] Wang, G.; Na, S.-I.; Kim, T.-W.; Kim, Y.; Park, S.; Lee, T. *Org. Electron.* **2012**, *13*, 771-777.

[32] Wold, D. J.; Frisbie, C. D. *J. Am. Chem. Soc.* **2001**, *123*, 5549-5556.

[33] Tomfohr, J. K.; Sankey, O. F. *Phys. Rev. B* **2002**, *65*, 245105.

[34] Salomon, A.; Cahen, D.; Lindsay, S.; Tomfohr, J.; Engelkes, V. B.; Frisbie, C. D. *Adv. Mater.* **2003**, *15*, 1881-1890.

[35] Dhungana, K. B.; Mandal, S.; Pati, R. *J. Phys. Chem. C* **2012**, *116*, 17268-17273.

[36] Ye, S.; Sato, Y.; Uosaki, K. *Langmuir* **1997**, *13*, 3157-3161.

[37] Song, H.; Lee, H.; Lee, T. *J. Am. Chem. Soc.* **2007**, *129*, 3806-3807.

[38] Wang, G.; Kim, T.-W.; Jo, G.; Lee, T. *J. Am. Chem. Soc.* **2009**, *131*, 5980-5985.

[39] Diez-Perez, I.; Hihath, J.; Hines, T.; Wang, Z.-S.; Zhou, G.; Muellen, K.; Tao, N. *Nat. Nanotechnol.* **2011**, *6*, 226-231.

[40] Jang, Y.; Kwon, S. J.; Shin, J.; Jeong, H.; Hwang, W. T.; Kim, J. W.; Koo, J.; Ko, T. Y.; Ryu, S.; Wang, G.; Lee, T. W.; Lee, T. W.; Lee, T. *ACS Appl. Mater. Interfaces* **2017**, *9*, 42043-42049.

Chapter 3. High-Yield, Reliable Fabrication for Molecular Junctions: Direct Metal Transfer Method

3.1. A New Approach for High-Yield Metal-Molecule-Metal Junctions by Direct Metal Transfer Method

In this chapter, we introduce a new approach for obtaining high-yield, vertically structured metal-molecule-metal junctions in which the top metal electrodes are formed on alkanethiolate self-assembled monolayers by a direct metal transfer method without the use of any additional protecting interlayers in the junctions. The fabricated alkanethiolate molecular devices exhibited considerably improved device yields (~70 %) in comparison to the typical low device yields (less than a few %) of molecular junctions in which the top metal electrodes are fabricated using the conventional evaporation method. We compared our method with other molecular device fabrication methods in terms of charge transport parameters. This study suggests a potential new device platform for realizing robust, high-yield molecular junctions and investigating the electronic properties of devices. Also this approach can allow improvement of rectification ratio (i.e. asymmetric ratio) of ferrocene-alkanethiolate molecular junctions as we discussed in previous section because the low rectification ratio was resulted from work function mismatch of both electrodes.

3.1.1. Introduction

The realization of high-yield, stable molecular junctions has been a long-standing challenge in the field of molecular electronics research, and it is an essential prerequisite for characterizing and understanding the charge transport properties of molecular junctions prior to their device applications. To investigate the mechanism and characteristics of

charge transport through molecular junctions, a variety of approaches for constructing molecular junctions, such as mechanically controllable break junction techniques, scanning probe microscopy-based techniques, and solid-state device-based methods, have been demonstrated as mentioned in chapter 1.[1-18] Specifically, the simple vertically structured, solid-state device-based metal-molecule-metal junctions were considered to be a general testbed for studying the charge transport characteristics of molecular junctions and their device applications.[5,9,11,13,16,17] However, one of the typical obstacles that may be encountered when forming molecular junctions using this method is that conducting filamentary paths may be formed through the molecules by the metal electrode evaporated on the molecular layers, which results in a very low device yield of molecular junctions and renders them inappropriate as a reliable testbed platform of molecular junctions.[8,9,19-23] To overcome this obstacle, methods that utilize an intermediate protecting layer between the molecular layer and the top electrode have been reported. For example, a conducting polymer of PEDOT:PSS, Aedotron P, graphene, and reduced graphene oxide (rGO) have been adopted as the interlayer to improve the device yield of molecular junctions by prohibiting the formation of conducting filamentary paths.[5,13,16,24-29] Despite this improvement, these methods also have some drawbacks: (1) the device fabrication procedure may be more complicated because of the introduction of an additional interlayer, (2) the molecular layer can be damaged or contaminated by the additional interlayer, (3) the interlayer limits the potential choices of top electrodes that can enrich the functionality of molecular junctions through interactions between the molecular layer and top electrode, (4) the formation of symmetric molecular junctions is generally impossible, and (5) the junction conductivity is relatively poor compared to metal-molecule-metal junctions without interlayers. Especially, the limited choice of top

electrodes prohibits diverse applications of molecular species because of uncontrollable molecule-electrode contact properties. For these reasons, pure metal-molecule-metal junctions without any additional interlayers are generally more desirable.

In this study, we propose a new approach for creating high-yield molecular devices as a vertical metal-molecule-metal junction. We fabricated the top metal electrodes using a direct metal transfer (DMT) method in which the top electrodes are formed on a different substrate and then transferred to the molecular junctions, similar to the well-known graphene transfer method.[30-32] Using this method, we were able to fabricate highly stable and reliable metal-molecule-metal junctions without the use of any additional interlayers, and the resulting junctions exhibited considerably improved device yields (~70 %) compared to those (typically less than a few %) of the molecular junctions in which the top electrodes are formed using the conventional metal-evaporation method.[9,33] We compared this method with other molecular device fabrication methods in terms of characteristic charge transport parameters, especially the electronic coupling interaction between the molecular layer and electrodes. Also we summarized the strengths and weaknesses of our method in comparison with other methods.

3.1.2. Experimental

Figure 3.1.1 presents a schematic illustration of the process for fabricating the molecular junctions using the DMT method. In this study, we selected alkanethiolate ($HS(CH_2)_{n-1}CH_3$) SAMs for the molecular junctions because alkanethiolates, which have a structure composed of repetitively connected alkyl chains with thiol end groups, are one of the most widely studied molecules for use in a variety of junction fabrication techniques. Many research groups have reported the charge transport properties of alkanethiolates in

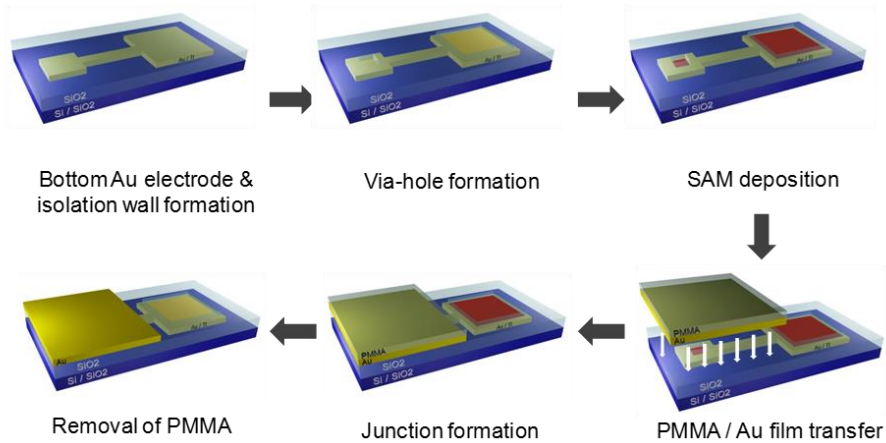

Figure 3.1.1. Device fabrication procedure.

molecular junctions based on the use of various techniques, such as scanning tunneling microscopy,[18] mechanically controllable break junction,[4,34,35] conducting-probe atomic force microscopy,[36] nanopores,[17] electromigration nanogap,[14,37] and solid-state device testbeds.[5,9,13,16] Therefore, the alkanethiolates can be considered as reference molecules for evaluating the characteristics of the newly proposed molecular junction testbeds. Here, we used three different lengths of alkanethiolate molecules: octanethiol ($HS(CH_2)_7CH_3$, denoted as C8), dodecanethiol ($HS(CH_2)_{11}CH_3$, denoted as C12), and hexadecanethiol ($HS(CH_2)_{15}CH_3$, denoted as C16). The reasons for choosing these three molecules are because (1) sufficient difference in alkane lengths is necessary for definite distinction in electrical properties especially current density. This definite distinction of current density enables the statistical analysis to be quite distinguishable, and (2) similar alkane lengths of molecules should be chosen as previous works for proper comparison of each method.[5,16,26,28,38,39] The chemical structures of these molecules are presented in Figure 3.1.2.

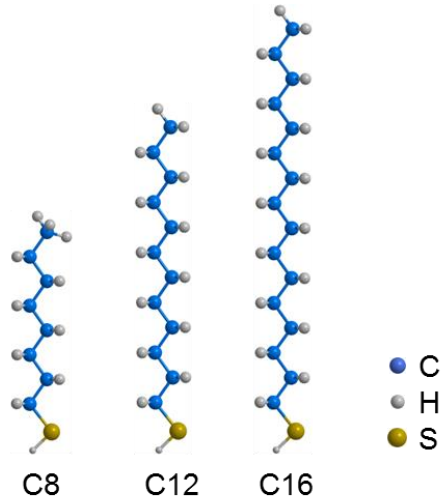

Figure 3.1.2. The three types of alkanethiolates along with their chemical structures: C8 (octanethiol), C12 (dodecanethiol) and C16 (hexadecanethiol).

To form the molecular junctions, we employed a fabrication procedure that was previously reported by our group.[9,13,16] First, conventional optical lithography was first used to pattern the bottom electrodes on Si/SiO_2 (p-type, 100 nm thick SiO_2 layer) substrates. After the evaporation of the bottom electrodes (50-nm-thick Au/5-nm-thick Ti), the residual photoresist was removed using the lift-off technique, and the SiO_2 insulating walls (50 or 100 nm) were generated by plasma-enhanced chemical vapor deposition. Then, circular holes with radii of 2, 3, 4, and 5 μm were created on the insulating wall through optical lithography to expose the Au top surface which is used as bottom electrodes. These via-holes for SAMs were made by optical lithography and reactive ion etch (RIE) (5 sccm of O_2 gas, 50 sccm of CF_4 gas, 150 W of RF power, 0.055 torr, 1-1.5 min) of SiO_2, exposing the Au top surface which is used as bottom electrodes. Because the bottom gold electrode is the top surface of the evaporated gold, it is necessary to investigate roughness of the gold surfaces for the molecular junction. For this, we have included surface morphology image

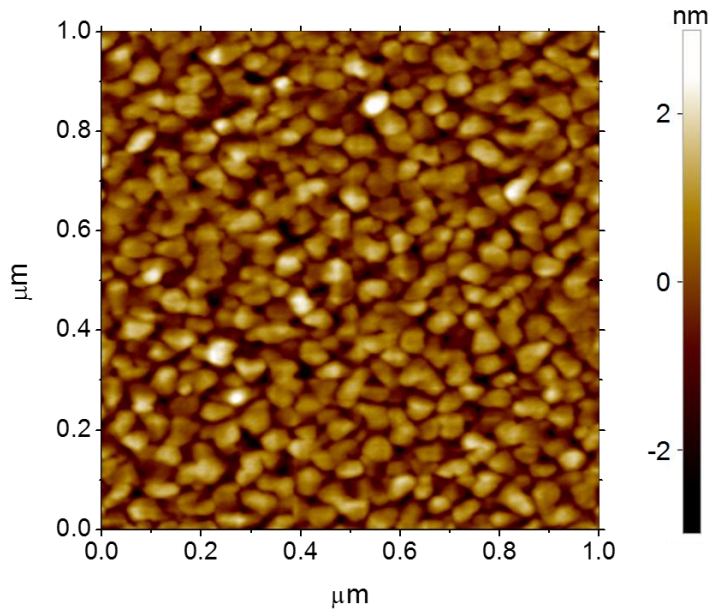

Figure 3.1.3. Surface morphological image of the bottom Au electrodes.

of the bottom gold electrodes, obtained with an atomic force microscope in Figure 3.1.3. Figure 3.1.3 displays the surface morphological image of bottom Au electrodes with an AFM (NX-100, Park systems). The RMS roughness from the image of Figure 3.1.3 (scan size = 1.0 μm × 1.0 μm) was estimated to be about 0.82 nm. Therefore, the rough surface can be a defect source of SAMs on gold. The rough surface of the bottom electrode results in large dispersion of the experimental data, it is quite recommendable to make the surface of the bottom electrode as flat as possible. Generally, there are some ways to achieve flatter surface of the bottom electrode.[39] In our case, however, we couldn't adapt this kind of methods to generate the bottom electrode because we used conventional optical lithography technique to fabricate the bottom electrode for mass production of molecular junctions. Then, alkanethiolate SAMs were formed on the exposed Au surfaces by immersing the substrates in an ethanolic solution of alkanethiolate molecules (~5 mM in anhydrous ethanol) in N_2-filled glove box for 1-2 days. A prepared transfer film was transferred on the

substrate. Before transferring, a couple of drops of isopropyl alcohol (IPA) were added on the substrate to enhance the soft contact between the molecular layer and metal film by surface tension. By drying the transferred substrate for enough time (~4 h), the metal-molecule-metal junctions were formed. Finally, the residual PMMA layer on top metal electrodes was removed with acetone. Generally, when one creates vertical metal-molecule-metal junctions, the device yield is very poor (less than a few %) because of the formation of conducting filamentary paths through the molecular layer during the evaporation of the top metal electrode.[8,9,19-23] To prevent this problem, methods for inserting an intermediate layer between the top electrode and molecular layer have been demonstrated, in which the interlayer acts as the electrode to contact molecules and as the blocking layer for the Au top electrode.[5,13,16,24-29] These interlayer-electrode molecular junctions exhibited considerably higher device yields, but at the same time, they may complicate the interpretation of the molecular junction's properties because of the additional interfaces resulting from the introduction of the interlayer.[40]

In this study, we transferred a patterned top metal sheet as the top electrode onto the molecular layers. Figure 3.1.4 presents photographic images of the preparation procedure steps for transferring the top Au electrodes. As the first step for preparing the transfer film, we deposited the patterned top Au electrodes onto a dummy substrate (SiO_2/Si) with an electron beam evaporator using a shadow mask, as shown in Figure 3.1.4(a). The inset of Figure 3.1.4(a) presents a schematic image of the Au electrodes on the dummy substrate. Then, poly(methyl methacrylate) (PMMA) was spin-coated onto the dummy substrate to support the Au electrodes while the film was detached from the substrate (Figure 3.1.4(b)). After coating, we applied a support tape to the top of the substrate (Figure 3.1.4(c)).

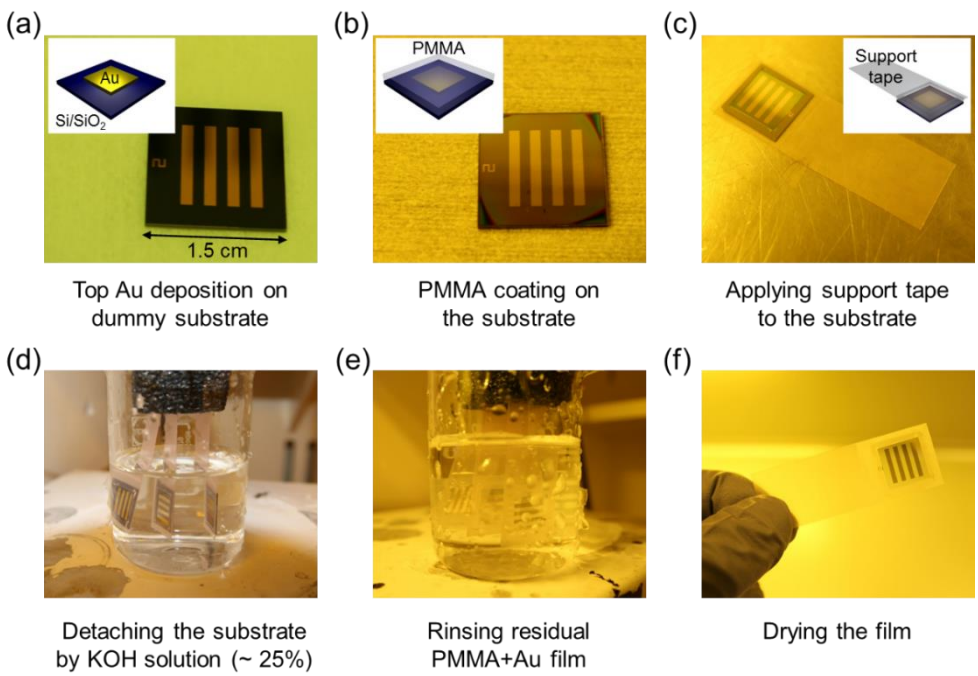

Figure 3.1.4. Optical and schematic images of the preparation procedure for transferring the Au film. (a) Patterned top Au electrode deposited on a dummy substrate. (b) PMMA was spin-coated on the dummy substrate. (c) A support tape was applied to support the substrate. (d) To detach the substrate, the film was immersed in a KOH solution. (e) Residual film was removed by rinsing the substrate. (f) Drying the residual film.

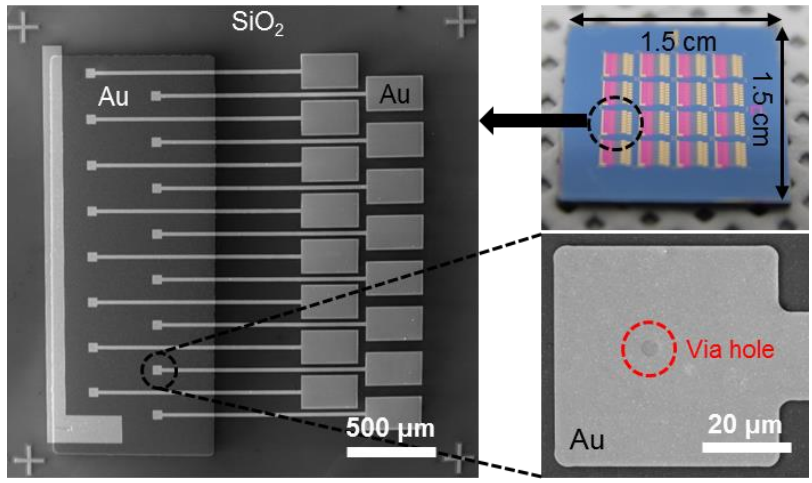

Figure 3.1.5. SEM and optical microscopy images of the fabricated molecular devices.

Because the tape is used for immersing the substrate in the etching solution, we attached a dummy sample on one end of the tape. Additionally, to prevent mechanical damage to the Au electrodes while handling the film, we removed the part of the tape above the substrate. Then, the top Au electrodes with a thin PMMA layer were detached from the dummy substrate by immersing the film into a potassium hydroxide (KOH) solution (~25 %) for approximately one hour. Because the SiO_2 layer on the substrate will be etched by this etching solution, the Au electrode can be detached. Finally, the detached transfer film was gently rinsed several times with deionized water and gently dried with a N_2 stream (see Figures 3.1.4(e) and 3.1.4(f)). By applying this film on the molecular monolayer, vertical metal-molecule-metal junctions were generated. To facilitate fine contact between the Au electrodes and the molecular layer, we added a couple of drops of isopropyl alcohol (IPA) to the molecular junction substrate before making contact with the transfer PMMA film. The capillary action resulting from the surface tension of IPA during vaporization enables

Molecules	# of fabricated devices	Fab. failure	Short	Open	Non-working	Working	Device yield
C8	128 (100.0%)	0 (0.0%)	25 (19.5%)	0 (0.0%)	1 (0.8%)	102 (79.7%)	
C12	128 (100.0%)	3 (2.3%)	14 (10.9%)	0 (0.0%)	19 (14.8%)	92 (71.9%)	272 (70.8%)
C16	128 (100.0%)	11 (8.6%)	12 (9.4%)	26 (20.3%)	1 (0.8%)	78 (60.9%)	

Table 3.1.1. Summary of the statistical analysis results for the molecular devices fabricated using the DMT method in this study.

the transfer film to make a fine contact with the molecular layer. Also we granted very low aspect ratio i.e. isolation wall height to junction width of the maximum 1:200. With this low aspect ratio, at least it is possible to make fine contact around the center of the junction except the edge of the isolation wall. Finally, the remaining PMMA was removed by dipping the samples in acetone. Figure 3.1.5 presents optical and scanning electron microscopy (SEM) images of the molecular junctions fabricated using this method. Through the use of this method, we were able to considerably improve the device yield (~70 %) with a pure metal-molecular monolayer-metal junction structure (Table 3.1.1). Finally note that this method is similar to previously reported polymer-assisted lift-off (PALO) method.[41]

3.1.3. Results and Discussion

One of the most remarkable advantages of fabricating molecular junctions using a solid-state device structure is the capability of mass production because the fabrication can be performed using conventional manufacturing processes. Mass production provides a statistically sufficient number of molecular devices to be analyzed. Additionally, the statistical analysis enables us to distinguish the genuine transport characteristics of

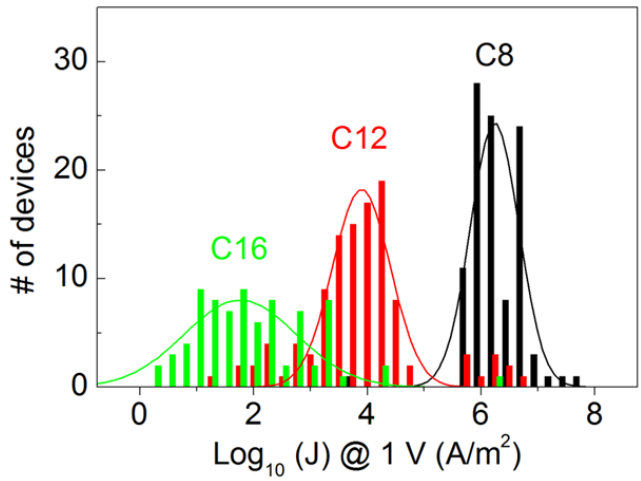

Figure 3.1.6. Histogram of the logarithmic current densities at 1 V for all 'candidate' molecular devices. Solid curves represent the Gaussian fitting results.

molecular junctions from uncertainly collected electrical information.[9,16,23,42] In this study, we fabricated a statistically meaningful number of molecular junctions. Specifically, 128 molecular junctions for each C8, C12 and C16 molecule were fabricated and analyzed (a total of 384 molecular junctions). Additionally, we found that the device yields were ~70 %, indicating that approximately 70% of the molecular junctions fabricated using this method exhibited molecularly determined charge transport properties (see Table 3.1.1). We defined 'molecularly working' devices based on the previously reported statistical criteria [9] and observed that the device yield remarkably improved compared to that (less than a few %) for the same device structure of metal-molecule-metal junctions in which the top electrodes were created using conventional evaporation.[9,19,21,23] For a brief explanation of the criteria, Figure 3.1.6 presents the histograms of $\log_{10}$ (current density (J)) values measured at 1.0 V for each 'candidate' C8, C12 and C16 molecular device. The candidate devices represent the molecular junctions that exhibit non-linear current-voltage characteristics, with the exception of obvious electrical shorts or open and fabrication

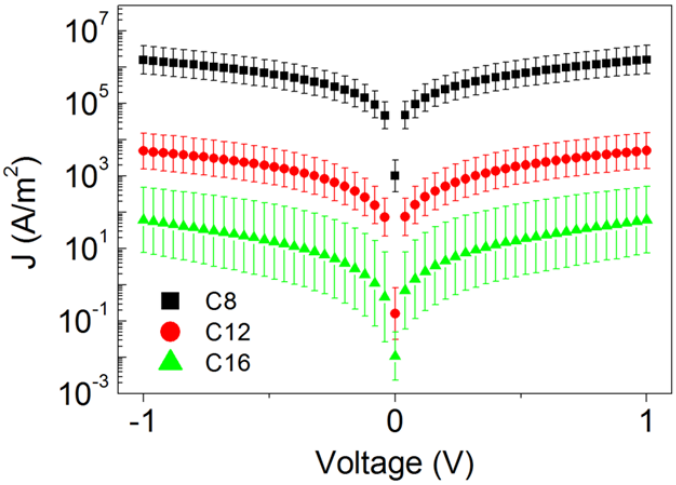

Figure 3.1.7. Statistical J-V data for all C8, C12, and C16 working devices. (b) Histogram of the logarithmic current densities at 1 V for all 'candidate' molecular devices. Solid curves represent the Gaussian fitting results.

failure. Then, we performed Gaussian fittings using the least squares method on the histograms using normal distribution functions,

$$f(x) = \frac{1}{\sqrt{2\pi\sigma^2}} \exp\left[-\frac{(x-\mu)^2}{2\sigma^2} \right] \qquad (1)$$

where μ is the Gaussian average, and σ is the Gaussian standard deviation. Finally, we limited the range of working devices such that the $\log_{10}$ (J) value lies within the arbitrarily chosen 3σ range corresponding to μ-3σ and μ+3σ. Through these criteria, we were able to select 99.7 % of the working devices from the entire population of candidates and determined the device yield to be ~70%.

Figure 3.1.7 shows the representative J-V characteristics of the working molecular devices in this study. Here, the error bars indicate the previously obtained Gaussian standard deviations of working molecular devices. According to a number of studies, the primary conduction mechanism through alkanethiolates is known as off-resonant

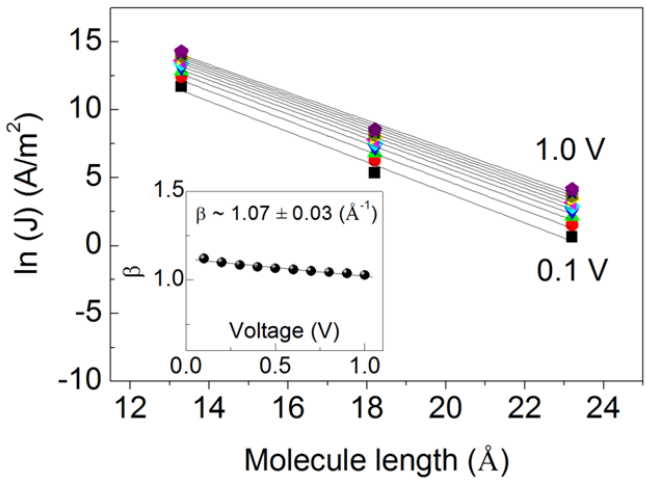

Figure 3.1.8. A semi-log plot of the current densities measured at different biases as a function of the molecular length. Solid lines represent the exponential fitting results, in which the slope is related to the decay coefficient β. The inset shows the values of deduced from the plot versus the applied bias.

tunneling.[9,43-45] Therefore, the exponential dependence of the current density on the molecular length (i.e., $J = J_0 \exp(-\beta d)$, where β is the decay coefficient and d is the molecular length) can be evidence for the actual realization of alkanethiolate molecular junctions.[5,9,13,16,23,43,44] We found that the current density was exponentially dependent on the molecular length, as shown in Figure 3.1.8. Figure 3.1.8 displays the semi-log plot of the current densities versus the molecular length from 0.1 to 1.0 V in increments of 0.1 V. From the magnitude of each linear fitting slope, which corresponds to the decay coefficient, we could determine β for each bias. The determined values of β for each bias are shown in the inset of Figure 3.1.8. The average value of β was determined to be 1.07 ± 0.03 Å^{-1}, which is in agreement with many previously reported studies on alkanethiolate molecular junctions.[43,46-51] To verify the off-resonant tunneling transport mechanism through alkanethiolates, we investigated the relationship between the

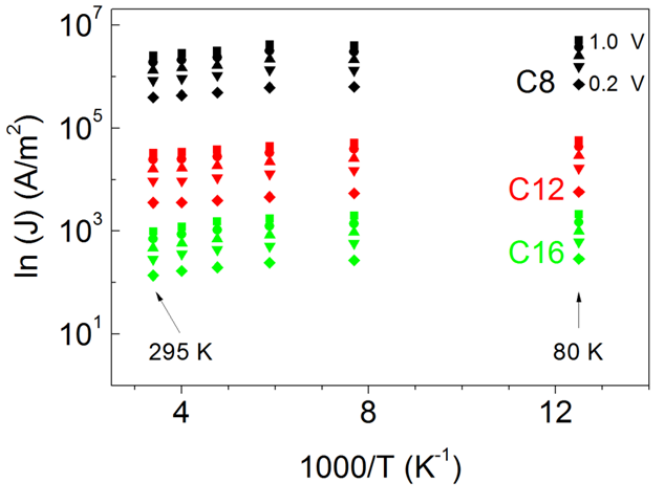

Figure 3.1.9. Arrhenius plot of the logarithmic current densities for C8, C12 and C16 molecular devices at different biases from 0.2 to 1.0 V in 0.2 V increments. The temperature was varied from 80 to 295 K in 40 K increments.

current density and temperature (T). Figure 3.1.9 shows the Arrhenius plots (i.e., ln (J) as a function of 1/T) at different biases ranging from 0.2 to 1.0 V in increments of 0.2 V. Additionally, the temperature was changed from 80 to 295 K in increments of 40 K. As shown in this figure, the molecular devices exhibited almost temperature-independent current density characteristics, providing direct evidence of tunneling transport properties. Through these fundamental electrical characterizations of the molecular junctions (Figures 3.1.7 to 3.1.9), we were able to confirm the feasibility of the proposed method as a high-yield testbed with metal-molecule-metal junctions. Figure 3.1.10(a) shows the J-V characteristics of evaporated Au-Au junctions and transferred Au-Au junctions. The error bars indicate the Gaussian standard deviation values for five junctions for each junction type. For reference, the representative J-V characteristics of C8 molecular junctions are presented in this plot. The inset of this figure shows the J-V characteristics at low bias regime in linear scale. As depicted in the plot, the current density of evaporated Au-Au

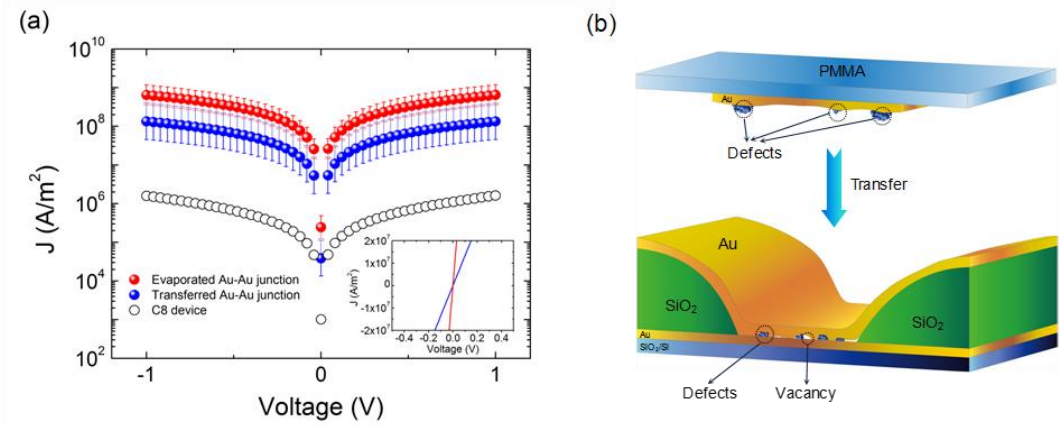

Figure 3.1.10. (a) Current density-voltage characteristics of evaporated Au-Au junction and transferred Au-Au junction. (b) Schematic illustration of transferred Au-Au junction.

junctions was found to be higher than that of transferred Au-Au junctions by a factor of ~3 in the magnitude. This may result from the transferring process to create top Au electrodes. Figure 3.1.10(b) shows a schematic image of the transferring process of top Au electrodes. Because the top Au electrodes are mechanically detached from a dummy substrate, there may exist contaminations on the surface of top Au electrodes like some defects and wrinkles as shown in Figure 3.1.10(b). Therefore, after the film is transferred on the exposed bottom Au/Ti electrodes, the defects and vacancy between the bottom and top electrodes will decrease the conductivity of transferred Au-Au junctions unlike evaporated Au-Au junctions.

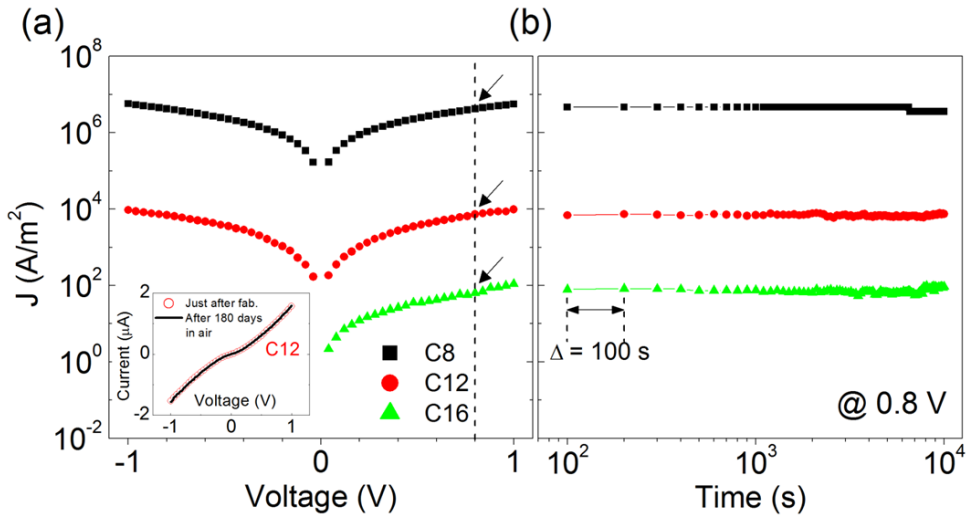

Figure 3.1.11. (a) J-V characteristics for representative C8, C12 and C16 molecular devices. The inset shows the J-V characteristics of a C12 molecular device measured immediately after fabrication (open circles) and after 180 days of exposure to ambient atmosphere (solid line). (b) Endurance characteristics of the molecular devices characterized by the current densities measured at 1.0 V for 10^4 s (measurement interval Δt = 100 s).

From the device application perspective, not only the device yield but also the stability and durability are crucial aspects of molecular junctions.[2,52,53] These aspects also reflect the reliability and reproducibility of the characteristics of molecular junctions. Therefore, the stability and durability should be considered one of the most important factors for verifying the validity of junction testbeds. Figure 3.1.11(a) presents the J-V characteristics of C8, C12 and C16 molecular junctions. Additionally, the inset of Figure 3.1.11(a) shows J-V curves of a representative C12 molecular junction. In this inset, we plotted the results that were measured immediately after the device was fabricated along with the results that were re-measured after 180 days after the device was exposed to ambient atmosphere. Although the molecular junction was exposed to oxygen and water vapor, no significant degradation in the transport characteristics was observed. Figure

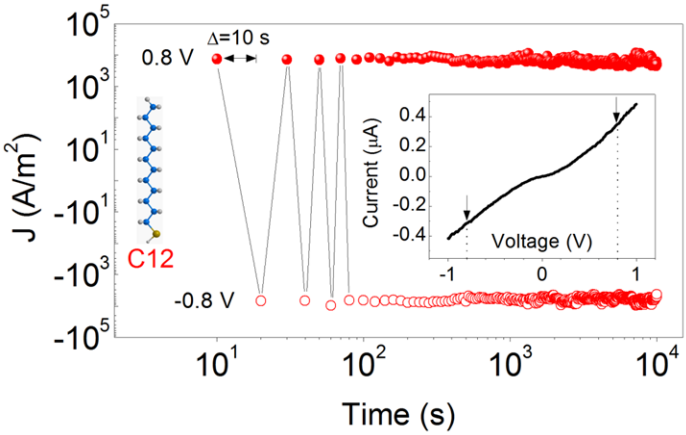

Figure 3.1.12. Retention characteristics of a C12 molecular device. The current densities were measured at positive bias (+0.8 V) and negative bias (-0.8 V) for 10^4 s with an interval $\Delta t = 10$ s.

3.1.11(b) presents the operational stability test results, in which the current densities were measured at 0.8 V (black arrows in Figure 3.1.11(a)) for each molecular junction as a function of time. The current density measurements were repeated every 100 s ($\Delta t = 100$ s) until 10^4 seconds, and it was observed that the current density characteristics were well maintained without significant degradation for 10^4 seconds. Furthermore, our molecular devices exhibited good retention properties, as indicated by the results shown in Figure 3.1.12. Even under repeated voltage stress conditions that varied from -0.8 to 0.8 V every 5 s for 10^4 s, the current densities measured at each bias did not notably change. These results reflect the excellent stability and durability of the molecular junctions fabricated using the DMT method in this study.

Now, we compare our method with other molecular device fabrication methods in terms of charge transport parameters. Among these parameters, junction conductivity (resistance) can be considered the main parameter for comparing each method. This parameter is related to the electronic coupling interaction between the molecular layer and

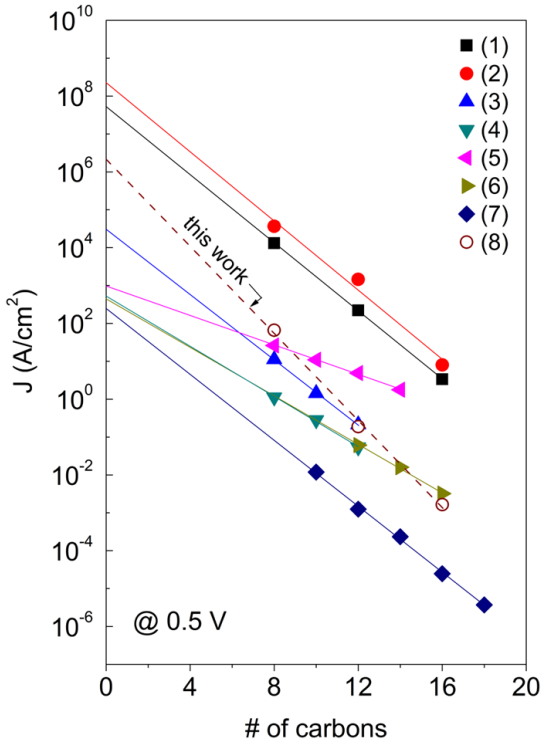

Figure 3.1.13. A semi-log plot of the current densities at 0.5 V as a function of the number of carbon bonds for various fabrication methods. Solid lines represent the exponential fitting results, in which the slope is related to the decay coefficient β and the y-intercept equals J_0. The symbols represent different device fabrication methods ((1) to (8); method (8) is the method proposed in this study), and the deduced parameters and detailed descriptions for the methods are presented in Table 3.1.2.

top electrode.[15,54,55] Strong electronic coupling is generally preferable because it can facilitate the observation of a variety of unique molecular transport properties via interactions between the molecular layer and electrode.[15,54,55] Figure 3.1.13 presents a semi-log plot of representative current densities (at a bias of -0.5 V) as a function of the number of carbon bonds for alkanethiolate molecular junctions fabricated using various methods that have been previously reported to be high-yield fabrication methods (device yield > 50 %; see Table 3.1.2). The solid lines represent the linear fits of the current densities in the semi-log plot. The magnitude of each slope is related to the decay

method #	Type of junction	Technique	β ($Å^{-1}$)	~J_0 @ 0.5 V (A/cm^2)	Yield (%)
(1) ■	Au-SAMs / Au	evporated Au / micropore	0.81-0.86	5.2×10^7	1.2-1.75
(2) ●	Au-SAMs / graphene- Au	graphene / micropore	0.85	2.3×10^8	90
(3) ▲	Au-SAMs / rGO-Au	solution-processed rGO	0.82	3.0×10^4	> 99
(4) ▼	Au-SAMs / polymer-Au	PEDOT:PSS / micropore	0.61	5.2×10^2	58
(5) ◀	Au-SAMs / polymer-Au	Aedotron P / nanopore	0.44	9.4×10^2	70-100
(6) ▶	Au-SAMs / Au	wedging transfer	0.58	4.4×10^2	38-50
(7) ◆	Ag-SAMs / GaO_x-EGaIn	thorugh-hole	0.80	2.5×10^2	78
(8) ○	Au-SAMs / Au	direct metal transfer	1.07	2.2×10^6	71

Table 3.1.2. Comparison of the experimental data between the DMT method of this study with other previously reported molecular device fabrication methods.

coefficient β, and the intercepts are equal to J_0, which gives to the inverse of the contact resistance. Each parameter determined from Figure 3.1.13 is summarized in Table 3.1.2. In Figure 3.1.13, each symbol from (1) to (7) represents a molecular junction fabrication method that has been previously reported by various research groups.[9,13,16,26,38,40,56,57] These fabrication methods are briefly explained in Table 3.1.2. The symbol (8) represents the molecular junctions fabricated using the DMT method in this study. The estimated value of β from our method was ~1.07 $Å^{-1}$, which is slightly larger than the values from other methods but in the range of previously reported values [43,46-51]. Comparison of this β value with other methods has been well established already can be an indirect and simple tool for judging whether the molecular junction is formed properly or not. In this respect, we can carefully conclude that our molecular junctions are appropriately generated by our new method. More importantly, the J_0 value using our method was determined to be ~2.2×10^6 A/cm^2, which is noticeably higher than the values obtained using other methods. In particular, most of the methods that adopt an intermediate layer exhibited relatively poor values of compared to our technique. This result suggests that the molecular junctions fabricated using our method possess good

contact properties and strong coupling between the molecular layer and top electrodes. However, the J_0 value in our method is less than that obtained in method (1) which directly evaporates the Au top electrode, mainly because of the transferring process to create top Au electrodes in our method, but method (1) typically exhibits a very low device yield (less than a few %). Here, we suppose that damage to the SAMs, nonconformal contact, and defects on the top Au film resulting from physical nature of our fabrication process may lead to degradation of electrical properties of our molecular junctions. Therefore, considering all these results, our DMT method can be considered a good molecular junction platform to provide a strong and stable electronic coupling between the top electrode and

Type of junction	Advantages	Disadvantages
Au-SAMs / Au (evaporated)	● relatively good contact ● various choice of top electrodes ● capability of mass production ● relatively easy fabrication ● low depedency of manufacturers ● low contact resistance ● nonvolatile, nontoxic	● very low yield (~1-2 %) ● physical damage to the SAM ● high dispersion in data ● waste of metals
Au-SAMs / graphene- Au	● high yield (~80-100 %) ● very stable over long period ● capacity of mass production ● low contact resistance ● nonvolatile, nontoxic	● physical contact of graphene (defects, damage to the SAM) ● high dispersion in data ● high dependecy of manufacturers ● restriction on choice of the top electrode ● fabrication is relatively difficult for practical applications
Au-SAMs / PEDOT:PSS-Au	● high yield (~100 %) ● very stable over long period ● capability of mass production ● relatively easy fabrication ● high reproducibility	● physical contact of polymer (defects, damage to the SAM) ● ambiguous interface between top contact ● restriction on choice of the top electrode
Si-SAMs / Hg	● relatively good contact ● high reproducibility	● restriction on choice of the top electrode ● damage to the SAM and bottom electrode ● low stability in time ● Hg is toxic and volatile. ● relatively low yield (~25 %)
Ag-SAMs / GaO_x-EGaIn	● high yield (~80-100 %) ● nonvolatile, nontoxic ● high reproducibility ● relatively good contact ● low damage to the SAM and bottom electrode	● restriction on choice of the top electrode ● ambiguous interface between top contact ● relatively low stability for practical applications
Au-SAMs / Au (this work)	● relatively high yield (~70 %) ● nonvolatile, nontoxic ● various choice of top electrodes ● capability of mass production ● stable over long period	● physical contact of the top electrode (defects, damage to the SAM) ● high dependecy of manufacturers ● high dispersion in data ● fabrication is relatively difficult for practical applications

Table 3.1.3. Comparison of the strengths and weaknesses between our method with other methods.

molecular layer with a high device yield.

Finally, we discuss in details the advantages and disadvantages of our method in comparison with other methods. To this end, we carefully selected five different methods which received the intensive attention of different research groups in this field and compared their advantages and disadvantages each other as summarized in Table 3.1.3. Based on the comparison, our new method has several strengths compared to other methods, for example: (1) the structure of our molecular junction is familiar and comfortably conservative system because the two electrodes are made of common metals. This familiarity provides convenience in utilization that enables to reproduce the molecular junctions easily. (2) Because of the usage of the common metals for the electrodes, the molecular junctions can be diversified simply by choosing the kind of metals to one's preference. Generally, it is known that various common metals have peculiar effects on molecules such as different energy band alignment, packing density, and magnetic effects. Therefore by choosing various kinds of metal electrodes for molecular junctions, we can also diversify the functionality of molecular junctions. (3) The capability of mass production with high-yield junctions enables us to distinguish the genuine transport characteristics of molecular junctions from uncertainly collected electrical information. Because of its very small size of molecules, generally it is very difficult to generate the perfectly same molecular junctions among each fabrication. This brings variation in experimental data among each molecular junction that makes it hard to investigate the genuine properties of molecular junctions. Therefore, statistical analysis being available by the mass production of molecular junctions makes it possible to overcome this problem. Together with these advantages, however, there are limits to our method. (1) Because of its physical nature of establishing the top electrode contact with the SAMs, it might not be

possible to achieve ideal conformal contact. While preparing thin gold film, there were several physical processes which can bring defects on the surface of the thin gold film such as etching, rinsing, drying the film that will eventually damage the SAMs. This damage and irregular contact can result in unexpected errors in the experimental data. (2) The electrical data of our molecular junctions show relatively large dispersion which implies the molecular junction lacks homogeneity. We suspect that this large dispersion originates from the physical nature of our fabrication process which results in damage to the SAMs and irregular contact properties as mentioned above. Also, the dispersion can be influenced by roughness of gold surface of bottom electrode. (3) Our fabrication method is not trivial and demands a hard effort to produce the molecular junctions because the fabrication process should be handled carefully. Therefore, this method may not be suitable for practical applications of molecular electronic devices. Based on these strengths and weaknesses, there are some cases where these junctions can be applicable, for example, (1) when the statistical analysis should be applied to distinguish the genuine transport characteristics of molecular junctions especially with metal-SAMs-metal structure from uncertainly collected electrical information, and (2) when the various choices of metal electrodes that have different contact properties with the SAMs should be utilized to enrich the functionalities of molecular junctions. These cases are commonly necessary to investigate the intrinsic properties of molecules from the scientific point of view.

3.1.4. Chapter Summary

Conclusively in this chapter, we have demonstrated a new technique for fabricating high-yield molecular junctions in a vertical metal-molecule-metal structure in which the top metal electrodes are formed on alkanethiolate molecules using a direct metal transfer

method. The molecular junctions fabricated using this method exhibited the well-known tunneling transport characteristics of alkanethiolates with good stability, durability, and device lifetime properties, which are important factors for the practical application of molecular devices. Based on the comparison of our method with other previously reported molecular device fabrication methods, our method appears to provide stronger and more stable electronic coupling between the top electrode and molecular layer, resulting in better contact properties. Our new approach may be a probable way to achieve a reliable platform for the precise characterization and practical application of molecular electronic junctions. Further study can be an improvement of the rectification ratio of ferrocene-alkanethiolate molecular junctions by utilizing proper top metal electrodes that are transferred onto the SAMs to exhibit both high device-yield and work function matching.

References

[1] Chen, J.; Reed, M. A.; Rawlett, A. M.; Tour, J. M. *Science* **1999**, *286*, 1550.

[2] Green, J. E.; Choi, J. W.; Boukai, A.; Bunimovich, Y.; Johnston-Halperin, E.; DeIonno, E.; Luo, Y.; Sheriff, B. A.; Xu, K.; Shin, Y. S.; Tseng, H. -R.; Stoddart, J. F.; Heath, J. R. *Nature* **2007**, *445*, 414.

[3] Lafferentz, L.; Ample, F.; Yu, H.; Hecht, S.; Joachim, C.; Grill, L. *Science* **2009**, *323*, 1193.

[4] Reed, M. A.; Zhou, C.; Muller, C. J.; Burgin, T. P.; Tour, J. M. *Science* **1997,** *278*, 252-254.

[5] Akkerman, H. B.; Blom, P. W. M.; de Leeuw, D. M.; de Boer, B. *Nature* **2006,** *441*, 69.

[6] Chen, X.; Yeganeh, S.; Qin, L.; Li, S.; Xue, C.; Braunschweig, A. B.; Schatz, G. C.; Ratner, M. A.; Mirkin, C. A. *Nano Lett.* **2009**, *9*, 3974.

[7] Choi, S. H.; Kim, B.; Frisbie, C. D. *Science* **2008**, *320*, 1482.

[8] Haick, H.; Cahen, D. *Acc. Chem. Res.* **2008,** *41*, 359-366.

[9] Kim, T. W.; Wang, G. N.; Lee, H.; Lee, T. *Nanotechnology* **2007,** *18*, 315204.

[10] Liang, W. J.; Shores, M. P.; Bockrath, M.; Long, J. R.; Park, H. *Nature* **2002,** *417*, 725.

[11] Loo, Y. L.; Lang, D. V.; Rogers, J. A.; Hsu, J. W. P. *Nano Lett.* **2003,** *3*, 913-917.

[12] Park, J.; Pasupathy, A. N.; Goldsmith, J. I.; Chang, C.; Yaish, Y.; Petta, J. R.; Rinkoski, M.; Sethna, J. P.; Abruna, H. D.; McEuen, P. L.; Ralph, D. C. *Nature* **2002,** *417*, 722.

[13] Park, S.; Wang, G.; Cho, B.; Kim, Y.; Song, S.; Ji, Y.; Yoon, M. H.; Lee, T. *Nat. Nanotechnol.* **2012,** *7*, 438.

[14] Song, H.; Kim, Y.; Jang, Y. H.; Jeong, H.; Reed, M. A.; Lee, T. *Nature* **2009,** *462*, 1039.

[15] Venkataraman, L.; Klare, J. E.; Nuckolls, C.; Hybertsen, M. S.; Steigerwald, M. L. *Nature* **2006,** *442*, 904.

[16] Wang, G.; Kim, Y.; Choe, M.; Kim, T. W.; Lee, T. *Adv. Mater.* **2011,** *23*, 755.

[17] Wang, W. Y.; Lee, T.; Kretzschmar, I.; Reed, M. A. *Nano Lett.* **2004,** *4*, 643-646.

[18] Xu, B. Q.; Tao, N. J. *Science* **2003,** *301*, 1221-1223.

[19] de Boer, B.; Frank, M. M.; Chabal, Y. J.; Jiang, W. R.; Garfunkel, E.; Bao, Z. *Langmuir* **2004,** *20*, 1539-1542.

[20] Fisher, G. L.; Walker, A. V.; Hooper, A. E.; Tighe, T. B.; Bahnck, K. B.; Skriba, H. T.; Reinard, M. D.; Haynie, B. C.; Opila, R. L.; Winograd, N.; Allara, D. L. *J. Am. Chem. Soc.* **2002,** *124*, 5528.

[21] Haick, H.; Niitsoo, O.; Ghabboun, J.; Cahen, D. *J. Phys. Chem. C* **2007,** *111*, 2318-2329.

[22] Walker, A. V.; Tighe, T. B.; Cabarcos, O. M.; Reinard, M. D.; Haynie, B. C.; Uppili, S.; Winograd, N.; Allara, D. L. *J. Am. Chem. Soc.* **2004,** *126*, 3954-3963.

[23] Wang, G.; Kim, T. W. Lee, H.; Lee, T. *Phys. Rev. B* **2007,** *76*, 205320.

[24] Jeong, H., et al. *Adv. Funct. Mater.* **2014**, *24*, 2472-2480.

[25] Min, M.; Seo, S.; Lee, S. M.; Lee, H. *Adv. Mater.* **2013,** *25*, 7045-7050.

[26] Seo, S.; Min, M.; Lee, J.; Lee, T.; Choi, S. Y.; Lee, H. *Angew. Chem., Int. Ed.* **2012,** *51*, 108-112.

[27] Seo, S.; Min, M.; Lee, S. M.; Lee, H. *Nat. Commun.* **2013**, *4*.

[28] Li, T.; Hauptmann, J. R.; Wei, Z.; Petersen, S.; Bovet, N.; Vosch, T.; Nygard, J.; Hu, W.; Liu, Y.; Bjornholm, T.; Norgaard, K.; Laursen, B. W. *Adv. Mater.* **2012**, *24*, 1333.

[29] Li, T.; Jevric, M.; Hauptmann, J. R.; Hviid, R.; Wei, Z.; Wang, R.; Reeler, N. E. A.; Thyrhaug, E.; Petersen, S.; Meyer, J. A. S.; Bovet, N.; Vosch, T.; Nygard, J.; Qiu, X.; Hu, W.; Liu, Y.; Solomon, G. C.; Kjaergaard, H. G.; Bjornholm, T.; Nielsen, M. B.; Laursen, B. W.; Norgaard, K. *Adv. Mater.* **2013**, *25*, 4164.

[30] Kang, J.; Shin, D.; Bae, S.; Hong, B. H. *Nanoscale* **2012**, *4*, 5527.

[31] Li, X.; Zhu, Y.; Cai, W.; Borysiak, M.; Han, B.; Chen, D.; Piner, R. D.; Colombo, L.; Ruoff, R. S. *Nano Lett.* **2009**, *9*, 4359.

[32] Reina, A.; Jia, X.; Ho, J.; Nezich, D.; Son, H.; Bulovic, V.; Dresselhaus, M. S.; Kong, J. *Nano Lett.* **2009**, *9*, 30.

[33] Song, H.; Lee, T.; Choi, N. J.; Lee, H. *Appl. Phys. Lett.* **2007,** *91*, 253116.

[34] Kim, Y.; Hellmuth, T. J.; Sysoiev, D.; Pauly, F.; Pietsch, T.; Wolf, J.; Erbe, A.; Huhn, T.; Groth, U.; Steiner, U. E.; Scheer, E. *Nano Lett.* **2012,** *12*, 3736-3742.

[35] Xiang, D.; Jeong, H.; Lee, T.; Mayer, D. *Adv. Mater.* **2013**, *25*, 4845.

[36] Engelkes, V. B.; Beebe, J. M.; Frisbie, C. D. *J. Am. Chem. Soc.* **2004,** *126*, 14287.

[37] Chu, C. W.; Na, J. S.; Parsons, G. N. *J. Am. Chem. Soc.* **2007,** *129*, 2287-2296.

[38] Wan, A.; Jiang, L.; Sangeeth, C. S. S.; Nijhuis, C. A. *Adv. Funct. Mater.* **2014,** *24*, 4442-4456.

[39] Nijhuis, C. A.; Reus, W. F.; Barber, J. R.; Whitesides, G. M. *J. Phys. Chem. C* **2012,** *116*, 14139-14150.

[40] Wang, G.; Yoo, H.; Na, S. I.; Kim, T. W.; Cho, B.; Kim, D. Y.; Lee, T. *Thin Solid Films* **2009,** *518*, 824-828.

[41] Vilan, A.; Cahen, D. *Adv. Funct. Mater.* **2002**, *12*, 795–807.

[42] Kim, Y.; Wang, G.; Choe, M.; Kim, J.; Lee, S.; Park, S.; Kim, D. Y.; Lee, B. H.; Lee, T. *Org. Electron.* **2011,** *12*, 2144-2150.

[43] Wang, W. Y.; Lee, T.; Reed, M. A. *Phys. Rev. B* **2003,** *68*, 035416.

[44] Wang, W. Y.; Lee, T.; Reed, M. A. *Rep. Prog. Phys.* **2005,** *68*, 523-544.

[45] Zhitenev, N. B.; Erbe, A.; Bao, Z. *Phys. Rev. Lett.* **2004**, *92*, 186805.

[46] Bumm, L. A.; Arnold, J. J.; Dunbar, T. D.; Allara, D. L.; Weiss, P. S. *J. Phys. Chem. B* **1999**, *103*, 8122.

[47] Fan, F. R. F.; Yang, J. P.; Cai, L. T.; Price, D. W.; Dirk, S. M.; Kosynkin, D. V.; Yao, Y. X.; Rawlett, A. M.; Tour, J. M.; Bard, A. J. *J. Am. Chem. Soc.* **2002**, *124*, 5550.

[48] Holmlin, R. E.; Haag, R.; Chabinyc, M. L.; Ismagilov, R. F.; Cohen, A. E.; Terfort, A.; Rampi, M. A.; Whitesides, G. M. *J. Am. Chem. Soc.* **2001,** *123*, 5075.

[49] Kaun, C. C.; Guo, H. *Nano Lett.* **2003,** *3*, 1521-1525.

[50] Smalley, J. F.; Feldberg, S. W.; Chidsey, C. E. D.; Linford, M. R.; Newton, M. D.; Liu, Y. P. *J. Phys. Chem.* **1995**, *99*, 13141.

[51] Wold, D. J.; Haag, R.; Rampi, M. A.; Frisbie, C. D. *J. Phys. Chem. B* **2002,** *106*, 2813.

[52] Nijhuis, C. A.; Reus, W. F.; Whitesides, G. M. *J. Am. Chem. Soc.* **2009**, *131*, 17814.

[53] Van Hal, P. A.; Smits, E. C. P.; Geuns, T. C. T.; Akkerman, H. B.; De Brito, B. C.; Perissinotto, S.; Lanzani, G.; Kronemeijer, A. J.; Geskin, V.; Cornil, J.; Blom, P. W. M.; De Boer, B.; De Leeuw, D. M. *Nat. Nanotechnol.* **2008,** *3*, 749-754.

[54] Joachim, C.; Ratner, M. A. *P. Natl. Acad. Sci. U.S.A.* **2005**, *102*, 8801.

[55] Venkataraman, L.; Klare, J. E.; Tam, I. W.; Nuckolls, C.; Hybertsen, M. S.; Steigerwald, M. L. *Nano Lett.* **2006**, *6*, 458.

[56] Krabbenborg, S. O.; Wilbers, J. G. E.; Huskens, J.; van der Wiel, W. G. *Adv. Funct. Mater.* **2013**, *23*, 770.

[57] Neuhausen, A. B.; Hosseini, A.; Sulpizio, J. A.; Chidsey, C. E. D.; Goldhaber-Gordon, D. *ACS Nano* **2012,** *6*, 9920-9931.

3.2. Investigation of Inelastic Electron Tunneling Spectra of Metal-Molecule-Metal Junctions Fabricated Using Direct Metal Transfer Method

In this chapter, we measured the inelastic electron tunneling spectroscopy (IETS) characteristics of metal-molecule-metal junctions made with alkanethiolate self-assembled monolayers. The molecular junctions were fabricated using DMT method, which we previously reported for high-yield metal-molecule-metal junctions. The measured IETS data could be assigned to molecular vibration modes that were determined by the chemical structure of the molecules. We also observed discrepancies and device-to-device variations in the IETS data that possibly originate from defects in the molecular junctions and insulating walls introduced during the fabrication process and from the junction structure.

3.2.1. Introduction

In the field of molecular electronics, extensive studies on the electrical properties of single molecules or SAMs have been performed to understand the intrinsic charge transport mechanisms of molecular junctions and for realization of molecular-scale electronic devices.[1,2] Many researchers have reported numerous structures and platforms for fabricating molecular electronic junctions.[1,2] Among these, solid-state junction-based molecular electronic devices have the virtue of simple and massive production of molecular junctions for studying the charge transport characteristics using current-voltage characterization, temperature-variable analysis,[3] transition voltage spectroscopy,[4] and inelastic electron tunneling spectroscopy (IETS). In particular, IETS has been a powerful tool not only for verifying the existence of molecules in molecular junctions but also for investigating the effects of the molecules on the electronic charge transport characteristics,

molecule-metal contact information, etc.[5-9] Most of the IETS data were successfully obtained and analyzed from “pure” metal-molecule-metal junctions where the molecules are simply bridged between two metal electrodes. Here, a pure metal-molecule-metal junction means a molecular junction fabricated without the involvement of any interlayers, such as conducting polymers or graphene films, in the junctions.[10] However, pure metal-molecule-metal junctions exhibit very low device yield because of the difficulty of forming a reliable electrical contact with the molecules because of electrical short problems.[11] To overcome this issue in a pure metal-molecule-metal junction structure, we presented a new approach for high-yield molecular junctions in previous section,[12] in which we performed various electrical characterizations, for example, current-voltage characterization and statistical analysis to confirm the molecular junctions. However, to strongly verify the formation of metal-molecule-metal junctions and the existence of molecules in the junctions, a more direct detection technique of molecules such as IETS is essential for this purpose. In addition, by investigating the IETS data, one can obtain information about the condition of molecular junctions such as the contact geometry and molecular conformation in the junctions.[5,13,14] Despite the importance, however, only a few studies have been reported, especially for SAMs-based molecular junctions, mainly because of the difficulty of forming reliable junctions.[6,8,15,16] Therefore, it is necessary to perform the IETS experiments in a high-yield and reliable device testbed to accessibly investigate the intrinsic properties of the molecules.

In this chapter, we report on the IETS characteristics of alkanethiolate metal-molecule-metal junctions fabricated using the DMT method, which we previously reported for high-yield metal-molecule-metal junctions without involving any interlayers. We could assign the measured IETS data to molecular vibration modes, which are clearly sensitive

to the chemical structure of the molecules. With the observation, interestingly, we also observed discrepancies and device-to-device variations in the IETS data, such as negative values or dips and peaks that cannot be assigned to any possible vibrational modes of the alkanethiolate molecules. We determined that these types of discrepancies and variations originate from the defects in the SAMs, which result from the specific molecular device structure and device fabrication process.

3.2.2. Experimental

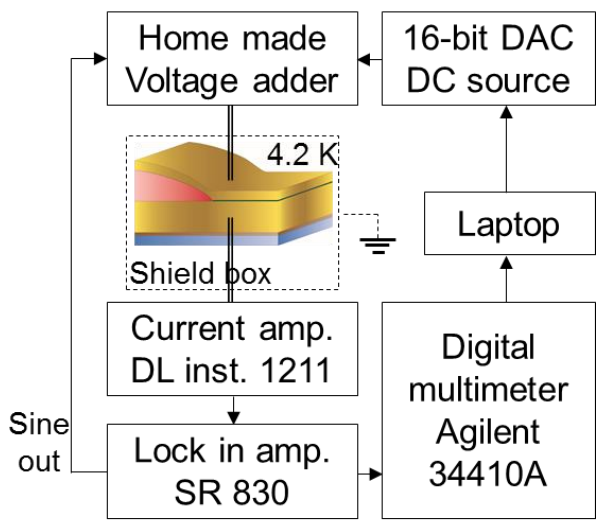

Figure 3.2.1. Circuit diagram of the IETS measurement system.

To fabricate the molecular junctions, we followed the same fabrication process reported in chapter 3.1. The IETS measurements can be performed using various measurement circuit techniques.[17] Specifically, in our study, we adopted a standard AC modulation technique to investigate the IETS characteristics. Figure 3.2.1 explains the schematic circuit diagram of our homemade IETS measurement system. The IETS measurement was performed at 4.2 K to reduce thermal broadening of the main signals

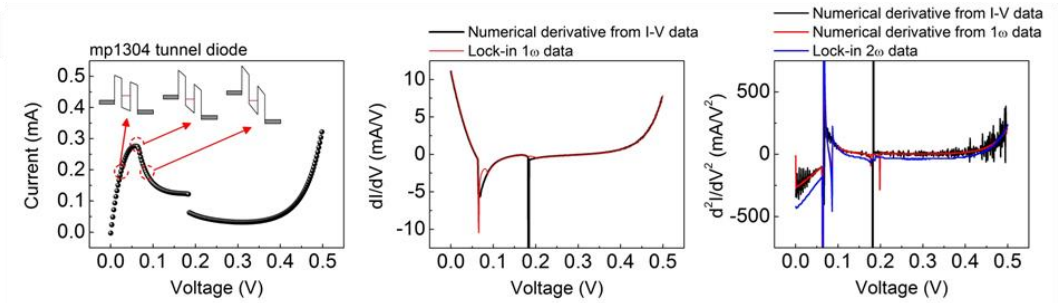

Figure 3.2.2. dI/dV, d^2I/dV^2 characteristics of a resonant tunnel diode (M-pulse Microwave, mp1304 tunnel diode) measured at room temperature.

with cryogenic measurement equipment.[5,6,8] The molecular devices were mounted on a 16-pin IC chip carrier socket on the sample stage inside a vacuum chamber that was electrically isolated from a power ground by a shield box before being dipped into a liquid-He-filled dewar. To measure the dI/dV and d^2I/dV^2 data directly, a standard AC lock-in technique was employed.[6,8] In practice, because only a small portion (< 1 %, as shown in Figure 1.3.3 in chapter 1.3) of electrons exhibit inelastic tunneling behavior,[18] a high signal-to-noise measurement technique is essential to detect the IETS data. We used a 16-bit digital-to-analog converter (DAC), which was controlled by a laptop for DC bias voltages, and we used a reference signal of the lock-in amplifier (Stanford Research Systems 830) as an AC modulation bias. The DC bias voltages were swept from 0 to 0.4 V with an increment of 305 μV, and an AC modulation bias of 7.8 mV (RMS value) at a frequency of 1033 Hz was applied. After these two biases were added using a home-made voltage adder,[7,19] the bias was applied to the sample to obtain the second harmonic signals, proportional to d^2I/dV^2. Then, the output current signal was converted and amplified from a current signal to a voltage signal with a low-noise current amplifier (DL instrument 1211). Finally, using a phase-sensitive detector (PSD) in the lock-in amplifier and a digital multimeter (Agilent 34410A), the second harmonic signal, which is directly

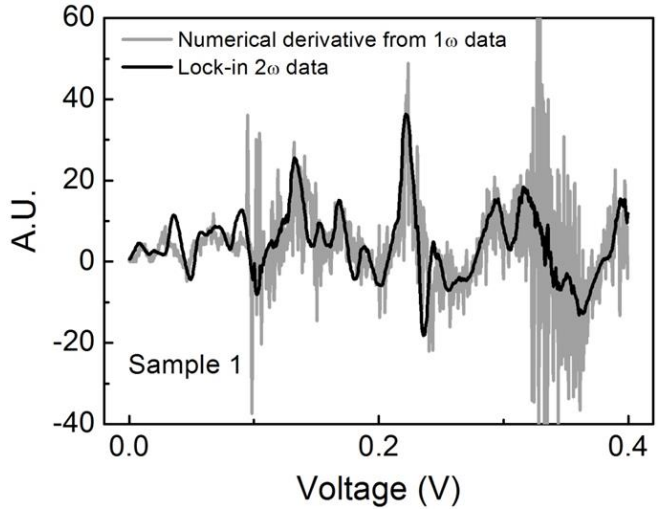

Figure 3.2.3. Comparison between the lock-in 2ω data and the numerical derivative of the lock-in 1ω data obtained for a C12 molecular junction.

proportional to d^2I/dV^2, was measured.[7,8,19] Note that because of this PSD technique, the second harmonic signal has a higher signal-to-noise ratio than the numerical differentiation of the dI/dV data. To verify the inelastic tunneling process and our IETS measurement system, we performed IETS measurements on a resonant tunneling diode (RTD) device. An RTD is a diode with a resonant-tunneling structure for which the I-V characteristics often exhibit negative differential resistance regions (NDR).[20] This unique electrical characteristic enables an RTD to be a good test sample for examining our instrument setup. The lock-in 2ω measurement result, the numerical derivative of the lock-in 1ω measurement result, and the second numerical derivative of the I-V characteristics of an RTD test sample show similar trajectories with each other, which indicates that our measurement system is available to perform the IETS experiments (see Figure 3.2.2). Figure 3.2.2 shows the I-V, dI/dV, and d^2I/dV^2 characteristics of a RTD sample (M-pulse Microwave, mp1304 tunnel diode) at room temperature. In the left plot of Figure 3.2.2, there are two distinctive NDR regions that are associated with some resonant states in the

energy band diagram. These regions appear as NDR peaks in the dI/dV plot. As shown in the middle plot of Figure 3.2.2, the lock-in 1ω measurement result obtained by the aforementioned instrument setup and the numerical derivative of the I-V characteristics overlap well with each other except for a very low dip at ~0.17 V, which results from insufficient resolution of the measurement device to detect the abrupt change of 1ω value.

In addition, another important finding here is that the numerical differentiation of the I-V characteristics exhibits 2ω spectra with a low signal-to-noise ratio, making it difficult to distinguish individual IETS peaks (see also Figure 3.2.3). Figure 3.2.3 shows the lock-in 2ω data and the numerical derivative of the lock-in 1ω data of a C12 molecular junction. As shown in this figure, the overall trajectory of the numerical derivative of the first harmonic signal is compatible with the directly obtained second harmonic signal, but the numerical derivative curve is too noisy and the lock-in measurement yields a much more resolved spectra. Hence, a high signal-to-noise measurement technique such as the lock-in technique is essential to detect the IETS signal.

3.2.3. Results and Discussion

Figure 3.2.4 shows the current density-voltage characteristics (J-V) of six selected C12 molecular junctions with pore sizes of 3 and 4 μm in radius that were used for IETS measurements in this study. Note that the molecular devices fabricated by the DMT method had already been characterized at room temperature (see Table 3.1.1 in chapter 3.1), and in this present study we performed the IETS experiments of a few molecular devices that were randomly selected based on a convenient location for chip-cutting and wire-bonding. These six C12 J-V data sets are presented as orange-colored circular symbols in distributions of J-V data sets (see Table 3.1.1) for octanethiol ($HS(CH_2)_7CH_3$, denoted as C8), C12, and

hexadecanethiol ($HS(CH_2)_{15}CH_3$, denoted as C16) for comparison (These were measured at room temperature).[12] Because alkanethiolates are insulating molecules with saturated alkyl chains, the overall transport mechanism is direct tunneling, which results in sigmoidal-shape curves in the individual I-V curves (inset of Figure 3.2.4) and exponential dependence of the current densities on the molecular length.[8,21] This dependency makes the tunneling current density (or conductance) decrease as the molecular length increases (i.e., conductance ~ exp(-βd), where β is the decay coefficient and d is the molecular length). As observed in Figure 3.2.4, the current density of our working molecular junctions decreased as the number of carbon chains increased; we observed a β value of ~1.0 $Å^{-1}$, which agrees with the literature values.[22] The selected six C12 samples exhibited consistent current density values upon bias sweep in the range of the C12 devices. It is noteworthy that the J-V characteristics of the molecular samples exhibit no particular features corresponding to vibrational modes of the molecules (see Figure 3.2.4); however,

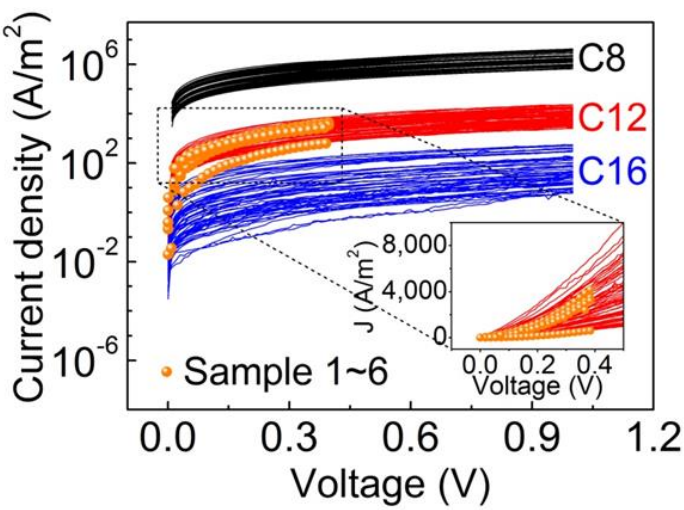

Figure 3.2.4. J-V characteristics of six different C12 molecular junctions (orange-colored circular symbols) with data sets of C8 and C16 molecular junctions. The inset shows J-V curves on the linear J scale.

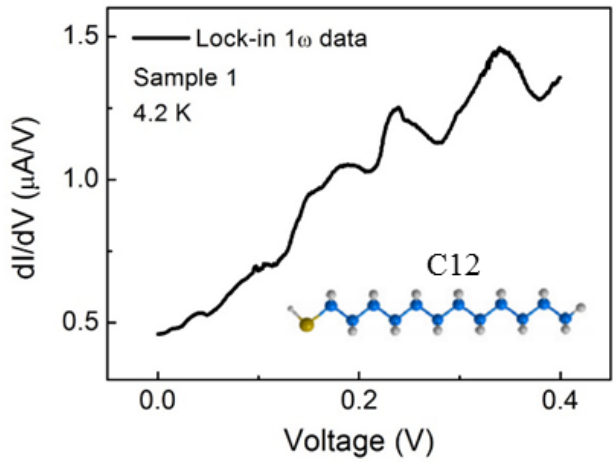

Figure 3.2.5. The first harmonic signal (dI/dV) of a C12 molecular junction obtained by lock-in technique at 4.2 K.

directly obtained dI/dV data (Figure 3.2.5) and d^2I/dV^2 data (Figure 3.2.6) proportional to the first and second harmonic signals from the lock-in amplifier exhibit distinctive trajectories, which can be assigned to the various vibrational modes of the C12 molecule.

Figure 3.2.6 presents the IETS data measured at 4.2 K for the six C12 molecular junctions fabricated using the DMT method. Note that the I-V measurement results at room temperature using the probe station presented high device yields,[12] but the IETS measurements at 4.2 K requires several processes such as sample cutting, wire-bonding, chip mounting, and heat cycle to 4.2 K. So, by doing these steps, the initially working ultra-thin molecular junctions can easily become malfunctioning (mostly becoming electrical short) during the IETS experiments. Therefore, measuring many devices' IETS data is time-prohibitive. The spectra were stable upon successive bias sweep (see Figure 3.2.7) which indicates the obtained IETS data are not randomly distributed artifact. On the other hands, a little bit varation in the singal is possibly related to dynamical molecular conformation changes induced by bias sweeping. And the characteristic vibration peaks of the molecules

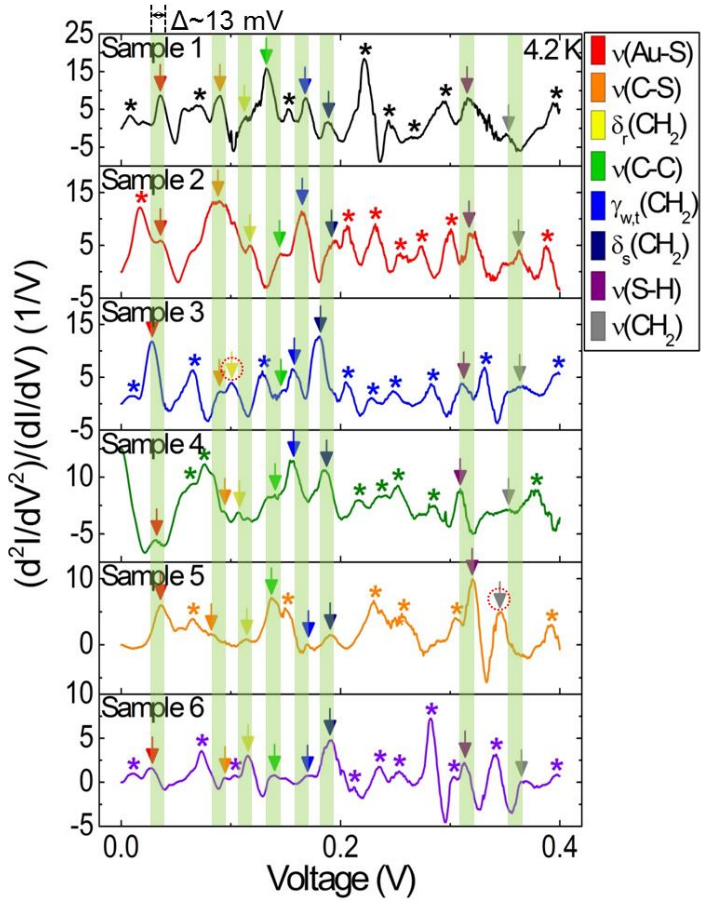

Figure 3.2.6. IETS data of six C12 molecular junctions measured at 4.2 K. Each arrow indicates the corresponding molecular vibration modes of the C12 molecule. Peaks that cannot be assigned to any possible vibrational modes of the molecule are marked with asterisks. In this plot, shaded squares are used to compare each characteristic peak from device to device.

were observed repetitively for different molecular junctions. We assigned the observed spectral peaks to specific molecular vibrations by comparison with previously reported infrared, Raman, high-resolution electron energy loss spectroscopy, and IETS measurements and density functional theory calculation results.[23-25] The peak positions related to molecular vibration of the six molecular junctions with its mean value and error (standard deviation) are summarized in Table 3.2.1. The peaks are observed at

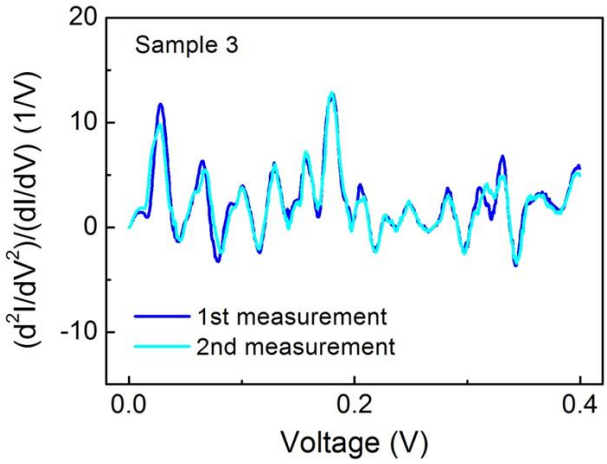

Figure 3.2.7. Plot of the IETS data of a C12 molecular junction under repeated measurements.

approximately 30, 85, 105, 135, 160, 185, 315, and 360 mV, which correspond to ν(Au-S) stretching, ν(C-S) stretching, $\delta_r(CH_2)$ rocking, ν(C-C) stretching, $\gamma_{w,t}(CH_2)$ wagging, $\delta_s(CH_2)$ scissoring, ν(S-H) stretching, and $\nu(CH_2)$ stretching modes, respectively. Most of these peaks except $\delta_r(CH_2)$ of sample 3 and $\nu(CH_2)$ of sample 5 (marked as red circles in Figure 3.2.6) that represent the CH_2 rocking mode and CH_2 stretching mode were observed from all six molecular junctions in a certain range of the bias window (~13 mV), which indicates that the molecular junctions truly consisted of C12 molecules. In addition to these

Peak position (in mV)						Mean value and Error (standard deviation)	Mode assignment
Sample 1	Sample 2	Sample 3	Sample 4	Sample 5	Sample 6		
35.4	35.1	28.1	31.7	35.4	27.8	32.3 ± 3.6	ν(Au-S)
89.1	88.5	89.1	93.4	85.1	94	89.9 ± 3.3	ν(C-S)
113.8	116.6	101.1	107.1	113.8	114.4	111.1 ± 5.9	$\delta_r(CH_2)$
133.9	144.6	146.5	138.6	137.3	139.2	140.0 ± 4.7	ν(C-C)
167.8	164.8	156.3	156.9	168.5	168.8	163.9 ± 5.8	$\gamma_{w,t}(CH_2)$
188.3	193.1	181	185.2	189.8	190.4	188.0 ± 4.3	$\delta_s(CH_2)$
317.1	318.9	311.9	310.7	319.8	312.8	315.2 ± 3.9	ν(S-H)
353.4	361.9	362.5	354.6	346.9	364.1	357.2 ± 6.7	$\nu(CH_2)$

Table 3.2.1. Summary of vibrational modes assigned to the IETS spectra of Au-dodecanethiol-Au junctions.

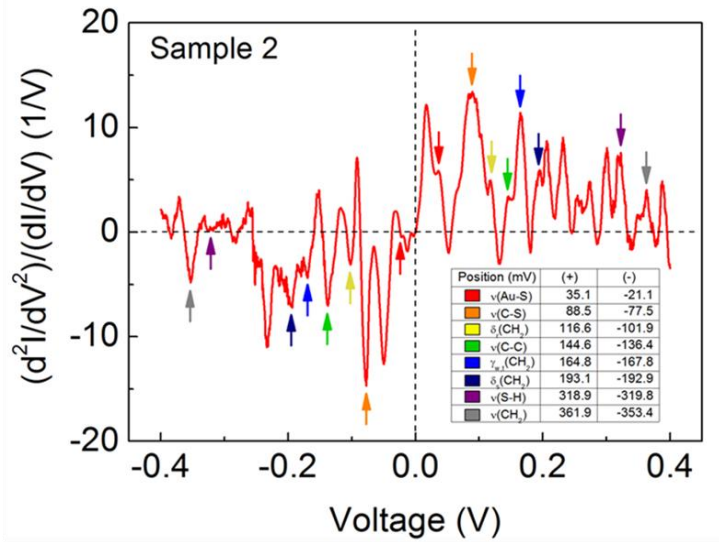

Figure 3.2.8. IET spectra of sample 2 at both bias regime.

peaks, however, unexpected features in the IETS characteristics were also observed; some peaks could not be assigned to any possible molecular vibration modes (marked as asterisks in Figure 3.2.6) and dips.[8,15,26] In addition, the overall trajectories of each signal and normalized intensity of peaks ($(d^2I/dV^2)/(dI/dV)$) exhibited different behavior from device to device despite having similar J-V characteristics. The origin of these discrepancies in the IETS characteristics of molecular junctions will be discussed in detail later. Nonetheless, the overall accordance between the peak positions and referential vibration modes suggest that the IETS signal in Figure 3.2.6 represents the vibrational characteristics of C12 molecular junctions. Also the spectra of opposite bias (negative bias) show almost anti-symmetric behaviors as expected (see Figure 3.2.8). The IET spectra shows almost anti-symmetric characteristics of the molecular vibrations.[27] The dips were observed at approximately -30, -85, -105, -135, -160, -185, -315, and -360 mV, which correspond to ν(Au-S) stretching, ν(C-S) stretching, $\delta_r(CH_2)$ rocking, ν(C-C) stretching, $\gamma_{w,t}(CH_2)$

wagging, $\delta_s(CH_2)$ scissoring, ν(S-H) stretching, and $\nu(CH_2)$ stretching modes, respectively. The discrepancies were also found similar to positive bias regime.

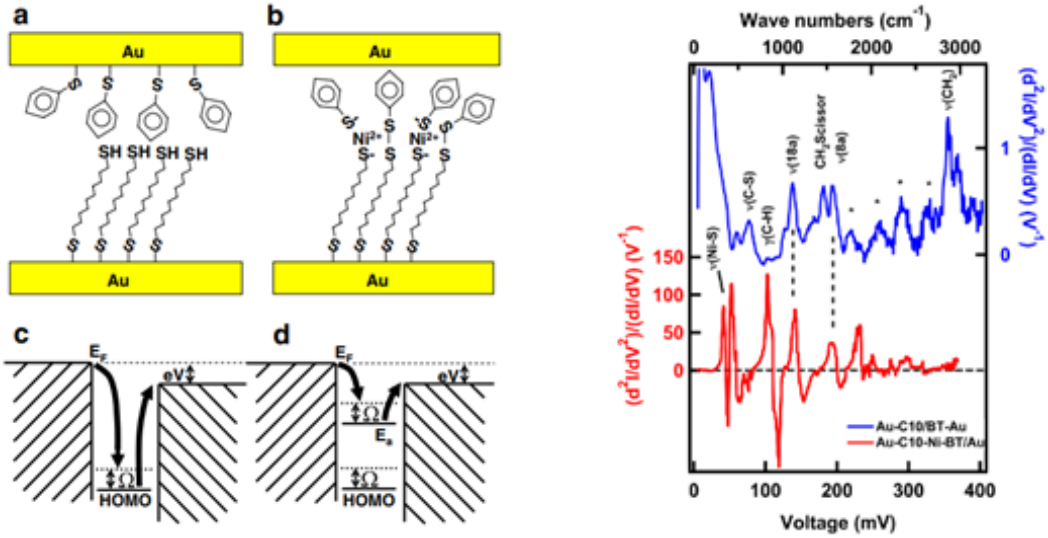

Figure 3.2.9. (Left figure) Schematic illustrations of metal particle-molecule hybridization in molecular junctions and their corresponding energy band diagram. (Right figure) IET spectra results from two different molecular junction system w/ and w/ metal particle-molecule hybridization. Reproduced from Ref. [31].

Now let us analyze the discrepancies in the IETS characteristics. From theoretical studies of IETS characteristics in metal-molecule-metal junctions, negative values or dips in the IETS signal (d^2I/dV^2) are unexpected features because inelastic conduction channels related to molecular vibration modes remain open over a sufficient bias regime.[28] In well-controlled experimental studies, especially regarding single-molecule junctions, the correct IETS characteristics were observed.[7] However, in some cases, especially for SAMs-based molecular junctions, an incorporation of defects, such as metal nanoparticles, into molecular junctions can introduce a hybrid metal particle-molecule electronic resonance state that can result in substantial modification of the intensity and line shape of the IETS signal, such as negative values or dips (see Figure 3.2.9).[29-31] In addition, the molecular

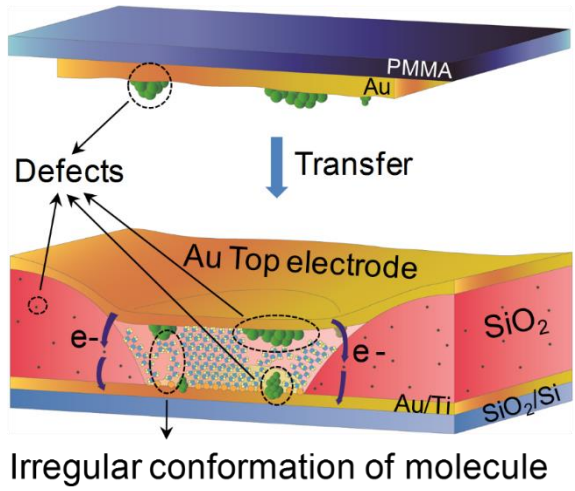

Figure 3.2.10. Schematic illustration of a molecular junction structure formed by the DMT method.

conformations and contact geometry induced by the interaction between the electrode metal and molecular layer play an important role in the substantial modification of the IETS characteristics.[5,13,14] Theoretical investigations based on the resonance model also predicted that depending on the energetic parameters of the system, the contribution from the elastic component may be negative and, furthermore, may outweigh the positive contribution of the inelastic component, resulting in dips in the IETS characteristics.[30,32] This effect is a second-order effect in electron-vibration coupling, which may be related to reabsorption of molecular vibration by the elastic current component.[33]

Figure 3.2.10 schematically illustrates the molecular junction structure that is formed by the DMT method in this study. Here, we draw the figure out of scale to emphasize the defects and irregular conformation of molecules. There can be several possible sources of defects as the electronic resonance states in the molecular junction. For example, the defects can be formed in the SAMs because of small grains on the surface of the bottom contact (see Figure 3.1.10 in chapter 3.1). Generally these substrate-induced defects are

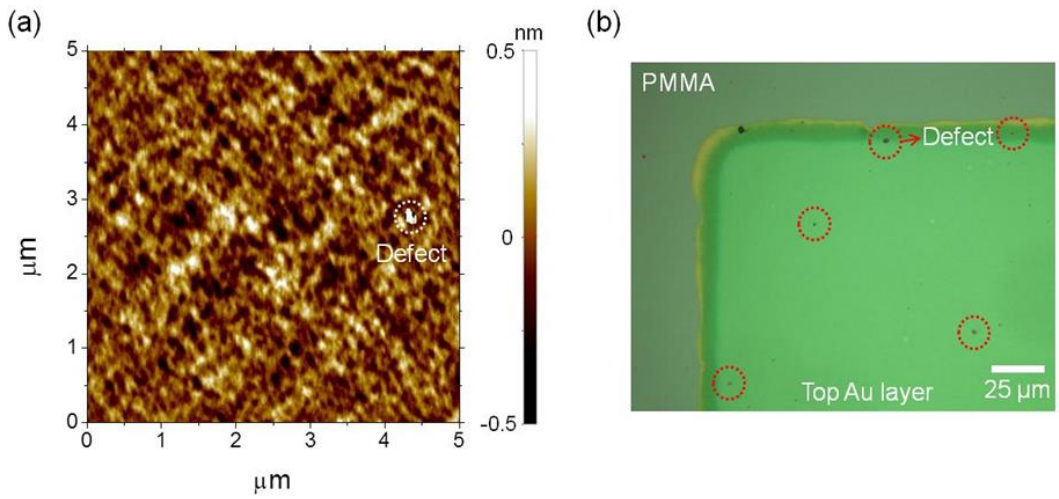

Figure 3.2.11. (a) Surface morphological image of the top Au layer. (b) Optical microscope image of the top Au layer.

proportional to the density of grain boundaries.[34] Also the top contact can induce defects in the SAMs. Due to the mechanical process while preparing the top contact layer such as the detachment of the metal film from dummy substrates or cleaning of the film, the top contact surface has also small grains and mechanical defects as shown in Figure 3.2.11. Figure 3.2.11 shows surface morphological image of the top Au electrodes which the top of SAMs were contacted and optical microscope image of the top Au layer. As shown in this figure, the top contact also comprises small grains which are directly related to large grain boundaries. Also mechanical defects induced while we are preparing the top contact can be found. These result in a poor contact with the SAMs, creating defects in the SAMs. The existence of these defects that results in poor contact properties with the SAMs can be indirectly revealed by estimating per-molecule conductance of our molecular junctions that would show relatively low conductance in comparison with the single molecule study cases assuming "perfect" array of single molecules. To compare the conductance per a single molecule between our molecular junctions and single molecule studies, we followed the

following procedures: (1) We get G_{mol} (conductance per a single molecule) of an octanethiol (C8) molecule from linear fit of the low-bias (-0.3 V $\leq$ V $\leq$ 0.3 V) statistical current-voltage data (adapted from Figure 3.2.4) along with assuming the ideal molecular grafting density (around 4.60 $\times$ 10^{18} m^{-2} for alkanethiols;[35] Then the G_{mol} value can be found to be around 2.68×10^{-13} S which is same with ~3.46×10^{-9} G_0 (G_0 is the conductance quantum which is defined as $G_0 = 2e^2/h \sim 7.75 \times 10^{-5}$ S). (2) A single octanethiol molecule study using STM shows that the Gmol value is around 6.83×10^{-11} S which is same with ~8.81×10^{-7} G_0 (the value is extracted using low-bias linear fit of Figure 4(b) from Ref. [36]). From the analysis, we could find that the G_{mol} value induced using our experimental data indeed shows smaller value than the ideal perfect array case. By performing the analysis, we could indirectly identify the irregular (i.e. imperfect) contact between the top Au layer and the SAMs (but the irregular contact may not be the "only" determinant factor of the decrease of conductance). Then, these types of additional resonance states can cause substantial modification to the intensity and line shape of the IETS characteristics, such as negative values or dips.[29-31] With this unexpected feature, there are peaks that cannot be assigned to any possible vibrational modes of the C12 molecule (marked as asterisks in Figure 3.2.6). Because of the small size of the C12 molecule (~1.8 nm), the insulating SiO_2 layer cannot perfectly block the charge flow, especially at the edge of the layer, and thus, the defects in the insulating SiO_2 layer placed at the edge of the layer may also participate in the charge flow as hopping sites (Figure 3.2.10). In this respect, these peaks are likely associated with the insulating SiO_2 layer or free thiol group.[16,19,37] According to previous studies regarding the vibrational modes of silicon-based materials, several asterisks in Figure 3.2.6 can be assigned to these vibrational modes.[37,38] With these background signals, the

defect-induced resonance states may introduce virtual molecular vibrations, which also create the artificial peaks in the IETS signal.[31] Furthermore, in this study, the device-to-device variations in the IETS characteristics, for example, different peak intensity and line shape, were observed (Figure 3.2.6). These variations are related to the irregular conformations of molecules randomly caused by defects in the SAMs (Figure 3.2.10) which can be clearly identified by the log-normal variations in electrical characteristics.[12,14,39,40] Because the J-V characteristics of molecular junctions are an averaged effect of the charge flow through the entire SAMs molecular junction, some randomly changed conformations of molecules in the molecular junction have less of an effect on the J-V characteristics, which eventually exhibit similar properties (Figure 3.2.4). The features of the IETS characteristics, such as peak positions or intensity, however, can be considerably modified by the individual change of conformations of molecules due to its highly sensitive nature on energy states between electrodes.[30,31] In addition, the irregular conformations of molecules change the scattering cross-sections of the molecular vibration modes along the transport pathway, which results in modification in the strength of electron-molecular vibration coupling and eventually the peak intensity.[17,41] Indeed, the modifications of IETS spectra by different molecular conformations have been observed even in the single molecule junction.[5] Therefore, defect-induced arbitrary changes of molecular conformations in the SAMs of each molecular junction result in device-to-device variations of the IETS characteristics. Although these analyses are fairly reasonable, we think that there should be more delicate investigations on the analysis of IETS characteristics in future.

Nonetheless, the overall accordance between peak positions and the referential vibration modes and its repeatability and similarity with the numerical derivative of the

first harmonic signal (Figures 3.2.3 and 3.2.7) demonstrate that the IETS signals obtained in this study represent molecular vibrational characteristics of C12 molecules along with other artificial features. It is suggested that one should fabricate defect-free and even molecular junctions without the insulating layer at the edge of the junction to obtain an accurate IETS signal and avoid the discrepancies. In another sense, it is helpful to eliminate the device-to-device variations of the IETS characteristics by statistically collecting the IETS peak positions from a sufficiently large number of molecular junctions.[42]

3.2.4. Chapter Summary

In summary in this chapter, we have demonstrated the measurements of molecular vibration spectra for alkanethiolate metal-molecule-metal junctions prepared by the direct metal transfer method using the IETS technique. We observed that the measured IETS signal can be assigned to molecular vibration modes that are sensitive to the chemical structure of the molecules. In addition, we were able to analyze possible defects in the molecular junctions which were not revealed by the current-voltage characteristics or temperature-variable analysis. The defects appeared as discrepancies and device-to-device variations in the IETS characteristics, which originated from the additional electronic resonant states and the irregular conformations of molecules induced by metal defects placed in the molecular junctions or the insulating SiO_2 layer.

References

[1] Love, J. C.; Estroff, L. A.; Kriebel, J. K.; Nuzzo, R. G.; Whitesides, G. M. *Chem. Rev.* **2005**, *105*, 1103-1169.

[2] Song, H.; Reed, M. A.; Lee, T. *Adv. Mater.* **2011**, *23*, 1583-1608.

[3] Choi, S. H.; Kim, B.; Frisbie, C. D. *Science* **2008**, *320*, 1482.

[4] Beebe, J. M.; Kim, B.; Gadzuk, J. W.; Frisbie, C. D.; Kushmerick, J. G. *Phys. Rev. Lett.* **2006,** *97*, 026801.

[5] Kim, Y.; Song, H.; Strigl, F.; Pernau, H. F.; Lee, T.; Scheer, E. *Phys. Rev. Lett.* **2011,** *106*, 196804.

[6] Kushmerick, J. G.; Lazorcik, J.; Patterson, C. H.; Shashidhar, R.; Seferos, D. S.; Bazan, G. C. *Nano Lett.* **2004**, *4*, 639.

[7] Song, H.; Kim, Y.; Jang, Y. H.; Jeong, H.; Reed, M. A.; Lee, T. *Nature* **2009,** *462*, 1039.

[8] Wang, W. Y.; Lee, T.; Kretzschmar, I.; Reed, M. A. *Nano Lett.* **2004,** *4*, 643-646.

[9] Yu, L. H.; Keane, Z. K.; Ciszek, J. W.; Cheng, L.; Stewart, M. P.; Tour, J. M.; Natelson, D. *Phys. Rev. Lett.* **2004**, *93*, 266802.

[10] Wang, G.; Kim, T.-W.; Lee, T. *J. Mater. Chem.* **2011**, *21*, 18117-18136.

[11] de Boer, B.; Frank, M. M.; Chabal, Y. J.; Jiang, W. R.; Garfunkel, E.; Bao, Z. *Langmuir* **2004,** *20*, 1539-1542.

[12] Jeong, H.; Kim, D.; Kim, P.; Cho, M. R.; Hwang, W. T.; Jang, Y.; Cho, K.; Min, M.; Xiang, D.; Park, Y. D.; Jeong, H.; Lee, T. *Nanotechnology* **2015,** *26*, 025601.

[13] Lin, L.-L.; Wang, C.-K.; Luo, Y. *ACS Nano* **2011**, *5*, 2257.

[14] Troisi, A.; Ratner, M. A. *Phys. Chem. Chem. Phys.* **2007**, *9*, 2421.

[15] Wang, W.; Richter, C. A. *Appl. Phys. Lett.* **2006**, *89*, 153105.

[16] Wang, W.; Scott, A.; Gergel-Hackett, N.; Hacker, C. A.; Janes, D. B.; Richter, C. A. *Nano Lett.* **2008**, *8*, 478.

[17] Lin, L.; Jiang, J.; Luo, Y. *Physica E* **2013**, *47*, 167.

[18] Persson, B. N. J. *Phys. Scr.* **1988**, *38*, 282.

[19] Song, H.; Kim, Y.; Ku, J.; Jang, Y. H.; Jeong, H.; Lee, T. *Appl. Phys. Lett.* **2009**, *94*, 103110.

[20] Tsu, R.; Esaki, L. *Appl. Phys. Lett.* **1973**, *22*, 562.

[21] Kim, T. W.; Wang, G. N.; Lee, H.; Lee, T. *Nanotechnology* **2007,** *18*, 315204.

[22] Song, H.; Lee, C.; Kang, Y.; Lee, T. *Colloid. Surface. A* **2006**, *284*, 583.

[23] Bryant, M. A.; Pemberton, J. E. *J. Am. Chem. Soc.* **1991**, *113*, 8284.

[24] Castiglioni, C.; Gussoni, M.; Zerbi, G. *J. Chem. Phys.* **1991**, *95*, 7144.

[25] Kato, H. S.; Noh, J.; Hara, M.; Kawai, M. *J. Phys. Chem. B* **2002**, *106*, 9655.

[26] Taniguchi, M.; Tsutsui, M.; Yokota, K.; Kawai, T. *Nanotechnology* **2009**, *20*, 434008.

[27] Okabayashi, N.; Paulsson, M.; Komeda, T. *Prog. Surf. Sci.* **2013**, *88*, 1.

[28] Lambe, J.; Jaklevic, R. C. *Phys. Rev.* **1968**, *165*, 821.

[29] Bayman, A.; Hansma, P. K.; Kaska, W. C. *Phys. Rev. B* **1981**, *24*, 2449.

[30] Galperin, M.; Ratner, M. A.; Nitzan, A. *J. Chem. Phys.* **2004**, *121*, 11965.

[31] Yu, L. H.; Zangmeister, C. D.; Kushmerick, J. G. *Phys. Rev. Lett.* **2007**, *98*, 206803.

[32] Mii, T.; Tikhodeev, S. G.; Ueba, H. *Phys. Rev. B* **2003**, *68*, 205406.

[33] Persson, B. N. J.; Baratoff, A. *Phys. Rev. Lett.* **1987**, *59*, 339.

[34] Weiss, E. A.; Chiechi, R. C.G. K. Kaufman, J. K. Kriebel, Z. Li, M. Duati, M. A. Rampi, and G. M. Whitesides, J. Am. Chem. Soc., **129**, 4336 (2007).

[35] Salomon, A.; Cahen, D.; Lindsay, S.; Tomfohr, J.; Engelkes, V. B.; Frisbie, C. D. *Adv. Mater.* **2003,** *15*, 1881-1890.

[36] Kockmann, D.; Poelsema, B.; Zandvliet, H. J. W. *Nano Lett.* **2009**, *9*, 1147.

[37] Irikura, K. K. *J. Phys. Chem.* **2007**, *36*, 389.

[38] Petit, C.; Salace, G.; Vuillaume, D. *J. Appl. Phys.* **2004**, *96*, 5042.

[39] Fu, Q.; Luo, Y.; Yang, J.; Hou, J. *Phys. Chem. Chem. Phys.* **2010**, *12*, 12012.

[40] Vitali, L.; Borisova, S. D.; Rusina, G. G.; Chulkov, E. V.; Kern, K. *Phys. Rev. B* **2010**, *81*, 153409.

[41] Hihath, J.; Tao, N. *Prog. Surf. Sci.* **2012**, *87*, 189.

[42] Fock, J.; Sorensen, J. K.; Loertscher, E.; Vosch, T.; Martin, C. A.; Riel, H.; Kilsa, K.; Bjornholm, T.; van der Zant, H. *Phys. Chem. Chem. Phys.* **2011**, *13*, 14325.

3.3. Statistical Investigation of the Length-Dependent Deviations in the Electrical Characteristics of Molecular Electronic Junctions Fabricated Using the Direct Metal Transfer Method

In this chapter, we analyzed the electrical transport characteristics of vertical type alkanethiolate molecular junctions fabricated using the DMT method and the electrical characteristics of the molecular junctions were statistically collected and investigated in terms of current density and transport parameters based on the Simmons tunneling model. In particular, we examined the statistical variations in the length-dependent electrical characteristics, especially the Gaussian standard deviation σ of the current density histogram. From the results, we found that the magnitude of the σ value can be dependent on the individual molecular length due to specific microscopic structures in the molecular junctions. The probable origin of the molecular length-dependent deviation of the electrical characteristics is discussed.

3.3.1. Introduction

As a future alternative for conventional Si-based electronics, molecular electronics that utilize functional molecules as active device components have attracted significant attention from both scientific and application points of view. Since the first conceptual model of a molecular rectifier was proposed, interest in the research field has been growing rapidly, and many research groups have extensively studied electronic charge transport through molecular layers with various device structures to reveal the intrinsic charge transport mechanism and realize real device applications.[1-6] In particular, alkyl-based molecular junctions have been one of the most widely investigated systems to examine transport characteristics because alkyl molecules with specific end groups are known to

form stable and well-ordered molecular monolayer films on various substrates (such as Au surfaces).[7,8] Despite their abundant virtues compared with conventional microelectronics, molecular electronic device applications have been hampered by many obstacles, preventing reliable, reproducible, and high-yield electronic transport characteristics of molecular systems. To overcome these obstacles and understand genuine charge transport characteristics of the junctions, analyzing a statistically sufficient number of molecular devices is highly desirable because the statistical investigation can single out the accurate characteristics of molecular systems from the ambiguously collected experimental data by observing the statistical distribution of the data. Actually, many research groups have reported these kinds of statistical results,[9-11] meanwhile there have been several efforts to achieve high-yield molecular junctions.[8,12,13] In most cases, only statistically 'representative' (i.e., averaged) electrical characteristics were treated as crucial parameters, while the deviations of these characteristics from junction to junction did not attract particular attention. Nevertheless, based on the fact that these deviations stem from variations in the specific microscopic structures of the molecular layers, it is worth investigating to gain insight into the structural states of the molecular layers for robust future electronics applications. Therefore, an investigation of the deviations in the electrical characteristics would be beneficial for these purposes.

Here, we analyzed a statistically significant number of alkanethiolate molecular junctions that were fabricated using the DMT method as metal-molecule-metal (M-M-M) structures. Statistical analysis with a simple tunneling model was performed, which enabled us to examine basics of the charge transport characteristics through alkanethiolate molecular layers. Specifically, by investigating some transport parameters derived from the modeling, we could obtain a brief insight into the molecular junction structure and

molecule-electrode interface. Additionally, the statistical deviations in the electrical characteristics as functions of the molecular length related to the specific molecular junction structures and interfaces have been observed and analyzed.

3.3.2. Experimental

To fabricate the molecular junctions, we followed the same fabrication process reported in chapter 3.1.

3.3.3. Results and Discussion

As mentioned in the introduction, examining the electrical characteristics of a statistically significant number of molecular junctions has the virtue of singling out the genuine charge transport properties of molecular junctions from ambiguously collected experimental data. To accomplish this task, we analyzed a large number (approximately 400) of molecular junctions, which are each composed of 128 junctions for C8, C12 and C16 alkanethiolate molecules and fabricated using our DMT method. From these devices, we determined so called 'working' molecular devices which can be recognized as statistically meaningful junctions based on the Gaussian distribution of the electrical characteristics (here current density, J) of the devices. The working devices were defined and selected from the all of the devices based on the criterion that they show statistically similar current densities at certain bias voltage to that of the majority of the devices in the Gaussian distribution, as shown in Figure 3.3.1(a). For a detailed explanation of the criterion for selecting the working devices, please see our previous reports.[10,14] In this report, we found that approximately 70 % of the devices can be regarded as working

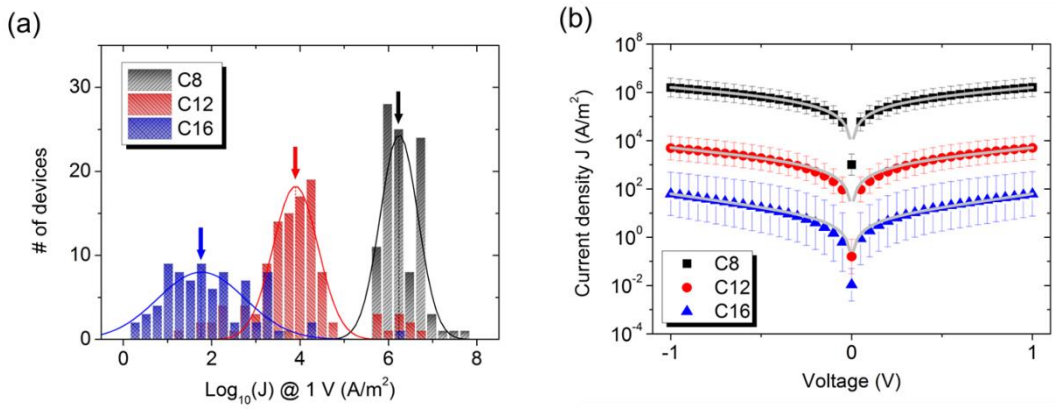

Figure 3.3.1. (a) Current density histogram at 1 V bias voltage for all candidate molecular devices. The Gaussian fitting results are shown as solid curves in the plot. (b) Statistically averaged representative J–V characteristics for all C8, C12, and C16 working devices. Gray solid curves represent the fitted results using the Simmons tunneling model.

devices with M-M-M junction structures, which means 70 % of our molecular junctions exhibited molecularly-based electrical characteristics.[14]

We can obtain representative J-V characteristics by log-averaging the current densities of the working devices as shown in Figure 3.3.1(b). To plot the graph, we found the logarithmic current densities of each working device and log-averaged them. Note that the error bars for each data point indicate the Gaussian standard deviations (σ) from the fitting functions of the logarithmic J values of each working device in Figure 3.3.1(a). In the following section, we will discuss the length-dependent variations of the σ values in detail. It is widely known from various studies that the charge transport mechanism through alkanethiolate SAMs is non-resonant tunneling transport.[15,16] which can be simply described by the well-known Simmons tunneling model that describes the metal-insulator-metal junction as a rectangular shaped tunneling barrier system:[17-19]

$$J = \left(\frac{e}{4\pi^2\hbar d^2}\right)\left[\left(\Phi_B - \frac{eV}{2}\right)\exp\left\{-\frac{2\sqrt{2m}}{\hbar}\alpha\left(\Phi_B - \frac{eV}{2}\right)^{1/2} d\right\}\right.$$
$$\left. -\left(\Phi_B + \frac{eV}{2}\right)\exp\left\{-\frac{2\sqrt{2m}}{\hbar}\alpha\left(\Phi_B + \frac{eV}{2}\right)^{1/2} d\right\}\right] \quad (1)$$

where d is the width of the barrier, m is the electron mass, Φ_B is the barrier height, V is the applied bias voltage, and α is an adjustable unitless parameter that reflects slight changes in the potential barrier shape or the effective electron mass. Especially in case of the low bias ohmic regime, J can be expressed approximately as

$$J \approx \frac{\sqrt{2m\Phi_B}e^2}{4\pi^2\hbar^2 d}\alpha V \exp\left(-\frac{2\sqrt{2m\Phi_B}}{\hbar}\alpha d\right) \quad (2)$$

$$\beta_0 = \frac{2\sqrt{2m\Phi_B}}{\hbar}\alpha \quad (3)$$

where β_0 is the decay coefficient, which reflects the exponential decrease of J versus molecule length (i.e., the width of the molecular tunnel barrier) in the low bias regime. However, note that these extracted fitting parameters, such as the decay coefficient or α from the Simmons model, do not imply certain exact quantitative meanings about the charge transport characteristics of the molecular junctions. Nonetheless, by analyzing the molecular transport junctions based on the model, we could gain a general idea of the charge transport characteristics of the junctions from a qualitative point of view.

To statistically investigate the charge characteristics of each working molecular junctions, we fitted (nonlinear least-squares fitting) the J-V characteristics of each working C8, C12 and C16 device in the Simmons tunneling model using Eq. (1) and obtained the transport parameters, including the Φ_B, α, and β_0 values. Here, each C8, C12 and C16

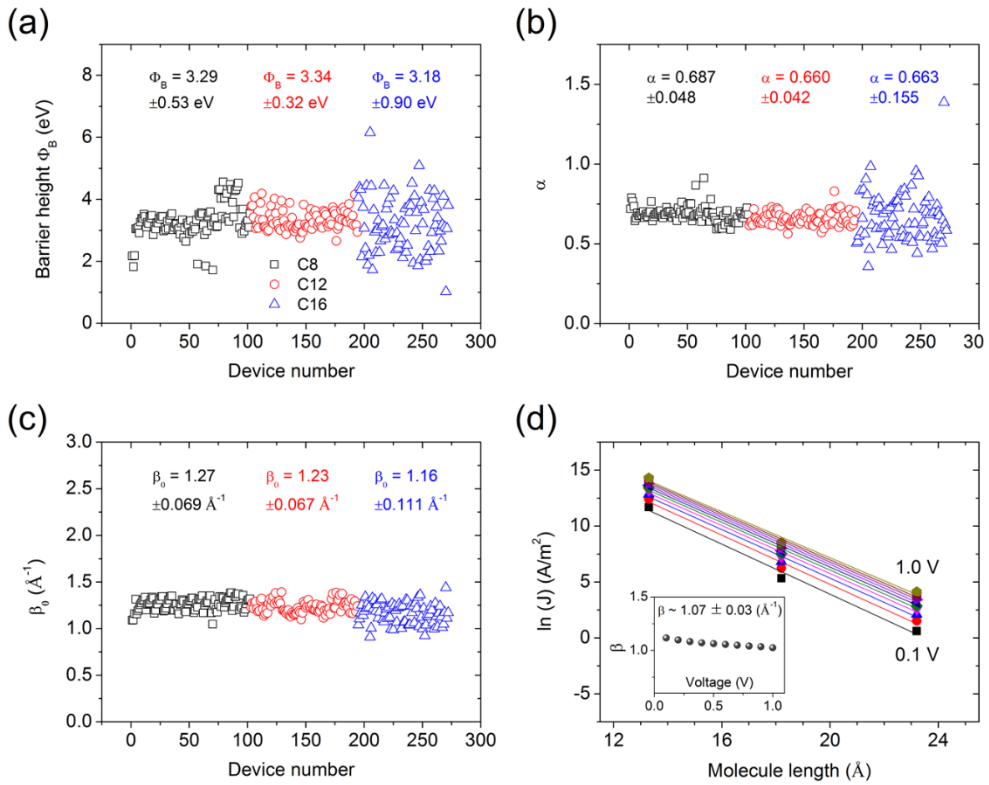

Figure 3.3.2. (a-c) Transport parameters derived from fitting the Simmons model for each individual working device. (a) Barrier height Φ_B, (b) adjusting parameter α, and (c) decay coefficient β_0. (d) Logarithmic current densities at bias voltages of 0.1 V to 1.0 V in 0.1 V increments versus the molecular length. Each solid linear line represents the exponential fitting results ($J \propto \exp(-\beta d)$). The inset depicts the deduced decay coefficient values (β) from the fitting results versus bias voltage.

molecule has molecular lengths d of 13.3, 18.2 and 23.2 Å, respectively.[20] Based on the molecular lengths, we extracted the transport parameters, and Figures 3.3.2(a) and 3.3.2(b) show the fitting results for the Φ_B and α values of all the individual working molecular devices. In addition, Table 3.3.1 summarizes these parameters and J values at 1 V bias voltage that are averaged over all the working molecular devices. Note that the Φ_B and α values from the fitting results show relatively similar values despite the different molecular lengths. The α values were similar those from to previously reported studies, but the Φ_B

Molecules	J at 1 V (A/m^2)	Φ_B (eV)	α	β_0 ($Å^{-1}$)
C8	$\sim 1.62\times10^6$	3.29±0.53	0.69±0.05	1.27±0.07
C12	$\sim 5.05\times10^3$	3.34±0.32	0.66±0.04	1.23±0.07
C16	$\sim 6.22\times10^1$	3.18±0.90	0.66±0.15	1.16±0.11

Table 3.3.1. Summary of the statistically averaged transport parameters from all of the working molecular devices.

values were not; instead, they showed higher values.[10,15] Here, as mentioned previously, the α values do not possess an exact physical meaning, but they make the Simmons fitting on the molecular junctions possible by acting as an adjustable parameter for the factors that one cannot take into account while modeling the tunneling junction as a rectangular barrier.[19,21,22] In addition, Φ_B reflects the relative energy alignment of the molecular frontier orbital with the electrode Fermi level, which depends on the nature of the contact properties at the molecule-electrode interface.[23,24] Therefore, higher values of Φ_B may represent non-conformal contact properties of our molecular junction structure, which will result in an overall increase in the values.[25,26] By applying these averaged parameters to Eq. (1), the estimated J-V characteristics for each molecular junction are presented as gray solid curves in Figure 3.3.1(b), which show similar trajectories to the representative experimental data. In addition, the β_0 values extracted from all of the individual working devices using each Φ_B and α value are shown in Figure 3.3.2(c). These values are found to be distributed in the range of 0.8-1.4 $Å^{-1}$, which are slightly larger values but mostly in agreement with previously reported β_0 values in pure (i.e., interlayer-less) M-M-M junction structures.[10,19-21] It is noteworthy that the β_0 values from molecular junctions with interlayers, for example, the well-known conducting polymer PEDOT:PSS, show

somewhat different values (0.5-0.6 $Å^{-1}$), which reflects the different natures of the contact properties (CH_3/Au versus CH_3/PEDOT:PSS).[8] Using the representative J-V characteristics of the devices, one can determine the decay coefficient values from length-dependent analysis ($J \propto \exp(-\beta d)$) without modeling the molecular junction. Here, we used β (the value that was determined from the length dependent analysis) versus β_0 (the value that was determined from the Simmons tunneling model in the low bias regime, Eqs. (2)-(3)) for comparison. For the length-dependent analysis, we plotted the J values of each molecular junction at bias voltages of 0.1 V to 1.0 V in 0.1 V increments versus the molecular length as shown in Figure 3.3.2(d). Based on the fact that the J values show exponential dependence on the molecular length ($J \propto \exp(-\beta d)$), we could extract β values for each bias voltage from the magnitude of each linear fitting slope as shown in the inset in Figure 3.3.2(d). From the analysis, we found that the averaged β value was approximately 1.1 $Å^{-1}$, which is in good agreement with previous studies on alkanethiolate molecular junctions.[23] Again, slightly larger values of β_0 from the Simmons fitting results may reflect the non-conformal contact properties of our molecular junction structure because of the strong dependence of the Simmons tunneling model on the $\alpha(\Phi_B)^{1/2}$ value (Eq. (3)).[23]

Based on the analysis of the representative charge transport characteristics of our molecular junctions, we investigated the length-dependent variation of electrical characteristics of the molecular junctions; specifically, the Gaussian standard deviation σ of the Gaussian fittings on the current density histogram as shown in Figure 3.3.1(a). Here, the Gaussian fittings have been performed using a normal distribution function as

$$f(x) = \frac{1}{\sqrt{2\pi\sigma^2}} \exp\left\{-\frac{(x-\mu)^2}{2\sigma^2}\right\} \qquad (4)$$

where μ is the Gaussian mean, and σ is its standard deviation. Then, as briefly mentioned above, the devices within a certain range of current density, depending on σ, can be considered working devices. Thus, the representative J-V characteristics could be derived in terms of statistically meaningful characteristics. Meanwhile, we also found that the degree of the distribution of the logarithmic J values of each molecular junction around the statistical mean value (i.e., the Gaussian mean μ) is dependent on the molecular length. Generally, this statistical distribution can be attributed to fluctuation factors causing such a distribution of tunneling current densities in molecular junctions. For example, these factors can be unexpected variations (i.e., fluctuations) in the molecular configurations of the molecular layers in the junction, such as the tilting angle of the SAMs on the bottom electrode, surface roughness of the bottom electrode, existence of defects or contaminants, and contact properties at the metal-electrode interface.[27-30] Note that such variations may stem from parameters that are controllable during the junction fabrication process, such as variations in the junction area; however, this type of fluctuation could cancel out because all of the molecular junctions in this study are generated by single batch processes, i.e., all of the devices were made at the same time. Instead, variations in intrinsic parameters that are mostly uncontrollable in the molecular junction, for example, the tunneling pathway, are more likely to be the main reasons for the fluctuations in the statistical distribution.[31] A detailed discussion of this observation will be given in the following section.

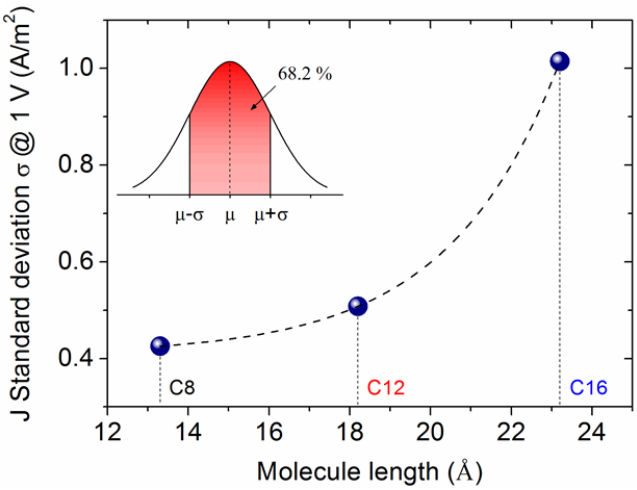

Figure 3.3.3. A plot of the Gaussian standard deviation σ extracted from Gaussian fitting of the current density histograms versus the molecular length. Black dotted curve represents the exponential fitting results.

Figure 3.3.3 shows the Gaussian standard deviation σ values of current density histograms at 1 V bias voltage for C8, C12 and C16 molecular junctions. As shown in the plot, the distribution of logarithmic J values depends on the molecular length, and the σ value increases as the molecular length increases. Here, to interpret the results quantitatively, we empirically assumed a simple exponentially dependent model of the σ value on molecular length as

$$\sigma = \sigma_0 + A \cdot \exp(\gamma d) \qquad (5)$$

where d is the molecular length, γ is a weighting factor, and σ_0 and A are adjusting factors. The idea of the model showing exponential dependence is based on the conformational degrees of freedom that are added to the alkyl chains with each methylene unit, which may accumulate to an exponential dependency of the overall structural configurations on the length. In statistical mechanics, the Boltzmann distribution describes the probability distribution of energy states as

$$f(E) = A \cdot \exp(-E / k_B T) \quad (6)$$

where E is the energy of the state, k_B is the Boltzmann constant, and T is the temperature of the system. Then, if we consider the various conformational states (i.e., disordered configuration) of the individual molecules as specific energy states of the system, the total conformational degrees of freedom that are related to the number of accessible conformational states can be considered proportional to the maximum energy of the system. Meanwhile, the maximum energy of an individual molecule, for example, the alkanethiolates in this study, increases with the addition of each alkyl chain unit based on the repetitively connected spring model of a molecule in which the internal energy increases with the length d ($E \propto d^2$). Thus, the total conformational degrees of freedom of the molecule grow with the molecular length d due to the higher probability of various conformational states. Indeed, it is known from the theoretical studies that the conformational degree of freedom of an individual molecule increases with an increase in the number of bonding chains and, eventually, the molecular length in case of a repetitive structure.[32] Therefore, as a simple presumption, a specific charge transport parameter that is determined by the conformational degree of freedom can be modeled as a growth model with increasing molecular length. Note that we utilized SAMs instead of individual molecules; thus, the charge transport medium should have different dynamic characteristics due to intermolecular interactions.[33] Nevertheless, disorder in the SAMs due to the uncontrollable parameters that we mentioned above makes the SAMs imperfect, and this argument might be applicable to our molecular junction system. Focusing on this study, one of the most likely origins of the variations in the J-V characteristics through SAMs can be thought of as the variation in the width of the tunneling barrier based on the Simmons

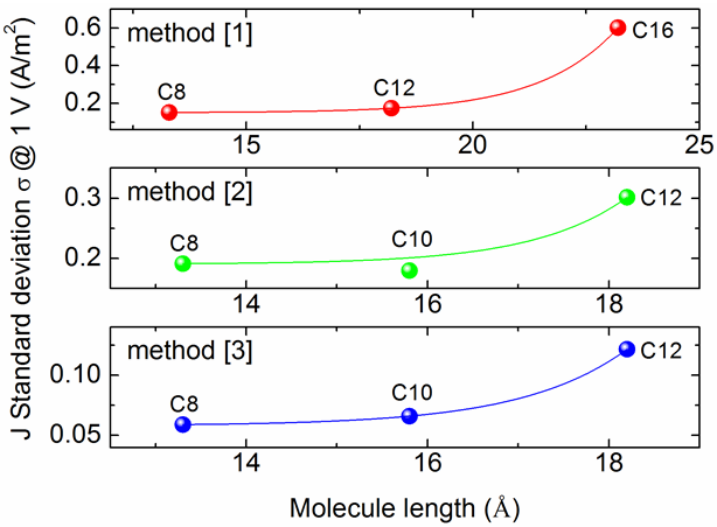

Figure 3.3.4. Plots of the Gaussian standard deviation σ for different device fabrication methods [1]-[3]. The deduced parameter, detailed descriptions, and the information from references [1]-[3] are presented in Table 3.3.2.

tunneling model. In this case, the molecule with longer lengths can produce larger variations in the thickness of the molecular layer than the shorter molecules due to intrinsic and extrinsic aspects, for example, more likely incorporation of defects and contaminants in the molecular layer or substantial molecular deformation due to the thicker cross-sectional area and higher structural degrees of freedom. Therefore, the thickness (i.e., the tunneling barrier width in terms of the Simmons tunneling model) of the molecular layer and, thus, the J-V characteristics that depend on the thickness might be proportional to the molecular length. Based on these observations, we empirically assumed that σ can be modeled as exponentially dependent on the molecular length d with a variable weighting factor γ. Though it is difficult to precisely define the physical implications of the γ value, this parameter reflects the relative strength of the dependence of the σ value on the molecular length. By applying this model to the σ values of C8, C12, and C16 devices, we plotted a fitting curve for C8, C12 and C16 as a black dotted curve in Figure 3.3.4, which

is in good agreement with the experimental data. However, we emphasize that there should be a rigorous quantitative explanation for the exponential dependence of the modeling based on molecular dynamics studies using the total interatomic potential of conformational energy [34,35] or DFT calculations.[36,37]

Method #	Type of Junction	Technique	γ	Ref
[1]	Au-SAMs / Au	evaporated Au / micropore	0.59	Phys. Rev. B 76, 205320 (2007)
[2]	Au-SAMs / polymer-Au	PEDOT:PSS / micropore	0.98	Nature Nanotech. 7, 438 (2012)
[3]	Au-SAMs / rGO-Au	solution-processed rGO	0.87	Angew. Chem. Int. Ed. 51, 108 (2012)
This work	Au-SAMs / Au	Direct metal transfer	0.36	

Table 3.3.2. Summary of the parameters deduced from the exponential fitting results of the σ values and detailed descriptions of the different fabrication methods.

To visualize the above discussion, we suggested a schematic illustration of our fabricated junction for cases with short chain molecules and long chain molecules, including examples of defects and contaminants in the substrate, SAMs, and top electrode that can affect the molecular configuration, which is shown in Figure 3.3.5. Usually, it is known that molecules with longer chains are incorporated via van der Waals attractions and form more ordered and dense molecular layers than short chain molecules.[33] However, because of the thicker cross-sectional areas of longer chain molecules, as we mentioned above, it is probable that SAMs formed with these molecules more frequently have artificial defects and contaminants. In addition, longer alkyl chains can induce more back-bending of the top end units of the molecules (that is, the top end units of the molecules fold back, pointing towards the bottom electrode) as schematically depicted in Figure 3.3.5.[38] Especially in our case, these kinds of defects can be more frequently incorporated due to the mechanical nature of our molecular device fabrication procedure resulting in disordering in the SAMs. For example, substrate-induced defects can be formed in the

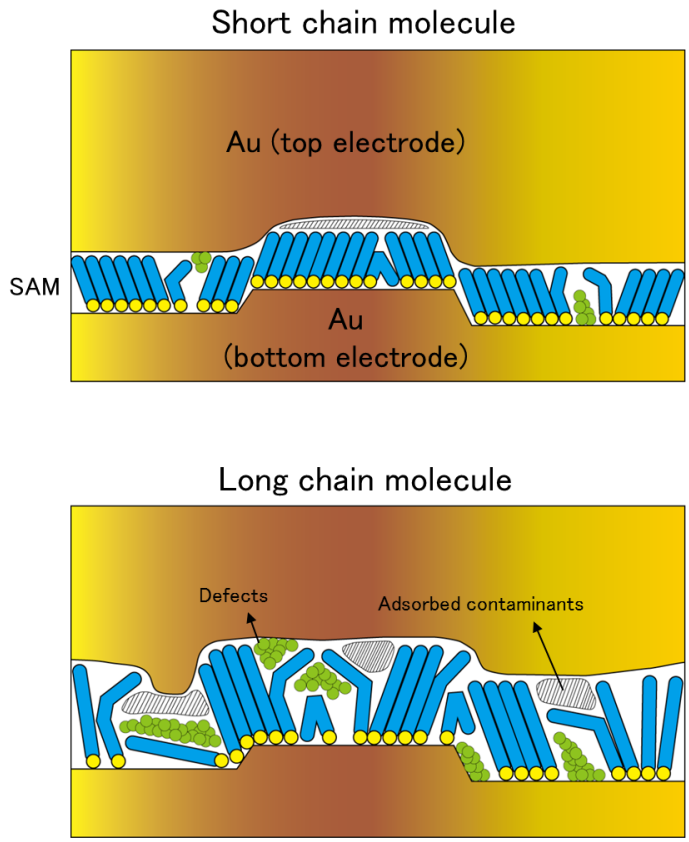

Figure 3.3.5. Schematic illustration of the molecular junction structures formed via the DMT method for both short and long chain molecules.

SAMs due to large grain boundaries from small grains on the surface of the bottom contact, and the top contact can also induce defects in the SAMs. Due to the mechanical processes used in the preparation of the top contact layer, the top contact surface might contain mechanical defects, such as metal particles. These kinds of defects result in poor contact with the SAMs, which cause variations in the electrical characteristics. Therefore, in spite of the possibility of better ordering of molecules with longer molecular chains, the effects of molecular configuration disordering that result from artificial defects and contaminants may surpass the intermolecular interaction, which result in a larger variation in the electrical transport characteristics. Note that the different molecular conformations may

also result from the intrinsic chemical properties of each molecule, such as the reactivity of the thiol groups or differences in orientation. Because each molecule has a different number of alkyl units, the reactivity of the thiol groups on the Au electrode surface varies due to the different thermodynamics. Specifically, there is a strong preference for the adsorption of the longer thiols than the shorter ones.[39] This property can also be observed from the results obtained by analytical chemistry.[40,41] Therefore, in our case, there is a possibility that the C8 molecules form more imperfect SAMs than the longer molecules, which might result in a larger deviation in electrical characteristics. However, as we mentioned in the experimental section, we immersed the clean Au electrode into a dilute ethanolic solution of the alkanethiolate for enough time (24-48 h) to generate the full coverage structure of a densely packed monolayer of standing molecules for each molecular length.[42] Thus, the different reactivities of thiols with different molecular lengths may have only a slight effect on the deviation of the electrical characteristics; instead, other properties, for example, the incorporation of defects and disorder in the SAMs will have a dominant effect. Second, there is a chain-length dependent distinction of the structures and phases of the alkanethiolate SAMs.[43] However, slight differences in the overall structures and phases cannot change the electrical properties dramatically. The structural and morphological characterization results for the SAMs on the Au surface using SEM, AFM and X-ray diffraction (XRD) are shown in Figures 3.3.6, 3.3.7, and 3.3.8. Figure 3.3.6 shows XRD characteristics of bare Au and C8, C12, C16 SAMs on the Au surface. In our case, the SAMs were formed on a Au/Ti (50 nm/5 nm) surface prepared by an electron-beam evaporator onto SiO_2/Si (50 nm thickness of SiO_2; p++ Si(100)) To prepare the SAMs, we immersed the substrates into a 5 mM ethanolic solution for approximately 30 h. After taking the substrates out from the solution, we rinsed the sample with anhydrous ethanol

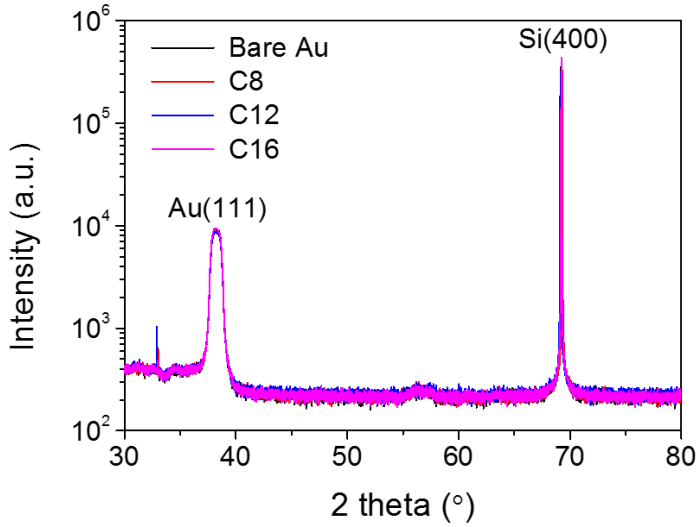

Figure 3.3.6. XRD characteristics of bare Au and C8, C12, C16 SAMs on the Au surface.

for 10 sec. We investigated the structure properties, θ-2θ scans and ω rocking curves, of the substrates by using a PANalytical X'Pert Pro diffractometer with Cu Kα x-ray source of 1.54056 Å wavelength. From the figure, it can be seen that XRD peaks were located around at a diffractometry angle of 2θ = 38.18º and 69.17º which could be assigned to Au(111) and Si(400) planes, respectively. Also there was broadening effect around the Au(111) peak which can be dedicated to the poly-crystallinity of Au on the substrates. However, we couldn't find any special difference in the peaks between bare Au and molecules deposited substrates regardless of the molecular length. It can be originated from too thin thickness of SAMs (1-2 nm) which might not be possible to be detected by an ordinary XRD instrument. Instead, more promising surface characterization technique, for example, grazing incidence X-ray diffraction technique or STM can observe the crystallinity (i.e. molecular orientation) of the SAMs.[44] Figure 3.3.7 shows SEM images of bare Au and C8, C12, C16 SAMs on the Au surface. From the figure, we could only observe blurred images of the substrate due to a relatively low resolution of thermal-type SEM. Usually it

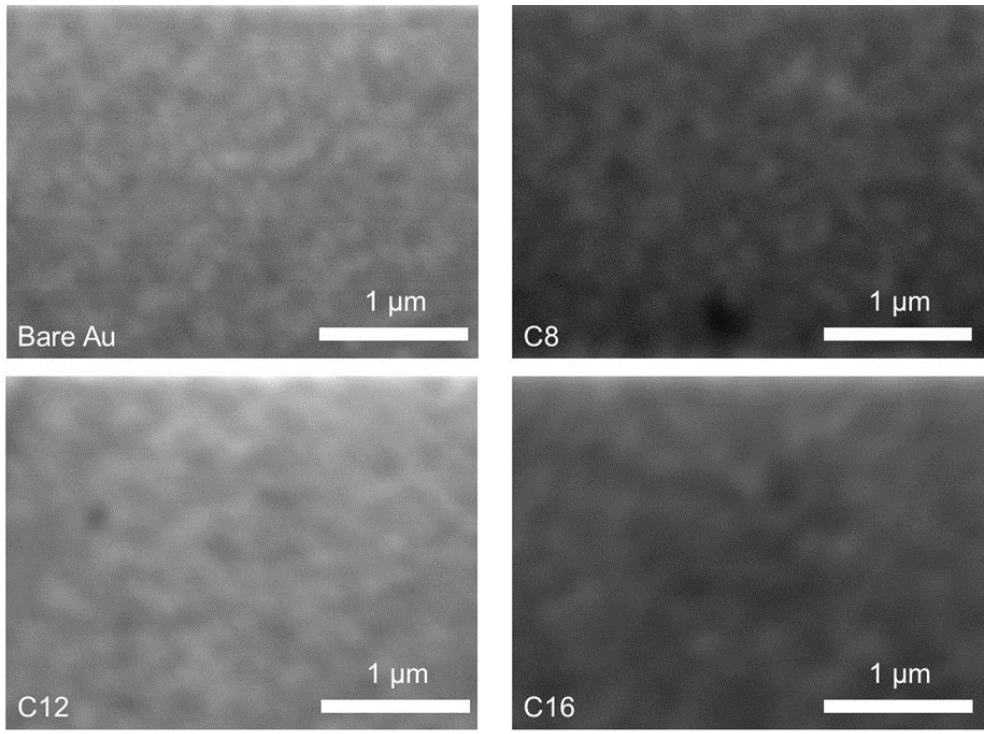

Figure 3.3.7. SEM images of bare Au and C8, C12, C16 SAMs on the Au surface.

is known that the morphology characterization of molecules deposited surfaces is more difficult than other promising surface characterization techniques, for example, AFM.[45] Therefore an accurate quantitative analysis of these pictures was not possible, but the average size of Au grains on the substrate is found to be distributed from several tenth of nanometer to a hundred nanometer of radius. In comparison with SEM, AFM has the capability to provide clearer information on the surface morphology. Figure 3.3.8 shows non-contact AFM images of bare Au and C8, C12, C16 SAMs on the Au surface. Usually it is known that the surface morphology characteristics and even crystal structures of the SAMs can be observed by AFM images.[46] The NC-AFM images were taken by a NX-10 from Park Systems using a PPP-NCHR probe. The scan size of each image was 500×500 nm^2. As shown in the figure, small Au grains were observable for each substrate with

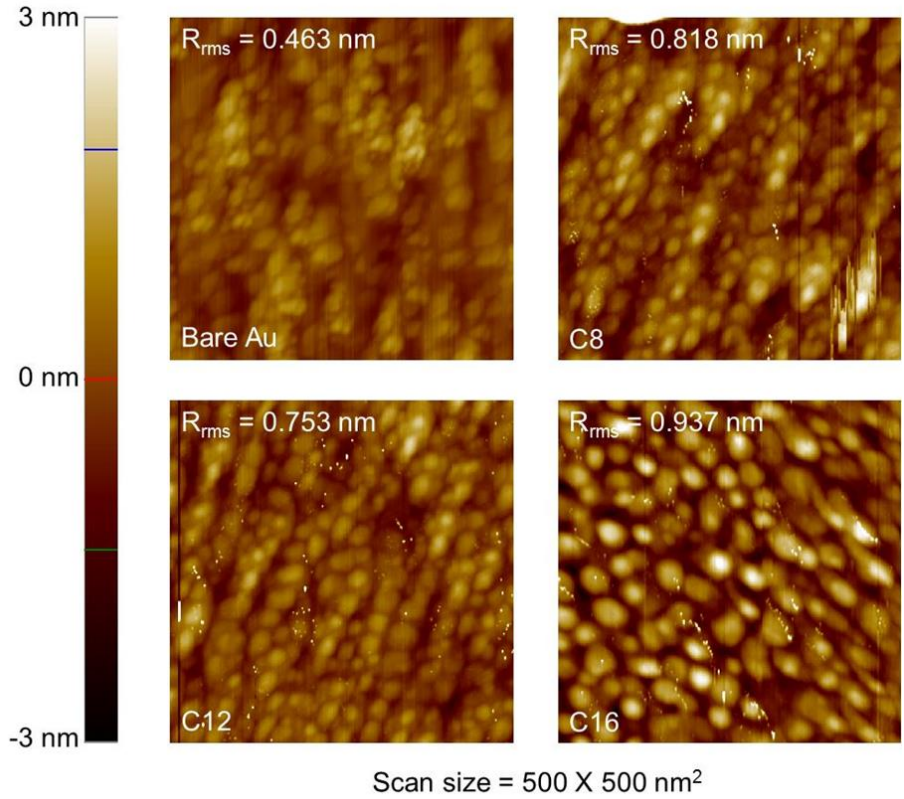

Figure 3.3.8. Non-contact AFM images of bare Au and C8, C12, C16 SAMs on the Au surface.

approximately 50 nm of radii. And the surface roughness (R_{rms}) was found that the bare Au has the value of 0.463 nm and 0.818 nm, 0.753 nm, 0.937 nm for each C8, C12 and C16 SAMs on the Au surface. From the results, we could identify that the surface roughness was increased when the SAMs were deposited on the Au surface mainly due to disorder of the SAMs which can be induced from artificial defects.[47] However we couldn't confirm the impact of carbon length on the morphological properties.

To identify this effect in other similar molecular junction structures, we compared the fitting results for the σ values in our previously reported studies using alkanethiolate molecules but different device fabrication methods. Figure 3.3.4 shows a plot of three

different kinds of fitting results using Eq. (5) assembled using a similar device fabrication technique, i.e., vertical type microfabricated molecular junctions. As shown in the plot, each method shows good agreement with the fitting curves and different weighting factors, γ, below unity. Roughly speaking, it implies that the degree of molecular configuration disordering couldn't exceed the length of each molecule. The summary of the fitting results is presented in Table 3.3.2. Note that there have been other studies in which the standard deviation (or full width at half maximum) of the Gaussian distribution of current density does not change monotonically with the molecular length and, therefore, disagree with our argument.[8,11,48] The reasons for the disagreement can be analyzed based on the following factors: (1) The distribution of the current density can be affected by not only the effects of molecular configuration disordering resulting from artificial defects and contaminants but other parameters, for example, the surface morphology of the bottom electrode, different SAM deposition times and environments, etc. Therefore, in other cases, these parameters could be controllable factors for the deviation rather than uncontrollable factors. (2) Ultra clean junctions, i.e., defect-free molecular junctions, can be achieved using different molecular junction fabrication methods that are almost free from the degradation of electrical characteristics that result from artificial defects.[48] (3) The molecular devices for the comparison should be generated in a single batch; in other words, the devices with different molecular lengths should be formed at the same time so that all of the environmental parameters that are likely to change the quality of the molecular junctions are the same. Therefore, the solid-state molecular junctions fabricated using our molecular junction fabrication method and the other methods in Figure 3.3.4 were synthesized in single batches. (4) The manner of colleting the J-V characteristics statistically can be different. In the case of our measurements, we obtained only one J-V

trajectory per molecular junction, but in other cases, several trajectories were collected by repeating the J-V measurement on few molecular junctions, which can result in significantly different results depending on the junction selection.[11]

3.3.4. Chapter Summary

Conclusively in this chapter, we have analyzed alkanethiolate molecular electronic junctions fabricated using the DMT method in terms of the electrical transport characteristics. In particular, we collected statistically significant transport parameters based on the Simmons tunneling model and determined representative current-voltage characteristics for the molecular junctions. The parameters mostly agreed well, but the barrier heights showed somewhat higher values, reflecting the non-conformal contact of the molecule-electrode interfaces in the molecular junctions. Additionally, we examined the statistical variations of the length-dependent electrical characteristics, especially the Gaussian standard deviation value σ. From the results, the σ values increase as the molecular length increases, and the relation might could be expressed using an exponential growth model based on empirical analysis. Finally, the probable origin of the length-dependent statistical variation could be related to artificial defects and contaminants in the molecular junctions. These observations may help pave the way for the development of robust and stable molecular electronic junctions.

References

[1] *Molecular Nanoelectronics* Reed, M. A.; Lee, T. Ed., American Scientific **2003**.

[2] Chen, J.; Reed, M. A.; Rawlett, A. M.; Tour, J. M. *Science* **1999,** *286*, 1550-1552.

[3] Collier, C. P.; Wong, E. W.; Belohradský, M.; Raymo, F. M.; Stoddart, J. F.; Kuekes, P. J.; Williams, R. S.; Heath, J. R. *Science* **1999,** *285*, 391-394.

[4] Park, J.; Pasupathy, A. N.; Goldsmith, J. I.; Chang, C.; Yaish, Y.; Petta, J. R.; Rinkoski, M.; Sethna, J. P.; Abruna, H. D.; McEuen, P. L.; Ralph, D. C. *Nature* **2002,** *417*, 722.

[5] Nitzan, A.; Ratner, M. A. *Science* **2003**, *300*, 1384-1389.

[6] Green, J. E., et al. *Nature* **2007**, *445*, 414-417.

[7] Jiang, J.; Lu, W.; Luo, Y. *Chem. Phys. Lett.* **2004**, *400*, 336.

[8] Akkerman, H. B.; Blom, P. W. M.; de Leeuw, D. M.; de Boer, B. *Nature (London, U. K.)* **2006,** *441*, 69-72.

[9] Venkataraman, L.; Klare, J. E.; Nuckolls, C.; Hybertsen, M. S.; Steigerwald, M. L. *Nature* **2006,** *442*, 904.

[10] Kim, T. W.; Wang, G. N.; Lee, H.; Lee, T. *Nanotechnology* **2007,** *18*, 315204.

[11] Reus, W. F.; Nijhuis, C. A.; Barber, J. R.; Thuo, M. M.; Tricard, S.; Whitesides, G. M. *J. Phys. Chem. C* **2012**, *116*, 6714.

[12] Wang, G.; Kim, Y.; Choe, M.; Kim, T. W.; Lee, T. *Adv. Mater.* **2011,** *23*, 755-760.

[13] Seo, S.; Min, M.; Lee, J.; Lee, T.; Choi, S. Y.; Lee, H. *Angew. Chem., Int. Ed.* **2012,** *51*, 108-112.

[14] Jeong, H.; Kim, D.; Kim, P.; Cho, M. R.; Hwang, W. T.; Jang, Y.; Cho, K.; Min, M.; Xiang, D.; Park, Y. D.; Jeong, H.; Lee, T. *Nanotechnology* **2015,** *26*, 025601.

[15] Wang, W. Y.; Lee, T.; Reed, M. A. *Phys. Rev. B* **2003,** *68*, 035416.

[16] Zhitenev, N. B.; Erbe, A.; Bao, Z. *Phys. Rev. Lett.* **2004**, *92*, 186805.

[17] Simmons, J. G.; *J. Appl. Phys.* **1963**, *34*, 1793.

[18] Wold, D. J.; Frisbie, C. D. *J. Am. Chem. Soc.* **2001,** *123*, 5549.

[19] Cui, X. D.; Zarate, X.; Tomfohr, J.; Sankey, O. F.; Primak, A.; Moore, A. L.; Moore, T. A.; Gust, D.; Harris, G.; Lindsay, S. M. *Nanotechnology* **2002,** *13*, 5.

[20] Wold, D. J.; Haag, R.; Rampi, M. A.; Frisbie, C. D. *J. Phys. Chem. B* **2002,** *106*, 2813.

[21] Holmlin, R. E.; Haag, R.; Chabinyc, M. L.; Ismagilov, R. F.; Cohen, A. E.; Terfort, A.; Rampi, M. A.; Whitesides, G. M. *J. Am. Chem. Soc.* **2001,** *123*, 5075.

[22] Rampi, M. A.; Whitesides, G. M. *Chem. Phys.* **2002,** *281*, 373-391.

[23] Wang, W. Y.; Lee, T.; Reed, M. A. *Rep. Prog. Phys.* **2005,** *68*, 523-544.

[24] Beebe, J. M.; Kim, B.; Frisbie, C. D.; Kushmerick, J. G. *ACS Nano* **2008,** *2*, 827.

[25] Majumdar, N.; Gergel, N.; Routenberg, D.; Bean, J. C.; Harriott, L. R.; Li, B.; Pu, L.; Yao, Y.; Tour, J. M. *J. Vac. Sci. Technol., B: Microelectron. Nanometer Struct.-Process., Meas., Phenom.* **2005,** *23*, 1417-1421.

[26] Wang, G.; Yoo, H.; Na, S. I.; Kim, T. W.; Cho, B.; Kim, D. Y.; Lee, T. *Thin Solid Films* **2009,** *518*, 824-828.

[27] Xu, B. Q.; Tao, N. J. *Science* **2003,** *301*, 1221-1223.

[28] Engelkes, V. B.; Beebe, J. M.; Frisbie, C. D. *J. Phys. Chem. B* **2005**, *109*, 16801.

[29] Hu, Y. B.; Zhu, Y.; Gao, H. J.; Guo, H. *Phys. Rev. Lett.* **2005**, *95*, 156803.

[30] Loertscher, E.; Weber, H. B.; Riel, H. *Phys. Rev. Lett.* **2007**, *98*, 176807.

[31] Song, H.; Lee, T.; Choi, N. J.; Lee, H. *J. Vac. Sci. Technol. B* **2008,** *26*, 904.

[32] Rudnicki, W. R.; Lesyng, B.; Harvey, S. C. *Biopolymers* **1994**, *34*, 383.

[33] Xiao, X. D.; Hu, J.; Charych, D. H.; Salmeron, M. *Langmuir* **1996**, *12*, 235.

[34] Jimenez, A.; Sarsa, A.; Blazquez, M.; Pineda, T. *J. Phys. Chem. C* **2010**, *114*, 21309.

[35] Chang, W. -Y.; Fang, T. -H.; Fang, C. -N. *J. Phys. Chem. B* **2009**, *113*, 14994.

[36] *DFT Study of Alkanethiol Self-assembled Monolayers on Gold(111) Surfaces* Torres, E., Graz University of Technology Ph.D. Thesis, **2009**.

[37] Alexiadis, O.; Harmandaris, V. A.; Mavrantzas, V. G.; Site, L. D. *J. Phys. Chem. C* **2007**, *111*, 6380.

[38] Nerngchamnong, N.; Yuan, L.; Qi, D. C.; Li, J.; Thompson, D.; Nijhuis, C. A. *Nat. Nanotechnol.* **2013**, *8*, 113.

[39] Bain, C. D.; Whitesides, G. M. *J. Am. Chem. Soc.* **1989**, *111*, 7164.

[40] *Electroanalytical Chemistry* Finklea, H. O. Ed., Marcel Dekker **1996**.

[41] *Encyclopedia of Analytical Chemistry: Applications, Theory and Instrumentation* Finklea, H. O. Ed., Wiley & Sons **2000**.

[42] Love, J. C.; Estroff, L. A.; Kriebel, J. K.; Nuzzo, R. G.; Whitesides, G. M. *Chem. Rev.* **2005,** *105*, 1103-1169.

[43] Fenter, P.; Eisenberger, P.; Liang, K. S. *Phys. Rev. Lett.* **1993**, *70*, 2447.

[44] Torrelles, X.; Barrena, E.; Munuera, C.; Rius, J.; Ferrer, S. Ocal, C. *Langmuir* **2004**, *20*, 9396.

[45] Rolandi, R. Cavalleri, O.; Ricci, D.; Toneatto, C. *Thin Solid Films* **1994**, *243*, 431.

[46] O'Dwyer, C.; Gay, G.; Viaris de Lesegno, B.; Weiner, J. *Langmuir* **2004**, *20*, 8172.

[47] Hajisalem, G.; Min, Q.; Gelfand, R.; Gordon, R. *Opt. Express* **2014**, *22*, 9604.

[48] Weiss, E. A.; Chiechi, R. C.; Kaufman, G. K.; Kriebel, J. K.; Li, Z. F.; Duati, M.; Rampi, M. A.; Whitesides, G. M. *J. Am. Chem. Soc.* **2007,** *129*, 4336-4349.

Chapter 4. Summary

In this thesis, I described the research results mainly focusing on the electrical characterization of high-yield rectifying molecular junctions using ferrocene-alkanehiolate SAMs and the development of a fabrication method for high-yield, reliable M-M-M junction in solid-state device platform.

First, I investigated the electrical characteristics of ferrocene-alkanethiolate SAMs based molecular junctions fabricated in a high-yield solid-state device structure. The junctions were fabricated using a conductive polymer PEDOT:PSS interlayer between the top electrode and the SAMs on both silicon-based rigid substrates and plastic-based flexible substrates. I observed asymmetric electrical transport characteristics that originated from the ferrocene moieties. In particular, I found an abnormal temperature dependence of the current-voltage characteristics at a large reverse bias (i.e., a decrease in current density as temperature increases), which is associated with the redox-induced conformational change of the molecules in the molecular junctions. Also, I applied temperature dependent transition voltage spectroscopy analysis to verify the validity of this claim. I further demonstrated that the molecular devices could function on flexible substrates under various mechanical stress configurations with consistent electrical characteristics.

And secondly, I proposed a new approach for creating high-yield molecular devices as a vertically structured metal-molecule-metal junction. I fabricated the top metal electrodes using a direct metal transfer method in which the top electrodes are formed on a different substrate and then transferred to the molecular layers, similar to the well-known graphene transfer method. Using this method, I was able to fabricate highly stable and

reliable metal-molecule-metal junctions without the use of any additional interlayers, and the resulting junctions exhibited considerably improved device yields (~70 %) compared to those (typically less than a few %) of the molecular junctions in which the top electrodes are formed using the conventional metal-evaporation method. I compared this method with other molecular device fabrication methods in terms of characteristic charge transport parameters, especially the electronic coupling interaction between the molecular layer and electrodes. Also, inelastic electron tunneling spectroscopy analysis were applied to examine molecular vibrational properties of the molecular junctions. Finally, I investigated the statistical variations in the length-dependent electrical characteristics from the molecular junctions, especially the Gaussian standard deviation σ of the current density histogram.

To be specific, in chapter 2.1, we studied the redox-induced electronic transport properties of ferrocene-alkanethiolate molecules using a conducting polymer-interlayer device structure. We observed asymmetric electrical transport properties, which arise due to the existence of ferrocene moiety. In particular, we observed distinctive electrical characteristics that the current in the junction decreased with increasing temperature at high temperatures (> ~220 K) and when a large positive bias (> ~0.6 V) was applied to the ferrocene end-group side. This behavior is attributed to the redox process of the ferrocene moiety in the molecular junction. We also fabricated the same molecular junctions on flexible device substrates and demonstrated consistent electrical characteristics (i.e., asymmetric current-voltage characteristics and distinctive temperature dependence) under various bending configurations. This ensures that the unique feature originated from the intrinsic molecular reactions but not from the effect of substrates or device configuration. This study suggests the importance of consideration of intrinsic molecular reactions

especially redox process when one applies molecules to the robust functional molecular devices. And this work also provides a route toward the practical implementation of functional molecular devices with unconventional flexible configurations.

In chapter 2.2, we investigated the temperature dependent electrical characteristics of the ferrocene-alkanethiolate molecular junctions using the PEDOT:PSS interlayer. We fabricated and analyzed a statistically sufficient number of devices to ensure the reliability of the data. In particular, we consistently observed unusual temperature dependent electrical characteristics at a voltage polarity larger than +0.6 V and at temperatures higher than ~220 K. The origin of this distinctive behavior was attributed to the redox-induced conformational changes of the ferrocene-alkanethiolate molecules. We used the TVS analysis to understand the electrical characteristics of these molecular junctions. From the analysis, we found that the obtained TVS results were consistent and in good agreement with the measured electrical characteristics. Additionally, we performed a temperature dependent TVS analysis based on the MBT model to support the proposed redox-induced conformational changes of the molecules. This study suggests the significance of the consideration of the macroscopic structural organization of the molecular junction as well as the intrinsic molecular properties, which includes the redox processes or molecular conformations, to understand the charge transport characteristics of the molecular junctions.

In chapter 3.1, we have demonstrated a new technique for fabricating high-yield molecular junctions in a vertical metal-molecule-metal structure in which the top metal electrodes are formed on alkanethiolate molecules using a direct metal transfer method. The molecular junctions fabricated using this method exhibited the well-known tunneling transport characteristics of alkanethiolates with good stability, durability, and device lifetime properties, which are important factors for the practical application of molecular

devices. Based on the comparison of our method with other previously reported molecular device fabrication methods, our method appears to provide stronger and more stable electronic coupling between the top electrode and molecular layer, resulting in better contact properties. Finally this new approach may be a probable way to achieve a reliable platform for the precise characterization and practical application of molecular electronic junctions. Further study can be an improvement of the rectification ratio of ferrocene-alkanethiolate molecular junctions by utilizing proper top metal electrodes that are transferred onto the SAMs to exhibit both high device-yield and work function matching.

In chapter 3.2, we have demonstrated the measurements of molecular vibration spectra for alkanethiolate M-M-M junctions prepared by the direct metal transfer method using the IETS technique. We observed that the measured IETS signal can be assigned to molecular vibration modes that are sensitive to the chemical structure of the molecules. In addition, we were able to analyze possible defects in the molecular junctions which were not revealed by the current-voltage characteristics or temperature-variable analysis. The defects appeared as discrepancies and device-to-device variations in the IETS characteristics, which originated from the additional electronic resonant states and the irregular conformations of molecules induced by metal defects placed in the molecular junctions or the insulating SiO_2 layer.

In chapter 3.3, we have analyzed alkanethiolate molecular electronic junctions fabricated using the DMT method in terms of the electrical transport characteristics. In particular, we collected statistically significant transport parameters based on the Simmons tunneling model and determined representative current-voltage characteristics for the molecular junctions. The parameters mostly agreed well, but the barrier heights showed somewhat higher values, reflecting the non-conformal contact of the molecule-electrode

interfaces in the molecular junctions. Additionally, we examined the statistical variations of the length-dependent electrical characteristics, especially the Gaussian standard deviation value σ. From the results, the σ values increase as the molecular length increases, and the relation might could be expressed using an exponential growth model based on empirical analysis. Finally, the probable origin of the length-dependent statistical variation could be related to artificial defects and contaminants in the molecular junctions. These observations may help pave the way for the development of robust and stable molecular electronic junctions.

Appendix A

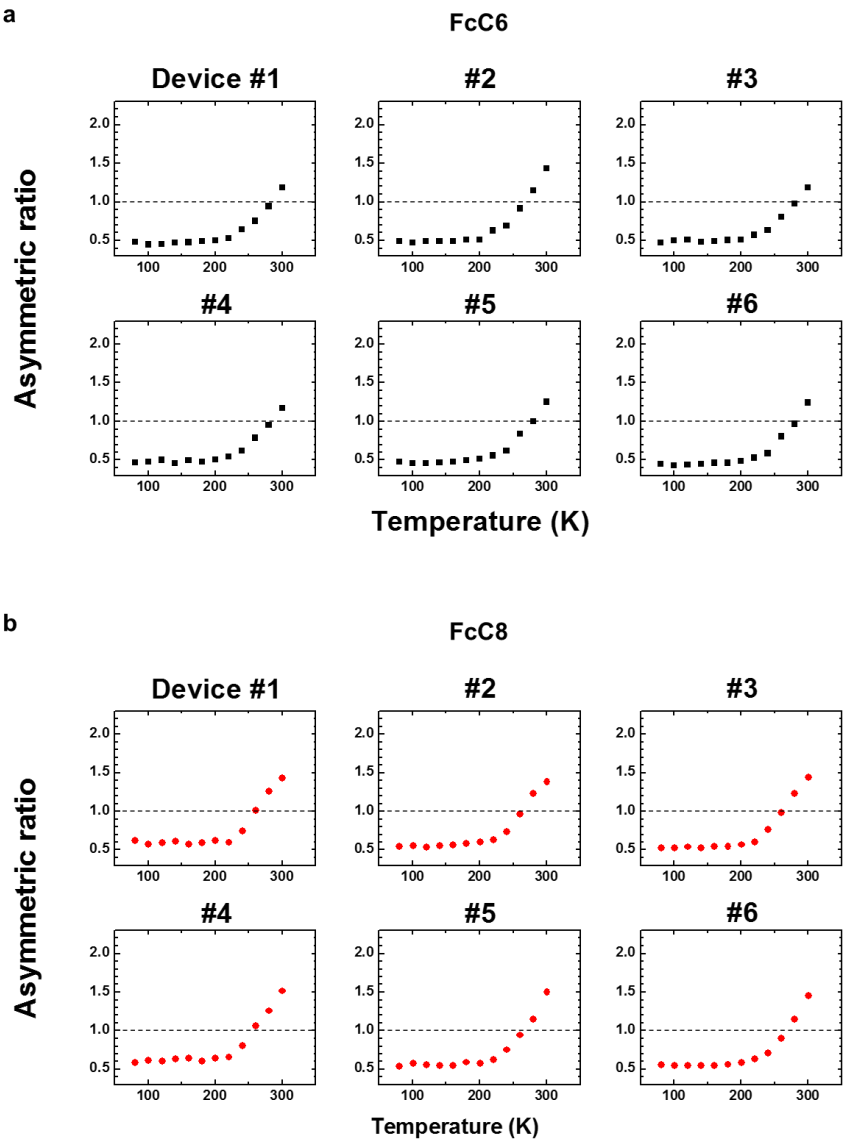
a
FcC6
Device #1
#2
#3
#4
#5
#6
Asymmetric ratio
Temperature (K)
b
FcC8
Device #1
#2
#3
#4
#5
#6
Asymmetric ratio
Temperature (K)

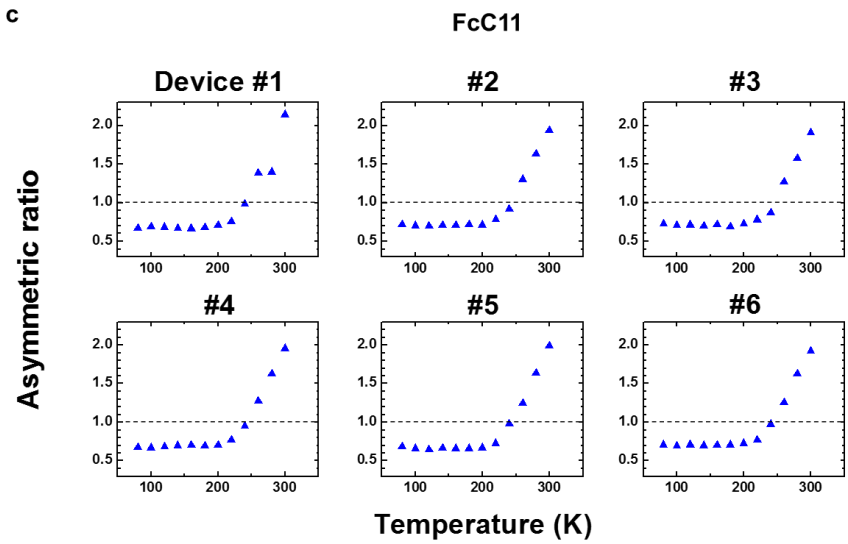

Figure A1. The change of asymmetric ratios for all the measured (a) FcC6, (b) FcC8, and (c) FcC11 molecular devices (18 devices in total) as a function of temperature.

Appendix B

Further discussion about our charge transport analysis of ferrocene-alkanethiolate molecular junctions

Here, we provide a further discussion about our charge transport analysis of ferrocene-alkanethiolate molecular junctions in response to the committee members' valuable inquiry raised during the final defense presentation. The main contents of the inquiry can be divided into two points: 1) Density of states of the HOMO of ferrocene moiety should be considered while describing charge transport phenomena in the molecular junction. 2) It should be careful when applying TVS analysis on the molecular junctions due to the participation of weak hopping transport by the HOMO of ferrocene moiety in the charge transport according to our analysis. In response to the inquiries, therefore, we suggest our rough discussion on these subjects:

1) Density of states of the HOMO of ferrocene moiety: Since only two electrons can occupy a single energy state of molecular orbital, tunneling electrons transmitted from alkyl chain body can suffer bottlenecks especially in case of high tunneling rate compared to hopping rate. Therefore, when we investigate the charge transport characteristics of molecular junctions while both tunneling transport and hopping transport participate in the overall transport, density of state of the HOMO of ferrocene moiety must be considered for an accurate analysis in terms of the electron transfer rate through alkyl chain body barrier and ferrocene-top electrode contact coupling. In our case, for example, the current density

of FcC6 molecular junctions at -1 V forward bias was ~1.2×10^4 A/m^2 (See Figure 2.1.7) which equals to ~7.5×10^{22} (= 1.2×10^4 / 1.602×10^{-19}) electrons per second·m^2. Meanwhile packing density of the ferrocene-alkanethiolate on the gold bottom electrodes can be approximated ~4.6×10^{18} per m^2 assuming the same packing density to alkanethiolate (Ref. Boer et al., *Adv. Mater.* 17, 5 (2005)), so the total number of electrons that can be occupied in the ferrocene moiety per m^2 is 9.2×10^{18} (= $2 \times 4.6 \times 10^{18}$). Therefore, if we assume that only one HOMO state of the ferrocene moiety participates in the charge transport, the hopping rate between the ferrocene-moiety and top electrode contact should exceed at least 8.2×10^3 (= 7.5×10^{22} / 9.2×10^{18}) Hz to prevent the bottlenecks. And if the rate exceeds the value, we may ignore the density of states of the HOMO of ferrocene-moiety anymore because even a single HOMO state of ferrocene moiety enables favorable transmission of the tunneling electrons without any bottleneck. But unfortunately because we couldn't estimate the hopping rate (in other words, coupling strength) in this analysis, we cannot surely conclude whether the density of states of the HOMO should be considered critically or not. However, note that density of states of molecular orbitals should be counted significantly in most cases.

2) Validity of applying TVS analysis: As the committee members pointed out, the TVS analysis is fundamentally based on the coherent tunneling transport assuming a single rectangular tunneling barrier. Therefore, when weak hopping transport is involved in the overall transport mechanism with two states model, one should be careful in applying the TVS analysis. In our case, we developed our analysis in analogy the MBT model we introduced in chapter 1, i.e. effective barrier height system from individual virtual rectangular barriers. Based on the MBT model, each electronic components in molecular junction system such as molecular backbone, molecule-bottom electrode contact,

molecule-top electrode contact can be regarded as stacking of individual rectangular barriers similar to series of resistors. This assumption can be rationalized by the fact that even in a single molecular component electron distribution can have spatial ununiformity as localized and delocalized states when they are properly separated by saturated molecular parts (Ref. McCreery et al., *Phys. Chem. Chem. Phys.* 8, 2572 (2006)). Therefore in such case, we can generalize the redox-probable ferrocene moiety-top electrode contact as a single contact barrier, which the tunneling barrier parameters such as barrier height can be changed with respect to the contact properties, in this case, redox process. Finally, by combining such individual barriers, one effective rectangular barrier can be assumed and the TVS analysis is applicable.

As a final note, an in-depth analysis on charge transport mechanism in ferrocene-alkanethiolate molecular junctions with different electrodes system has been presented in Ref. Garrigues et al., *Sci. Rep.* 6, 26517 (2016). In this article, for example, electrical screening by ferrocene moiety gives rise to a strongly non-linear profile across the junction.

국문초록

고수율 구조에서의 정류 특성을 갖는 분자 전자 접합에 관한 연구

정현학
서울대학교 물리천문학부

분자전자학의 역사는 일반적으로 1974년 Aviram과 Ratner의 분자 정류기라는 초기 이론적 제안을 통해 태동되었다고 일컬어진다. 위 연구의 중요한 제안은 실리콘 기반의 전자소자와 유사한 기능성을 발휘할 수 있도록 분자가 합리적으로 설계되었을 때, 전극 사이에 접촉된 단일 분자 접합이라는 궁극적인 미세한계의 영역대에서도 전자소자의 기능성을 충분히 발휘할 수 있을 것이라는 예측이었다. 이러한 제안 이후, 다양한 실험적 방법들을 통한 단일 분자나 자기조립분자박막 기반 전자 접합의 전기적 특성을 관측하기 위한 노력들이 이어져 왔다. 하지만 이와 더불어, 분자 접합이 갖는 미세한계 영역대의 크기로 인해 접합의 신뢰성 및 수율 측면에서 문제점들이 제시되었다. 이는 접합 구성요소인 분자가 갖는 독특하고 기능성을 갖춘 고유 성질들을 시험해 보기 위한 신뢰성 있고 고수율의 소자 플랫폼 부재로 인해 주로 발생하는 문제들이다. 최근에는 이러한 문제점을 해결하기 위한 노력에 힘입어 분자 접합 내에서 발생되는 분자의 화학 결합 변화, 산화 환원 과정, 빛 또는 전하에 의한 분자 형태 변화, 상변화 등과 같은 다양한 유형의 고유한 분자 특성들이 광범위하게 연구되고 있다. 하지만 여전히 분자 접합의 정밀한 특성 분석의 어려움으로 인해 분자가 갖는 다양한 기능성에 대한 이견들이 제시 되고 있다. 이 같은 문제는 앞으로 실용 가능한 차세대 전자 소자 기술로 발전하기 위한 분자전자학 분야의 오랜 숙원이라고 볼 수 있다.

본 학위 논문에서는 첫 번째로 고수율, 반도체 기반 소자 형태의 페로센-알칸싸이올레잇이 분자 접합의 전기적 특성에 관해 조사하였다. 이 연구에서

는 실리콘 기반의 고체 기판과 플라스틱 기반의 유연 기판 위에 전도성 고분자 중간층을 이용하여 분자 접합 소자를 제작하고 페로센 단말에 의해 발생되는 비대칭적 전기 특성을 확인하였다. 특히, 일정 크기 이상의 역 방향 전압에서 흔히 예측되는 전기적 특성의 온도 의존성과는 다른 양상이 나타났는데 (온도가 증가할수록 전류 밀도가 오히려 감소하는 특이 현상), 이는 페로센 단말의 산화, 환원 현상에 의해 발생되는 분자체의 배열 변화와 관련이 있다. 이러한 제안의 유효성을 검증해보기 위해 온도 의존적인 전이 전압 분광법을 이용하여 결과를 분석하였다. 또한, 이러한 분자 접합 소자가 유연 기판 위에서 다양한 기계적 응력 하에서도 안정적인 전기적 특성을 보일 수 있다는 사실을 실험적으로 확인하였다.

두 번째 연구주제로 고수율, 수직형 금속-분자-금속 접합을 제작하는 새로운 방법에 대해 연구하고 이를 제시하였다. 이를 위해 그래핀 전사방법을 응용하여 금속 박막 상부 전극을 분자 박막 위에 직접 전사하였다. 이를 통해 기존의 고수율 분자 접합을 제작하기 위한 방법으로 흔히 도입되었던 중간층 없이 높은 수율의 순수형 금속-분자-금속 접합을 제작할 수 있었으며, 이는 기존의 진공 금속 증착 방식을 통해 제작되는 분자 접합의 낮은 수율(수 %)에 비해 현격히 개선된 결과를 보였다 (약 70 %). 한편 이러한 방법을 통해 제작된 소자의 전기적 특성과 관련된 파라미터들을 다른 고수율 분자 접합 제작법을 통해 제작된 소자의 결과들과 비교하였다. 또한, 분자 접합 내의 분자의 고유한 진동 특성을 검토하기 위해 비탄성 터널링 전자 분광법을 적용하였고, 분자 길이에 따른 전기적 특성의 통계적 변화, 특히 전류 밀도 히스토그램의 가우시안 표준 편차의 변화에 대해서도 조사하였다.

Keywords: 분자전자학, 분자 접합, 자기조립분자박막, 전기적 특성, 분자 다이오드, 페로센-알칸싸이올레잇, 고수율, 직접 전사 기법, 비탄성 터널링 전자 분광법, 전이 전압 분광법

Student Number: 2011-20423

감사의 글

처음 대학에 입학하고부터 박사학위과정을 마무리하는 이 순간까지 정말 오랜 시간 학교라는 공간에 머물며 많은 경험들을 할 수 있었던 것 같습니다. 이 소중한 경험들은 어떤 방식으로든 제 스스로 성장할 수 있는 자양분이 되었다고 확신합니다. 사실 절망스러웠던 적도 많았지만 이를 극복할 수 있도록 부족한 저를 보듬어주신 많은 분들 덕분에 지금 이 자리에 앉아 한 자 한 자 감사의 글을 적을 수 있게 된 것이겠지요. 감사합니다. 곰곰이 생각해보면 한 평생을 살아가며 누군가에게 공식적으로(?) 감사를 표할 수 있는 기회가 별로 없을 것 같은데 이 기회를 빌어 소중한 분들께 감사를 표할 수 있게 되어 영광스럽게 생각합니다.

가장 먼저 저의 지도교수님이신 이탁희 교수님께 진심 어린 감사를 드립니다. 혼란 속에서 방황하던 저를 아무런 조건 없이 선뜻 거두어주신 교수님의 인자하신 성품과 부족한 저를 끝까지 믿고 이끌어주신 지도와 인내로 지금의 제가 있게 되었습니다. 언제나 교수님을 본받고 스승님의 이름에 부끄럽지 않은 제자가 되도록 노력하겠습니다. 항상 행복하시고 건강하시길 기원합니다.

사랑하는 MNELAB원 여러분들께도 감사의 말씀을 전하고 싶습니다. 먼저 연구실 원년멤버로 고락을 함께 한 진곤, 같은 팀 멤버로 알게 모르게 의지가 많이 되었던 동구에게 감사하다는 말을 전하고 싶습니다. 얼굴만 대충 알 때는 좀 차가워 보였는데 지내고 보니 성격이 너무 선해서 좋았던 태영, 제수씨와 항상 행복하길 기도할께. 랩장하는 걸 보면서도 느꼈지만 넌 어느 곳에서든 잘 해낼 사람이라 생각한다. 그리고 영걸(영굴), 사람들과 금방 친해지지 못하는 내 성격에도 너만큼은 금방 친해질 수 있어서 너무 좋았다. 덕분에 긴 연구실 생활 가운데 여러모로..(!) 의지가 많이 되어서 정말 고마웠어. 앞으로도 밝은 네 성격만큼 밝은 미래가 함께하길 빈다. 그리고 간지남 경준, 항상 도지는 나의 건망증에 가차없는 일격을 가해줘서 고마웠고 눈빛만큼이나 날카로운 너의 지성으로 언제나 좋은 연구해나가길 빈다. 분자팀 부사수 왕택, 허당 같지만 실험에서만큼은 꼼꼼한 너의 스타일을 항상 눈 여겨 보고 있었다. 그 능력이 조만간 빛을 발하길 바란다. 가끔 대화할 때면 생각의 깊이가 다르다는 느낌을 주곤 했던 젊은 연식이도 분자팀의 능력 있는 후배가 되어줘서 너무 고마웠어. 준우, 정민도 분자팀 선배역할을 제대로 못하고 떠나는 것 같아 아쉽지만 훗날 이 맘 때가 되면 분명 나보다 훨씬 뛰어난 박사들이 돼 있을 것이라 믿는다. 유기팀 후배들, 주말출근은 기본인 성실함의 대명사 대경, 진취적이고 빠릿빠릿한 영록, 여러 가지 일에도 항상 에너지가 넘치는 우철, 신사적이고 진중한 희범에게도 고마운 마음을 표하고 싶습니다. 그리고 무기팀 후배들, 왠지 잘 모르겠지만 어투에 이상하게 정이 가는 꾸준한 진수와 한다면 하는 인간승리의 살아있는 표본 GOD재근, 착하고 다정한 유리와 항상 인사할 때 웃어주는 성격 좋은 지원, 마지막으로 명랑한 재영에게도 그 동안 감사했다는 말을 전하고 싶습니다. 한기도 오랜 기간 못 봤지만 새로운 길에서 잘 해내고 있으리라 믿고, 인호도 그 동안 먼 길 오가느라 너무 고생 많았다. 국누나, 이고은씨도 길게든/짧게든 여러모로 도움 주셔서 감사합니다. 그리고 승준형, 형께는 이루 말로 다 할 수 없는 감사를 드리고 싶습니다. 연구적으로도 좋은 롤모델이 되어 주셨지만, 특히 졸업을 앞두고 아낌없는 조언과 정말 소중한 도움들 덕분에 학위과정을 잘 마무리할 수 있게 된 것 같습니다. 또한 강기훈 박사님도 오랜 기간 함께하지 못해 아쉽지만 그 짧은 기간 동안에도 본받을 만한 역량을 너무 많이 보여주셔서 스스로도 귀감이 많이 되었습니다. 감사합니다. 민미숙 박사님, 계시는 동안 여러 도움 주셔서 감사하고 잘 돌아오시길 기원합니다. Professor Xiang, thank you. I always wish all the best for you and your family.

이와 더불어 MNELAB선배님들께도 감사의 말씀을 전하고 싶습니다. 후배로 생

각해주실지 모르겠지만 감히 생각해 주신다면 저는 굉장히 기쁠 것 같습니다. 왕건욱 교수님, 연구적인 도움뿐만 아니라 진로 준비에 있어서도 많은 도움 주셔서 감사합니다. 건호 형님, 성훈 형님도 연구실 초기 도움 많이 주셔서 감사합니다. 송현욱 교수님, 김태욱 박사님, 조병진 교수님, 홍웅기 박사님께서도 조언 주셔서 감사 드린다는 말씀을 드립니다. 박성준 박사님도 항상 감사했습니다.

힘든 대학원 생활을 함께 버틸 수 있게 해주었던 많은 동료, 선후배님들께 감사합니다. 소중한 학부 동기들, 혁우(혁구), 융희, 환철, 명균, 현준. 대학원에 늦게 들어온 날 많이 도와줘서 너무 고마웠어. 연구적인 도움도 도움이지만 정서적으로 친구들이 주위에 함께 있다는 게 얼마나 든든한 일인지 너희들이 졸업하고 나서야 좀 느낀 것 같다. 각자의 길 위에서 항상 발전이 있길 바라고, 앞으로도 친구이자 동료로써 좋은 인연들 계속 이어갔으면 좋겠다. 대학원에서 처음 인연을 맺은 홍석, 너의 선한 성품 덕에 많은 도움을 받았던 것 같네. 고마웠고 학위과정도 잘 마치길 바라. 오랜 기간 공동연구를 같이 한 한빛, 함께 졸업할 수 있게 되어 기쁘다. 항상 앞날에 행운이 함께하길. 대학원 입학 초기 때 특히 자주 교류했던 필광, 따로 얘기는 못했지만 최근 논문 축하하고 비상한 너의 능력을 앞으로도 널리 발휘할 수 있길 빈다. 지금은 포닥 가신 명래형, 항상 친절함으로 저를 대해주시고 장비 사용 등에도 많은 도움 주셔서 감사합니다. 지윤, 준범도 그 동안 22동 복도를 오가며 여러모로 많이 고마웠어~ 제가 미처 여기 적지 못한 다른 많은 분들께도 모두 감사의 말씀을 전합니다.

그리고 지금 이 순간까지 묵묵히 저를 믿고 기다려 주신 사랑하는 저의 가족들에게 무한한 감사를 드리고 싶습니다. 아버지, 어머니. 어엿하게 낳아주시고 사랑으로 길러주셔서 감사합니다. 큰아들 바쁠까 봐 전화도 자주 안하고 그러지 마시고 오래오래 건강하셔서 항상 저의 버팀목이 되어주세요. 오랜 기간 공부만 하는 못난 아들 때문에 걱정 많이 하셨지만 이제 그 걱정 덜어드릴 수 있도록 의젓하게 살아가며 효도하겠습니다. 그리고 자주 찾아 뵐께요. 사랑합니다. 누나, 승규. 항상 동생/형 응원해줘서 너무 고마워. 앞으로도 지금처럼 힘들고 어려울 때 서로 의지하고 힘이 돼 주며 기쁠 때는 가장 먼저 함께 기뻐해주는 사람들이 되자. 매형, 누나와 언제나 행복하게 사시길 빌께요. 항상 손주들 잘 지내고는 있는지 걱정해주시는 외할머니, 앞으로도 건강히 오래오래 사시길 기원합니다. 저를 믿고 아껴주시는 장인어른, 장모님. 항상 감사합니다. 사랑하시는 딸 행복하게 살아가는 모습 보여드릴 수 있도록 항상 혜린 아끼고 위하며 살겠습니다. 원주에 갈 때마다 항상 반갑게 맞아주셔서 이제는 원주집도 제 고향 같고 좋습니다. 앞으로도 자주 찾아 뵙겠습니다. 처남 재영, 이제는 어엿한 사회인이 되었는데 항상 누나랑 매형 신경 써줘서 고마워. 친가/외가 친척 어르신들도 어린 시절부터 저를 아껴주시고 보살펴 주셔서 감사합니다.

끝으로 사랑하는 나의 아내 혜린. 항상 우스개 소리로 넌 정말 날 잘 만났다고 얘기하고 다녔지만 사실 내가 널 만날 수 있었던 게 하늘이 주신 가장 큰 축복이 아닐까 생각해. 항상 나를 믿고 사랑해줘서 너무 고마워. 힘들었던 학위기간이 우리를 더욱 성장시켜줬던 것처럼 앞으로도 힘들고 어려운 일 함께 헤쳐 나가며 성장하고 또 행복하게 살자. 하느님께서 항상 지켜주시겠지.^^ 사랑합니다.

한 고비를 넘어 끝이 아닌 새로운 출발점에 다시 서게 된 것 같습니다. 새로운 시작에 앞서 잠시나마 감사했던 분들을 돌이켜 볼 수 있게 된 것 만으로도 충분히 기쁘고 벅찬 감정을 느낍니다. 앞으로도 항상 겸손하게 모든 것에 감사하며 살겠습니다. 그리고 잊지 않겠습니다. 그 동안 수고 많았고 훗날 이 글을 다시 보게 된다면 언제나 지금 이 순간을 우직하게, 그리고 행복하게 살라고 얘기하고 싶다. 하느님 감사합니다. 성모님 저를 위하여 빌어주셔서 감사합니다.